Lappeenranta
University of Technology

Philipp Maydannik

ROLL-TO-ROLL ATOMIC LAYER DEPOSITION PROCESS FOR FLEXIBLE ELECTRONICS APPLICATIONS

Doctoral dissertation for the degree of Doctor of Science (Technology) to be presented with due permission for public examination and criticism in Mikkeli University Consortium auditorium, Lönnrotinkatu 5, 50100 Mikkeli, Finland, on the 16th of June, 2015, at noon.

Acta Universitatis
Lappeenrantaensis 641

Supervisor

Mika Sillanpää
Laboratory of Green Chemistry
Chemical Department
LUT School of Engineering Science
Lappeenranta University of Technology
Mikkeli, Finland

David Cameron
Current address:
R&D Centre for Low-Cost Plasma and Nanotechnology Surface Modification
Masaryk University
Brno, Czech Republic

Reviewers

Fred Roozeboom
Group Plasma & Materials Processing
Dept. of Applied Physics
TU Eindhoven
Eindhoven, Netherlands

Steven M. George
Depts. of Chemistry & Mechanical Engineering
University of Colorado,
Boulder, Colorado, USA

Opponent

Fred Roozeboom
Group Plasma & Materials Processing
Dept. of Applied Physics
TU Eindhoven
Eindhoven, Netherlands

ISBN 978-952-265-803-6
ISBN 978-952-265-804-3 (PDF)
ISSN-L 1456-4491
ISSN 1456-4491

Lappeenrannan teknillinen yliopisto
Yliopistopaino 2015

ABSTRACT

Philipp Maydannik
Roll-to-roll atomic layer deposition process for flexible electronics applications
Lappeenranta 2015
75 pages
Acta Universitatis Lappeenrantaensis 641
Diss. Lappeenranta University of Technology
ISBN 978-952-265-803-6, ISBN 978-952-265-804-3 (PDF), ISSN-L 1456-4491, ISSN 1456-4491

Atomic Layer Deposition (ALD) is the technology of choice where very thin and high-quality films are required. Its advantage is its ability to deposit dense and pinhole-free coatings in a controllable manner. It has already shown promising results in a range of applications, e.g. diffusion barrier coatings for OLED displays, surface passivation layers for solar panels. Spatial Atomic Layer Deposition (SALD) is a concept that allows a dramatic increase in ALD throughput. During the SALD process, the substrate moves between spatially separated zones filled with the respective precursor gases and reagents in such a manner that the exposure sequence replicates the conventional ALD cycle.

The present work describes the development of a high-throughput ALD process. Preliminary process studies were made using an SALD reactor designed especially for this purpose. The basic properties of the ALD process were demonstrated using the well-studied Al_2O_3 trimethyl aluminium (TMA)+H_2O process. It was shown that the SALD reactor is able to deposit uniform films in true ALD mode. The ALD nature of the process was proven by demonstrating self-limiting behaviour and linear film growth. The process behaviour and properties of synthesized films were in good agreement with previous ALD studies. Issues related to anomalous deposition at low temperatures were addressed as well.

The quality of the coatings was demonstrated by applying 20 nm of the Al_2O_3 on to polymer substrate and measuring its moisture barrier properties. The results of tests confirmed the superior properties of the coatings and their suitability for flexible electronics encapsulation.

Successful results led to the development of a pilot scale roll-to-roll coating system. It was demonstrated that the system is able to deposit superior quality films with a water transmission rate of $5x10^{-6}$ g/m^{2}day at a web speed of 0.25 m/min. That is equivalent to a production rate of 180 m^2/day and can be potentially increased by using wider webs.

State-of-art film quality, high production rates and repeatable results make SALD the technology of choice for manufacturing ultra-high barrier coatings for flexible electronics.

Keywords: atomic layer deposition, aluminium oxide, moisture barriers, flexible electronics, thin films, polymer substrate, roll-to-roll

PREFACE

I would like to express sincere gratitude to my supervisor and mentor Prof. David Cameron, who has been guiding me through the years of studies.

I would like to acknowledge contribution of my co-workers at LUT, Miktech and other universities for their work and support. Special thanks go to Tommi Kääriäinen, Kimmo Lahtinen and Tatyana Ivanova for their valuable impact on my work.

I am deeply thankful to Mikko Söderlund, Pekka Soininen, Mika Jauhiainen, Jorma Väisänen and Sampo Ahonen from Beneq Oy for their support on engineering and hardware.

My thanks also go to reviews of this dissertation Prof. Fred Roozeboom and Prof. Steven George for their work.

And of course I would like to express my gratefulness to my family for their endless support through these years. My very special thanks to Elina Iamsia for her care and support.

LIST OF PUBLICATIONS

The dissertation is based on the summary of the following original peer-reviewed articles and referred in the text by the Roman numerals.

I. **P.S. Maydannik**, T.O. Kääriäinen, D.C. Cameron, An atomic layer deposition process for moving flexible substrates, Chemical Engineering Journal 171 (1) (2011) 345-349

II. **P.S. Maydannik**, T.O. Kääriäinen, D.C. Cameron, Continuous atomic layer deposition: Explanation for anomalous growth rate effects, Journal of Vacuum Science & Technology A 30 (1) (2011) 01A122

III. **P.S. Maydannik**, A. Plyushch and M. Sillanpää and D.C. Cameron, Spatial Atomic Layer Deposition: performance of low temperature H_2O and O_3 oxidant chemistry for flexible electronics encapsulation, Journal of Vacuum Science & Technology A 33 (3) (2015) 031603

IV. **P.S. Maydannik**, T.O. Kääriäinen, K. Lahtinen, D.C. Cameron, M. Söderlund, P. Soininen, P. Johansson, J. Kuusipalo, L. Moro, X. Zeng, Roll-to-roll atomic layer deposition process for flexible electronics encapsulation applications, Journal of Vacuum Science & Technology A 32 (5) (2014) 051603

AUTHORS CONTRIBUTION IN THE PUBLICATIONS

I. The author performed the literature survey, most of the experimental and analysis work, and wrote the first draft of the paper.

II. The author performed the literature survey, most of the experimental and analysis work, and wrote the first draft of the paper.

III. The author performed the literature survey, most of the experimental and analysis work, and wrote the first draft of the paper.

IV. The author performed the literature survey, most of the experimental and analysis work except the Water Vapour Transmission Rate (WVTR) measurement, and wrote the first draft of the paper.

OTHER PUBLICATIONS BY THE SAME AUTHOR

I. G. Natarajan, **P.S. Maydannik**, D.C. Cameron, I. Akopyan, B.V. Novikov, Atomic layer deposition of CuCl nanoparticles, Applied Physics Letters 97 (24), 241905, 2010

II. T.O. Kääriäinen, **P.S. Maydannik**, D.C. Cameron, K. Lahtinen, P. Johansson, J. Kuusipalo, Atomic layer deposition on polymer based flexible packaging materials: Growth characteristics and diffusion barrier properties, Thin Solid Films 519 (10), 3146-3154, 2011

III. K. Lahtinen, **P.S. Maydannik**, T. Kääriäinen, D.C. Cameron, J. Kuusipalo, Utilisation of continuous atomic layer deposition process for barrier enhancement of extrusion-coated paper, Surface and Coatings Technology 205 (15), 3916-3922, 2011

IV. T.V. Ivanova, **P.S. Maydannik**, D.C. Cameron, Molecular layer deposition of polyethylene terephthalate thin films, Journal of Vacuum Science & Technology A 30 (1), 01A121, 2012

V. K. Lahtinen, **P.S. Maydannik**, T. Seppänen, D. C. Cameron, P. Johansson, S. Kotkamo, J. Kuusipalo, Protecting BOPP film from UV degradation with an atomic layer deposited titanium oxide surface coating, Applied Surface Science 282, 506-511, 2013

VI. K. Lahtinen, T. Kääriäinen, P. Johansson, S. Kotkamo, **P.S. Maydannik**, T. Seppänen, J. Kuusipalo, D. C. Cameron, UV protective zinc oxide coating for biaxially oriented polypropylene packaging film by atomic layer deposition, Thin Solid Films 570, 33-37, 2014

CONFERENCES

I. **Maydannik Philipp**, Kääriäinen Tommi, Cameron David, A Continuous ALD process for deposition of diffusion barriers on flexible substrates, Society of Vacuum Coaters - Annual Technical Conference, Volume 53rd ATC, 2010, Pages 16-19

II. **Maydannik Philipp**, Kääriäinen Tommi, Cameron David et al., Continuous Atomic Layer Deposition process: towards roll-to-roll ALD, AVS 10th International Conference on Atomic Layer Deposition, 2010

III. **Maydannik Philipp**, Kääriäinen Tommi, Lahtinen Kimmo et al., Continuous ALD Deposition on Moving Flexible Polymer Substrates, Society of Vacuum Coaters - Annual Technical Conference, 2011, Pages 82-88

IV. **Maydannik Philipp**, Kääriäinen Tommi, Lahtinen Kimmo et al., An Industrial Scale Roll-to-roll Atomic Layer Deposition Process for Coating Flexible Web Substrates, AVS 13th International Conference on Atomic Layer Deposition, 2013

Contents

ABBREVIATIONS

ALD - Atomic Layer Deposition

CIGS - Copper Indium Gallium Selenide

CVD - Chemical Vapour Deposition

FTIR - Fourier transform infrared

OLED - Organic Light-Emitting Diode

PECVD - Plasma Enhanced Chemical Vapour Deposition

PEN - Polyethylene naphthalate

PES - Polysulfone

PVD - Physical Vapour Deposition

QCM - Quartz Crystal Microbalance

RH - Relative Humidity

RPI - Redlich-Peterson Isotherm

SALD - Spatial Atomic Layer Deposition

SPD – Specific Precursor Dosage

TFT – Thin Film Transistor

TMA – Trimethyl aluminium

WVTR - Water Vapour Transmission Rate

I. Introduction

Flexible electronics is an emerging market with very high potential for growth. The current figure for the total market of printed, flexible and organic electronics is $24 billion with an estimated growth to $77 billion in 10 years [1]. The largest share of the market belongs to Organic Light-Emitting Diode (OLED) display and lighting products together with conductive inks [1]. Indeed, flexibility together with OLED technology brings a number of advantages both for consumers and manufacturers. OLED displays are known for their ability to provide very bright, high contrast and clear pictures with high viewing angles, low response time and attractive power consumption. Their suitability for roll-to-roll manufacturing can potentially minimize their costs. However, there are certain challenges arising, particularly with manufacturing of flexible OLED devices. Light emitting material can be easily oxidized by either moisture or oxygen penetrating from the ambient environment. Therefore, the device must be hermetically encapsulated to ensure a long life-span. The most commonly indicated maximum allowable permeation rate for OLED devices is in order of 10^{-6} g/m^{2}day. For devices produced on rigid substrates this does not exhibit any problem since encapsulation can be done by covering the device with transparent glass that has virtually zero water permeation rate. However, for devices on flexible substrates, additional requirements such as flexibility must be fulfilled. Polymeric substrate itself does not provide enough gas barrier properties with an intrinsic WVTR of 1 – 10 g/m^{2}day. The most common approach used to improve gas barrier properties of the polymer is to coat it with impermeable material such as metal oxides. Mostly vacuum coating methods are used for this purpose. E.g. methods based on physical processes such as vacuum thermal or electron beam evaporation and magnetron sputtering to name a few. These methods usually provide fairly high production rates but fail to produce adequate barrier coating and are mainly used for less demanding packaging technology. Methods based on chemical processes are able to produce coating with higher qualities. Chemical Vapour Deposition (CVD) especially Plasma Enhanced Chemical Vapour Deposition (PECVD) is able to produce high quality barriers with WVTR level of 10^{-5} g/m^{2}day [2]. Another technique which is based on a chemical process is Atomic Layer Deposition. It is a

deposition method that is based on chemical interaction between the solid substrate and gaseous reagents. The method has been used to deposit moisture barrier films with great success. Superior barrier properties of ALD films and their suitability for OLED encapsulation were proved in several studies [3-4]. Carcia et al. showed with accelerated calcium test (60 °C and 85% relative humidity (RH)) that 25 nm of Al_2O_3 film deposited with ALD can decrease moisture permeation of Polyethylene naphthalate (PEN) polymer by 6 orders of magnitude resulting in $6x10^{-6}$ g/m^{2}day of WVTR [3]. Superior protection of an actual OLED device was demonstrated by Ghosh et al. OLED encapsulated with 180 nm of Al_2O_3 ALD layer showed no signs of degradation for 1000 hours [4]. Although it is clear that ALD is the technology of choice for encapsulation solutions, it has some drawbacks related to its process throughput. Unfortunately, ALD is known for its slowness due to process features, which will be explained in later sections.

Considering such promising results in a field of ultra-high moisture barrier application, increase of its throughput is an essential step towards further industrialization of the technology. The Spatial ALD concept is an approach that allows the turning of low production ALD into a high-throughput technology including adaptation into roll-to-roll manufacturing line. However, there is a lack of process understanding due to complete absence of experimental data. The SALD concept implies employment of a reactor design, which is very different from those used in conventional ALD. Thus, it is very crucial to perform experimental work and carry out the following steps:

- Verifying the Spatial Atomic Layer deposition concept for various thin film materials
- Developing a thin film coating process based on the SALD concept
- Scaling up the process by implementing a roll-to-roll coating scheme

A. Atomic Layer Deposition process. General description and remarks.

The history of ALD starts in the beginning of 1960s in the USSR when the first hypothesis of a surface modification theory by Molecular Layering was proposed by Prof. Aleskovski [5-9]. It remained unknown until later on in the 1970s Suntola invented a coating process based on the same principle and described in his works [10-19]. Since then it has gained the attention of the scientific community. Today, the ALD method is a well-established technique with a robust technological base approved by use in industry. E.g. Intel Corporation implemented the ALD process to deposit HfO_2 and Al_2O_3 dielectric layers for microprocessor manufacturing. Another example is Lumineq (Finland) which is using a ZnS ALD process for thin film electroluminescence displays manufacturing.

The ALD process is known for a number of advantages such as uniform film growth, precise thickness control, high quality film deposition and the ability to coat complex shaped substrates. These advantages are brought by the self-limiting nature of the process. In ALD, growth of solid matter is a result of chemical interaction between gaseous reagents and reactive sites of the surface. During the ALD process precursor vapour is injected into the reactor where it reacts with surface sites of the substrate. Gas-solid reaction continues until the surface is saturated with the reagent and one monolayer of molecules is formed. Before the next reagent is introduced, the chamber must be purged with inert gas in order to remove leftovers and reaction by-product. This sequence is called the ALD half-cycle and needs to be performed a number of times depending on the required film thickness. The scheme of a full ALD cycle consisting of two sequential half-cycles is shown in figure 1.

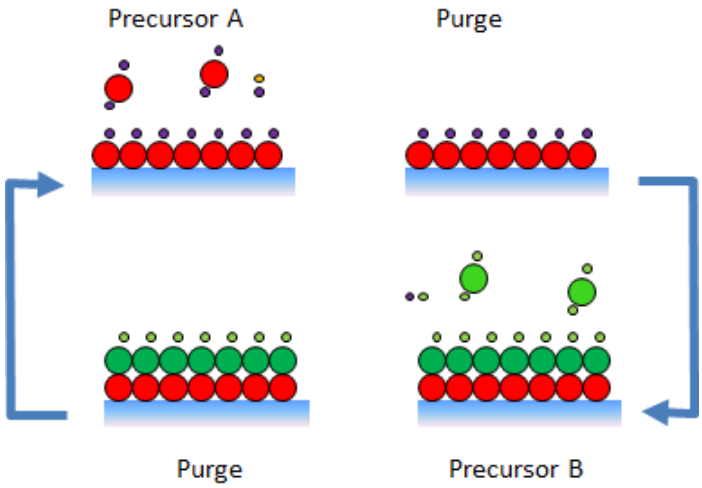

Figure 1. Schematic representation of the ALD process.

Conventional ALD is a vacuum based technology. Process-wise it is a sequence of reactant pulses intermittent with inert gas pulses in order to purge the chamber. Precursor injection time is usually relatively short and can be optimized by increasing the vapour pressure. For flow-through type ALD reactors, the precursor pulsing time depends on the gas flow rate, reactor volume, reagent vapour pressure and chemical kinetics between the particular reagent and the functional groups of the surface. Typical pulsing time is in the order of tenths of seconds for most of the processes and reactor chambers, but it can be longer in certain cases, e.g. slow reaction rates or large industrial deposition chambers.

In contrast, purging is a longer step. It varies from a few seconds to tens of seconds and greatly depends on the reactor shape and volume. As a rule purging is a limiting step as it requires a considerable amount of time for filling and flushing the chamber compared to the time for injection and chemical reaction. Purging is applied until the inert gas has completely removed the residuals. Thus, purging time depends on the inert gas flow rate, reactor geometry and volume and the desorption rate of the by-products. The time for purging varies greatly and can be up to 180 s at low temperatures [20]. As can be seen, the ALD cycle duration can be from a few seconds to up to one minute with the purging step being the limiting process.

Most of the studies dealing with process development pay great attention to showing self-limiting behaviour in order to prove the ALD nature of deposition. It is important indeed because the ALD growth mode can be easily turned into CVD type if the technological parameters are not set in a right way. Even in the case of partial CVD film quality can be compromised. The pulsing and purging procedure should be optimised in a way that the surface receives enough precursor and all its excess and reaction by-products are removed. In order to show this self-limiting behaviour so-called saturation curves are plotted. A saturation curve describes how the amount of material deposited per one precursor exposure depends on the precursor exposure time. A typical saturation curve for the TMA + H_2O ALD process is shown in figure 2. As ALD is based on a chemisorption process, usually the shape of the saturation curve can be described by one of the adsorption isotherms, e.g. Langmuir isotherm. The most common x-axis is either the pulsing time or partial pressure while the y-axis is film growth per cycle.

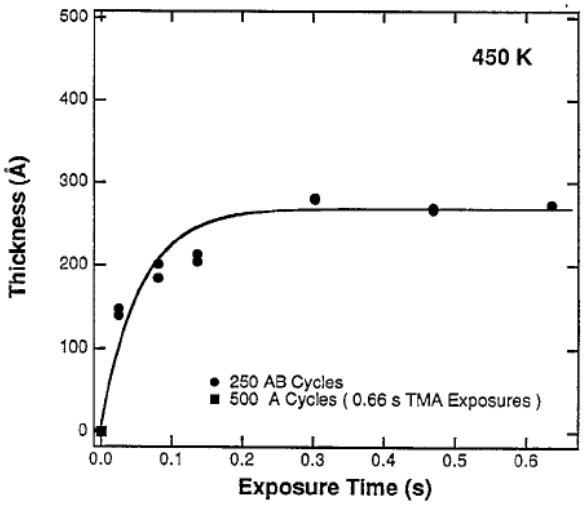

Figure 2. Typical saturation curve of the TMA+water process. Reprinted from [21].

Self-limiting behaviour brings another feature of the process: linearity of growth rate as a function of ALD cycles. This dependence should show a straight line as every ALD cycle produces a fixed amount of material to be deposited on a substrate. However, it can be

different in the initial stage because of slow nucleation and such effects as substrate induced or inhibited growth.

Another feature of the ALD technique is its inherent ability to produce uniform coatings even on complex shape substrates. Again, because of the gas-solid interaction based on chemisorption mechanism, precursor molecules attach to the surface, uniformly covering the surface.

The present work is based on the Al_2O_3 ALD process. There are several reasons for choosing Al_2O_3 over other oxides that can be grown by ALD. It is probably the most well studied chemistry with lots of data collected over years of studies. The behaviour of the process has been investigated by various techniques including in situ ellipsometry, Fourier transform infra-red spectroscopy (FTIR), quartz crystal microbalance (QCM), quadrupole mass spectrometry (QMS). A number of studies have been dedicated to the surface chemistry of Al_2O_3 ALD. For example, in situ FTIR confirmed the exchange ligand reaction between $–CH_3$ and –OH groups [22-25]. By-products of the reaction were determined by quadrupole mass spectrometry [26, 27]. Additional data on the deposition mechanism was acquired using QCM [28]. Density functional theory was used to model the interaction between surface and gaseous reagents [29].

Information on growth behaviour on different substrates including polymers has been obtained [24, 30]. Al_2O_3 by ALD is a material that is ready to be commercialized for several applications such as crystalline silicon solar cell passivation layers and moisture barrier layers for electronics.

Another good reason to go for the Al_2O_3 ALD process is that it follows the ideal ALD growth model with (almost) true saturation behaviour and absence of artifacts. This should be beneficial in avoiding possible confusion when moving to a completely new reactor setup.

The basic metal precursor is trimethyl aluminium (TMA) which is used together with an oxidizing precursor that replaces methyl ligands with hydroxyl groups. TMA is a pyrophoric compound and reacts violently with oxidizing agents by forming Al_2O_3. Thus, reaction time is very short which favors a high-speed process. Another advantage is that any process imperfection would be easily highlighted.

Generally, ALD studies concerning Al_2O_3 have been extensively reviewed and detailed information on the process, materials and applications can be found elsewhere [31-39].

B. Spatial Atomic Layer Deposition

1. Spatial ALD concept

Spatial Atomic Layer Deposition is a concept that facilitates increasing the production rate of ALD technology by eliminating steps that are limiting the ALD process such as gas filling and purging. While conventional ALD uses time-separated pulsing of gases to treat a fixed substrate, the SALD concept involves a different approach: the SALD concept utilizes spatially separated zones with steady gas flows arranged in such a way that: (i) when substrate is being moved between the zones gas the exposure sequence replicates the conventional ALD cycle; (ii) there is no intermixing between gases. Schematically the SALD approach is illustrated in figure 3.

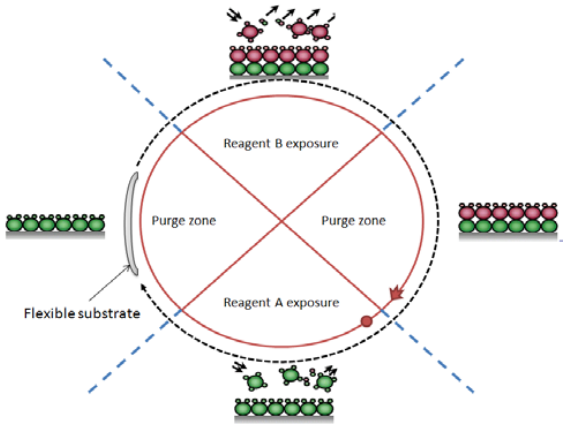

Figure 3. Scheme of spatially separated ALD process showing the flexible substrate moving between gas zones.

SALD brings a number of advantages. First of all, it allows continuous substrate treatment and implementation of roll-to-roll handling scheme. Secondly, it eliminates

process downtime due to loading/unloading and heating/cooling time. Implementation of steady gas flows does not need the presence of precise gas pulsing valves, thus making the equipment cheaper and more reliable. Finally, process speed is not limited by the hydrodynamic characteristics of the system but by the chemical kinetics of the particular reaction.

A number of attempts have been made to realize the SALD concept by building various coating systems. The most successful ones will be discussed in the next section.

2. *Spatial ALD systems*

Initially, the SALD concept was suggested by T. Suntola and described in two of his patents [18,40]. The patent discusses the reactor with inlet and exhaust slit intended for creating reactive zones separated by inert gas shields (figure 4).

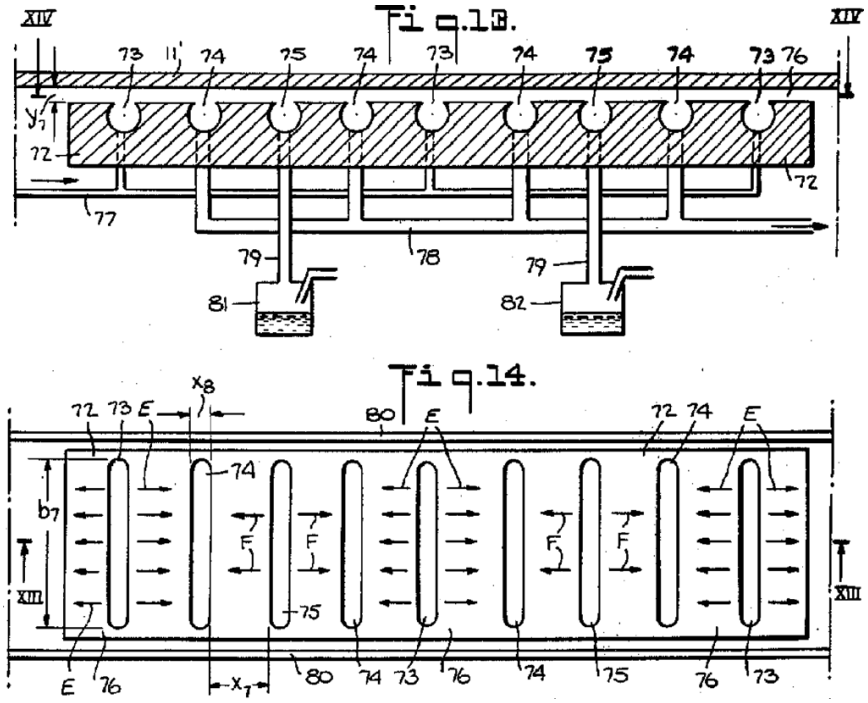

Figure 4. SALD concept by T. Suntola. Reprinted from patent [40].

The first report of a coating system that utilizes the SALD concept was published by Levy et al. [41,42]. The core of the system is a coating head with recessed channels suspended approximately 30 um above the substrate [43]. Gas is introduced on one end of the channel and removed from the other end. Film deposition is carried at atmospheric pressure and achieved by oscillating the head over the sample a certain amount of times in order to obtain the desired thickness. The reports describe the construction of the head (figure 5) and initial deposition results for Al_2O_3 and ZnO processes. The system was used to produce a Thin Film Transistor (TFT) device and its electrophysical characteristics were investigated [44].

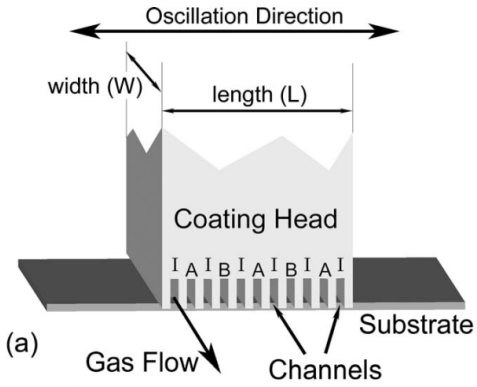

Figure 5. Eastman Kodak concept. I – nitrogen gas flow; A and B – oxidizing and metal precursors, respectively. Reprinted from [41].

TNO developed and described an atmospheric pressure SALD prototype intended for rigid substrate coating [45-49]. The design of the tool is schematically shown in figure 6. The tool consists of immobile coating head and rotating substrate holder. The coating head has linear gas injectors and pie-shaped recessions in a cylindrical body under which substrate is rotated. The gap between the gas bearing plane and the substrate was set to 20 um while the reagent inlet to substrate distance was 200 um. The head is mounted inside an oven that is capable of heating up 400 °C. An impressive coating rate of 1.2 nm/s was achieved. Deposited films were tested as a backside passivation for crystalline silicon solar cells very showing promising results [45].

The same prototype system was used to study a low temperature SALD process [46]. Reactor temperatures below 100 °C expectedly led to CVD type of growth due to the

excess of adsorbed water on the substrate surface. To avoid this effect an intermediate step of helium plasma treatment was added to the oxygen precursor. This approach showed good results but still further refinement was needed.

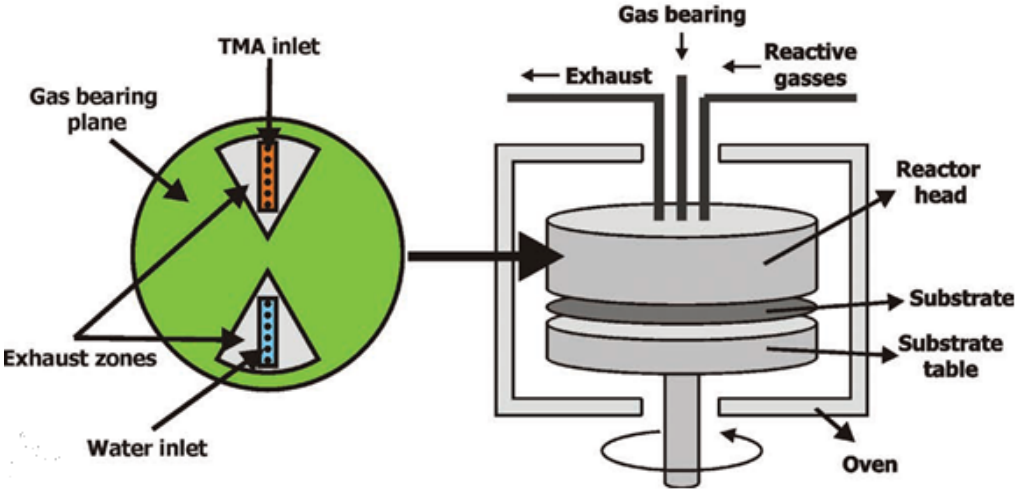

Figure 6. Schematic drawing of Spatial ALD reactor with stationary injector head and rotating substrate holder by TNO. Reprinted from [45].

The kinetics of the SALD process was studied experimentally and a model was developed. It was found that surface coverage is proportional to exp(√t).It was suggested that the reason for such dependence may be the fact that deposition rate is limited by a diffusion step [47].

The development of a high-speed roll-to-roll coating system was announced by TNO in 2012 [46]. The system comprises a rotating drum with combinations of inlet, exhaust ports and gas bearings. The substrate is wrapped over the drum and kept away typically 100-200 μm from the surface by applying high pressure from gas bearings. Deposition is achieved by rotating the drum while polymer web is being guided over it. The system is designed to handle 30 cm width webs. The operating principle of the device is illustrated in figure 7.

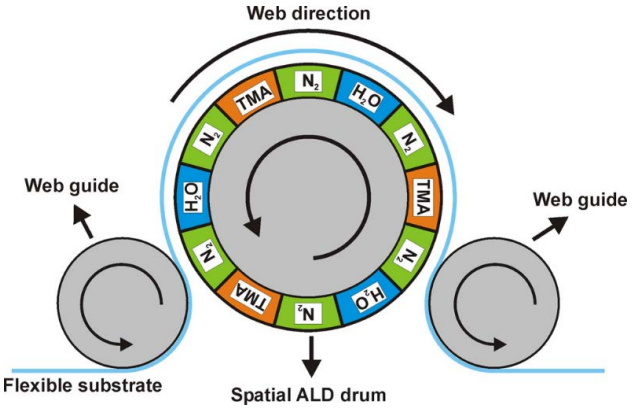

Figure 7. Roll-to-roll tool SALD coater by TNO. Reprinted from [46].

SoLayTec is a TNO spin-off company that developed a commercial sheet-to-sheet SALD system [50, 51]. The core of the system is a narrow channel with gas flowing from top and bottom sides with the substrate suspended in between as shown in figure 8. A silicon wafer is floating back and forth exposing itself to the reaction zones and building up monolayers of materials during each passage. Essentially the same approach is used by Levitech which is in turn a spin-off company from ASM International [52,53]. Unlike the SoLayTec system, the substrate is moved in one direction and the required thickness achieved by using a module that is long enough to accommodate the respective number of "reaction cells". Both systems are targeted for silicon solar cell passivation application.

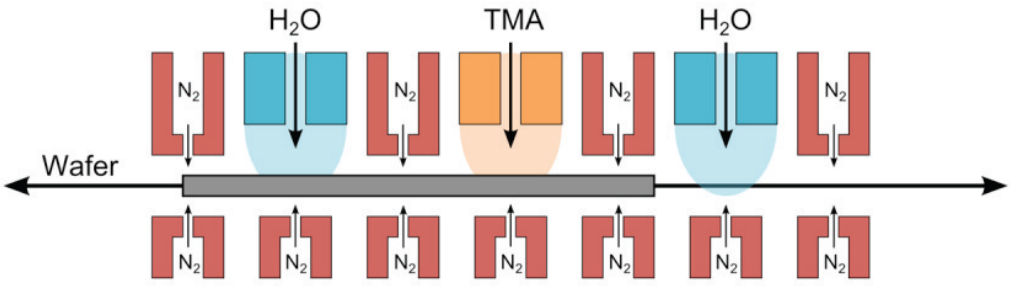

Figure 8. SoLayTec system. Reprinted from [54].

Lotus Applied Technology developed a roll-to-roll coating tool in a single chamber [55]. The chamber is divided into three zones by walls with slots to allow the web to pass through. Two zones are filled with reagent gases and one in between is filled with inert gas. The reactor scheme is shown in figure 9. Deposition is achieved by guiding the web

between zones multiple times in a serpentine fashion. The system is able to operate in roll-to-roll and single-loop mode. The first report describes deposition of TiO_2 film on PET substrate for moisture barrier application [56]. Growth rate saturation behaviour was shown and WVTR of TiO_2/PET structures was measured as a function of film thickness and web speed. Films exhibited moisture transmission levels of 10^{-2} g/m^{2}day at a web speed range of 0.2 – 5 m/s. The company was granted a number of patents related to the technology [57-62] including energy enhanced deposition [63, 64]

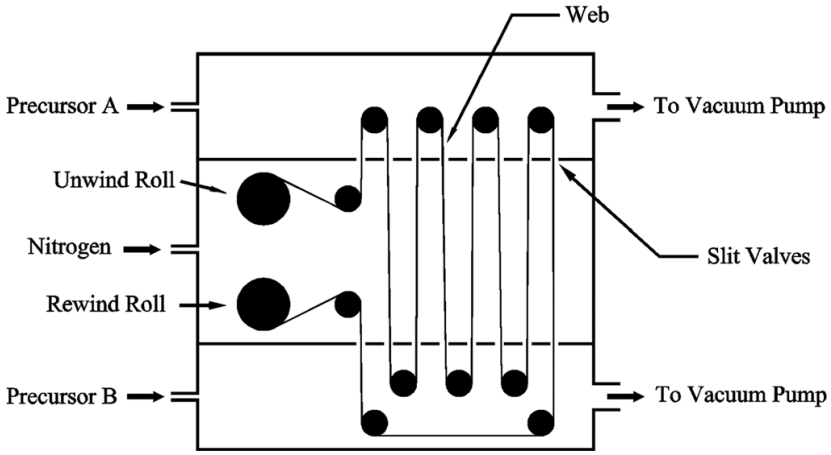

Figure 9. Lotus system. Reprinted from [65].

Improved results were reported by the same group by replacing water as a precursor with a plasma oxidation step. The motivation for introducing plasma was to eliminate a CVD-like deposition effect due to excess of water adsorption. Deposited coatings demonstrated very low WVTR of 10^{-4} g/m^{2}day. The damaging effect of the web rewinding step was demonstrated as well. Permeation level of rewound films was 10 times higher compared to films that were kept intact. The authors demonstrated that the issue can be solved by applying UV-curable coating on the top of ALD layer to prevent its damage [66].

Lotus Applied Technology announced the development of a scaled up reactor that will be able to handle 300 mm wide webs and rolls of 1000 m length. The system will be capable of coating layers with 100 ALD cycles resulting thickness ranging from 10 to 20 nm [67].

The research group from Colorado University carried out an extensive study on the operating conditions of a multiple slit coating head system [68]. The SALD system

operates at atmospheric pressure and in contrast to Eastman Kodak system uses variable mechanical spacing to maintain the gap. Helium was used as a tracer to detect possible gas intermixing and study the effect of gap spacing, pumping speed and N_2 purging pressure.

Another atmospheric roll-to-roll ALD system was developed by the research group from Jeju National University (South Korea). The authors report achieving a web speed of 7 mm/s and WVTR of ~10^{-3} g/m^2/day at 37.8 °C/100% for Al_2O_3 films with thickness ranging from 15 to 40 nm [69].

Since 2009, the ASTRaL group of Lappeenranta University of Technology has been developing a high-throughput process based on the SALD concept. This PhD thesis describes research work that has been carried out from 2009 to 2014.

C. Moisture barrier layers

1. Ultrahigh barriers by ALD

Probably the first demand for barrier coatings application was in the food industry to preserve food against moisture and oxygen in order to increase its shelf-life. The requirements for food packaging are not so stringent – in the order of 10^{-1} – 10^{-2} g/m^{2}day. Nevertheless, polymer alone is not able to provide suitable protection as its intrinsic barrier properties are 2 or 3 magnitudes higher (see figure 10). Then it was realized that coating polymer with an inorganic layer could solve the problem. The first methods used to coat the polymer were Physical Vapour Deposition (PVD) techniques such as physical vacuum evaporation and electron beam evaporation. Metallic aluminium was used as a barrier material. The resulting coating is flexible and provides virtually zero moisture permeation rates. Demand for transparent packaging pushed the development towards metal oxides such Al_2O_3, SiO_2, TiO_2, etc. Oxide coatings prepared with PVD techniques are good enough to use in food and pharmaceutical industry. Another advantage of using

PVD is its high production rate with web speeds of up to 370 m/min [70]. However, they were not good enough for electronics application.

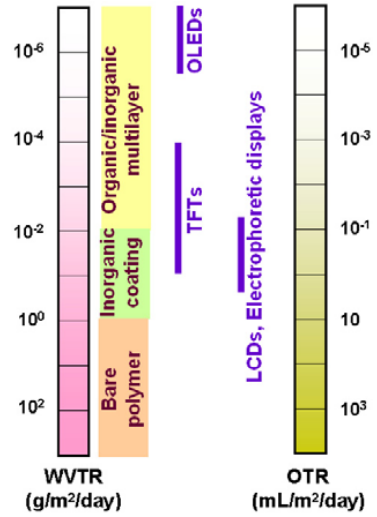

Figure 10. WVTR and OTR requirements for ultra-high barrier coatings. Reprinted from [71].

Magnetron sputtering is another deposition technique that belongs to PVD family. Its advantage is its ability to produce denser films by using higher energy species compared to other PVD techniques. Nevertheless, it is comparatively slow and has shadowing effects which make the coating sensitive even to small surface roughness.

Much better barrier films can be deposited using deposition techniques based on chemical interaction. One of the first attempts to use ALD for moisture barrier layers was made in 2004. Yun et al. [72] directly encapsulated an actual OLED device by depositing a 300 nm Al_2O_3 layer on top of an aluminium cathode contact using low temperature Plasma Enhanced ALD (PEALD). OLED lifetime was assessed by luminance degradation. The device could withstand 850 hours with decay of 4% compared to initial luminance values. Environment conditions were not reported.

Park et al. used a thermal ALD process to deposit 50 nm of Al_2O_3 on Polysulfone (PES) substrate [73]. Barrier layers were subjected to the WVTR test using MOCON Permatran-W1A at 38° C and 100% RH. Resulting transmission values were in the order

of 10^{-1} g/m^{2}day for single side coated and 10^{-2} g/m^{2}day for double side coated. OLED encapsulation performance was tested at 25° C and 80% RH with the result of 65.4% of the initial luminance value after 600 hours of exposure.

The first successful attempt to use the Al_2O_3 TMA+O_3 process for OLED encapsulation was made by Ghosh et al. [4]. 180 nm of Al_2O_3 were directly deposited on the OLED cathode layer followed by 2 um of parylene to avoid direct condensation of water onto the oxide layer. Encapsulated OLEDs were placed into an environmental chamber and subjected to 85 °C and 85% RH conditions for the permeability test. Regular radiometric measurements were performed that included device efficiency and emission spectra. Negligible degradation was observed after 1300 hours of accelerated test.

Similarly to Yun et al. [72], Langereis et al. investigated the suitability of the low temperature PEALD process for OLED encapsulation [74]. The WVTR was measured using the calcium test (21 °C and 60% RH). Permeation was studied as a function of film thickness and reactor temperature. Transmission values of 10^{-3} g/m^{2}day were obtained. No specific cleaning procedure was applied. Similar results were shown by Groner et al. [75]. WVTR of 10^{-3} g/m^{2}day and critical thickness of 10 nm was found.

A real breakthrough in terms of moisture barrier performance was made in 2006 by Carcia et al. [3]. For the first time it was demonstrated that ALD was able to produce single layer barrier films with WVTR of less than 10^{-5} g/m^{2}day. 25 nm of Al_2O_3 were deposited on PEN at 120 °C reactor temperature. The WVTR was measured using the calcium test at 38 and 60 °C and 85% RH with resulting values of $1.7x10^{-5}$ and $6.5x10^{-5}$ g/m^{2}day, respectively.

Potscavage et al. demonstrated the suitability of ALD films for encapsulation of pentacene/C60 organic solar cells [76]. 200 nm of Al_2O_3 were deposited straight on to the aluminium electrode of the prepared device and the structure was subjected to ambient atmosphere. Power conversion efficiency, fill factor and short-circuit current density were monitored. Some degradation of the parameters (6% of the initial values) was noted after 6145 hours of exposure.

Dameron et al. studied permeation of single and multilayer stack of Al_2O_3 prepared by thermal ALD and SiO_2 prepared by Rapid ALD [77]. WVTR values were measured by

the radioactive HTO tracer method. Barrier performance of a 26 nm Al_2O_3 single layer was ~10^{-3} g/m^{2}day, an Al_2O_3/ SiO_2 layer - ~10^{-4} g/m^{2}day and an Al_2O_3/ SiO_2 bilayer reduced transmission rate to ~$5x10^{-5}$ g/m^{2}day. Further increase of Al_2O_3/ SiO_2 layer numbers showed higher permeability than a single Al_2O_3 layer. Poorer results were attributed to the greater brittleness of thick layers.

Carcia et al. published thorough studies on comparison between barriers prepared by PECVD and ALD [78]. WVTR measurements were performed by a Ca test at 38 °C and 85% RH. A single Al_2O_3 layer by ALD with thickness of 10 nm exhibited a water transmission rate of $\leq 5x10^{-5}$ g/m^{2}day while 100 nm of SiN PECVD layer had a 100 times the transmission rate. At the same time, only 5 nm of ALD layer deposited on top of PECVD film reduced its permeability to $\leq 5x10^{-5}$ g/m^{2}day. Notably, the authors reveal some details on the substrate cleaning procedure. Polymer substrates were rinsed with methanol followed by soft scrubbing and again rinsing with methanol. Finally, substrates were rinsed with water and dried by blowing with N_2.

The suitability of ALD technology to protect Copper Indium Gallium Selenide (CIGS) solar cells against moisture was demonstrated by Carcia et al. [79]. CIGS modules covered by 55 nm of Al_2O_3 were exposed to harsh environmental conditions of 85 °C and 85% RH together with simulated solar illumination. Monitoring the main parameters (power conversion efficiency, fill factor and short-circuit current density) did not show any signs of degradation after 1020 hours of exposure.

This survey shows that ALD technology has advanced in the field of moisture barriers over the past 10 years. ALD films were thoroughly investigated and their barrier properties were quantified using different types of WVTR tests, demonstrating the readiness of ALD technology to fulfil the stringent protection requirements for organic electronics. However, there are several questions remaining obscured. There is clear scattering in the results between the studies – about 10^{-3} to 10^{-5} g/m^{2}day. One of the obvious reasons for this scattering is the absence of metrological standards for WVTR test conditions. The level of surface contamination is the key parameter for high quality moisture barrier production as it can be easily compromised by the presence of airborne particles, aerosols, etc. Most of the studies do not provide any information on the

cleaning procedure or the level of environmental contamination at which the experiments were carried out.

2. Permeation mechanism

Numerous studies have been dedicated to understanding the moisture and gas permeation mechanism. Generally, permeation through the material is a complex phenomenon with difference in chemical potential as the driving force. Permeation through material proceeds in several steps. The first stage is adsorption of the permeant molecule on the surface followed by its diffusion through the material layer and subsequent desorption out to the environment. Intramaterial diffusion is obviously a limiting step and governed by Fick's law which for thin barriers is:

$$F = -D\frac{\Delta c}{x} \quad (1)$$

where F is the molecular flux; Δc – concentration difference across the barrier; x – barrier thickness; D – diffusion coefficient.

In turn D is a function of temperature and described by the Arrhenius equation:

$$D = D_0 \exp(-\frac{E_d}{RT}) \quad (2)$$

where D is the diffusion coefficient at temperature T; D_0 is the maximum diffusion coefficient; E_d – the activation energy; R – the gas constant.

Another factor that contributes to permeation is the degree of porosity. It can be caused either by an imperfect deposition process or airborne contaminants. It has been shown that there is a correlation between density and size of pinholes with density and size of the atmospheric dust particles [80]. Intentional contamination was used to verify this hypothesis by Wang et al. [81]. Particles with known diameter were spread on the protective cover of the device in order to create artificial dark spots. The development of the dark spots was monitored with respect to time and particle diameter which led to the conclusion that formation of dark spots is due to airborne dust.

A number of studies used activated rate theory to investigate the permeation mechanism [82-84]. Tropsha et al. found out that activation energies of four different polymer substrates coated with SiO_2 by PECVD are identical suggesting the chemical interaction between water molecules and the SiO_2 structure [82].

3. *Measurement techniques*

Such low permeation rates require advanced measurement methods with very high sensitivity level. All the methods are based on the same principle where tested sample serves as a membrane between a “test gas” zone and a “sensor” or “detection” zone. The only difference is in the means of detecting and quantifying the gas which has penetrated through the membrane. Sensing and quantifying are based on either physical or chemical interaction of the sensing material with moisture. Typically used methods are mentioned below.

Most commonly and industrially approved are coulometric methods. A typical representative is the latest generation of MOCON Aquatran 2 WVTR measurement device which is able to detect moisture transmission rates down to $5x10^{-5}$ g/m^{2}day [85]. The disadvantage of the method is the quite high level of background leakage through the edge seal.

Another recently developed WVTR measurement system is Vacutran. Quantification, based on mass spectrometry and claiming sensitivity levels down to 10^{-6} g/m^{2}day [86]. The advantage of the tool is virtually zero background signal due to leakage because it uses deuterium oxide as a permeant. Another benefit of using mass spectrometry is the ability to measure permeability of the membrane with any gas, e.g. O_2, CO_2, etc. The downside of the method is very high cost of the equipment compared to other methods.

The calcium test is a measurement technique that is based on chemical conversion of metallic calcium into calcium hydroxide via reaction with water [87]. A thin layer of Ca deposited on glass is sealed with the barrier structure and exposed to predefined environmental conditions. Moisture penetrating inside oxidizes the Ca making it

transparent and conductive. Therefore, quantification is based either on measuring optical transmittance [88] or electrical conductivity of the film [89] as a function of time. A schematic illustration of the optical Ca-test is shown in figure 11. The great advantage of the method is that it gives an insight into the permeation mechanism. By looking at the sample with an optical microscope it is possible to spot local defects as well.

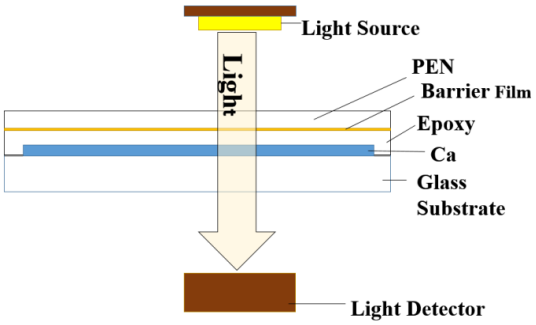

Figure 11. Calcium test scheme.

Another sensitive technique is the tritium diffusion test. The working principle is based on measurement of radioactive emission counts of tritiated water (HTO) permeating through the polymer (figure 12). The method possess very low theoretical detection limit but is not so common due to the hazardous nature of HTO [90-93].

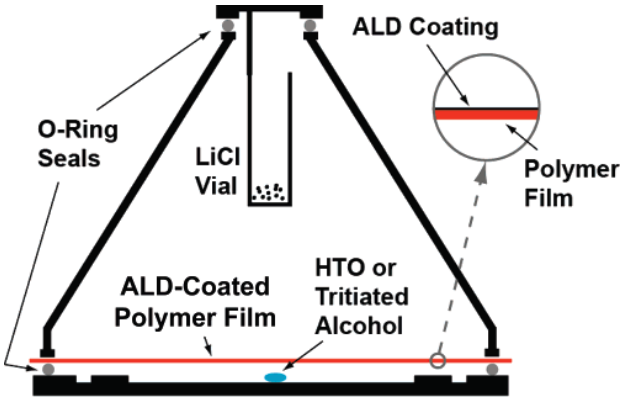

Figure 12. Drawing that represents HTO permeation test setup showing HTO source, polymer sample and vial with hygroscopic LiCl for HTO collection. Reprinted from [77].

Finally, the suitability of barrier layers for particular application can be non-arguably proven by simply encapsulating the device with the barrier coating. Respective

characteristics are being measured as a function of time to verify the level of protection. For example, for OLED devices measured parameters include luminance, current density, and degradation due to local defects. Encapsulation for photovoltaic devices is considered to be successful if the power conversion factor, fill factor and short-circuit current density do not change overtime [94, 95].

Despite the diversity of measurement methods and techniques, there is a fairly good agreement between them. Nisato et al. made a comparative study by measuring the same barrier structure using different methods, namely: Ca- test (CCD, optical and electrical); cavity ringdown spectroscopy; tuneable diode laser absorption spectroscopy; isotope marking mass spectroscopy and a coulometric test. Results of the comparison study are shown in figure 13.

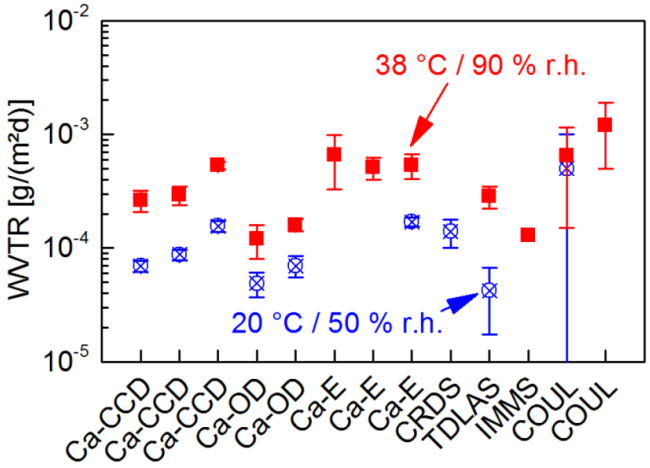

Figure 13. Comparison of WVTR measurement methods. Ca-CCD – calcium CCD test; Ca-OD – calcium optical test; Ca-E – calcium electrical test; CRDS – cavity ring-down spectroscopy; TDLAS – tuneable diode laser absorption spectroscopy; IMMS – isotope marking mass spectroscopy; COUL – coulometric. Reprinted from [92].

II. Experimental part

A. Spatial ALD system

ASTRaL began the development of an SALD prototype reactor in 2008. The first system was built as a test-bed to check the feasibility of the approach and acquire preliminary data before moving to the next step and scaling up the process. The system was built in conjunction with the Finnish ALD tool manufacturer Beneq Oy. In 2010, the reactor of the system was replaced with its second revision followed by development of a pilot roll-to-roll ALD system in 2012. The current section describes the construction of the main layout of the system and both revisions of the reactor.

1. General layout

The main components of the system are the vacuum chamber, precursor sources, filter unit and vacuum pump (figure 14). The system consists of two chambers: an outer stainless steel vacuum-tight cold wall vessel and an aluminum inner cylindrical shape reactor. The outer chamber contains the reactor heating system and gas supply lines. It plays an auxiliary role while the actual deposition takes place in the inner reactor. The construction of the inner reactor is discussed in the next sections.

The precursor source units comprise heated vessels with shut-off valves. These can be heated up to 100 °C to provide sufficient reagent pressure in case of low volatility precursors or high substrate rotation speed which will demand a higher vapour flow. The gas delivery lines are heated to create a temperature gradient to prevent precursor condensation in them. For controlling and adjustment of precursor flows, pneumatic valves and needle valves are installed. Carrier gas flows are adjusted by respective mass flow controllers.

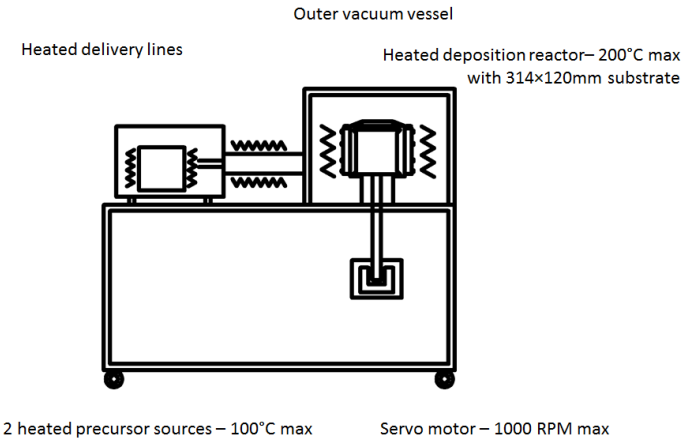

Figure 14. General layout of SALD tool by ASTRaL.

2. *Reactor description*

The core of the system is a cylindrical reactor which has four vertically aligned inlet slits for incoming gases (two for precursors and two for inert gas) and four similar outlet slits for outgoing gases (reaction products, excess of precursors) which are connected to the vacuum pump. These slits are arranged in the following sequence: precursor A inlet – pump out –N_2 inlet– pump out– precursor B inlet – pump out – N_2 inlet. The substrate is mounted on a 100 mm diameter rotating aluminum cylindrical drum with the surface to be coated facing the gas slits. The reaction vessel and the substrate holder form a narrow reaction chamber in the space between them. The spacing between the slits and rotating drum is 1mm and was chosen on the basis that on the one hand, small reactor volume would decrease the precursor consumption and make the gas separation more efficient; while on the other hand large spacing would make mechanical assembly easier because of the need to avoid any drum vibrations affecting the reactor volume and as a result the flow dynamics. Moreover, a large spacing gives more freedom in choosing the substrate thickness without affecting the process.

Schematic radial and axial cross-sections of the reactor and the arrangement of the inlets and outlets are depicted in Figure 15. The principle of operation is as follows: as the

drum rotates, the substrate is led through the various gas zones formed by continuous flows between respective precursor and exhaust slits – see Figure 15. The purge zones and exhaust lines serve to isolate the precursor zones so that no gas phase mixing occurs between the precursors. One rotation of the drum is equivalent to one cycle of the ALD process. Additional gas flows can be set from top and bottom to ensure precursor confinement and stop precursor leakage from the ends of the drum. The drum is rotated by a servo motor and the maximum rotation speed used was 250 rpm.

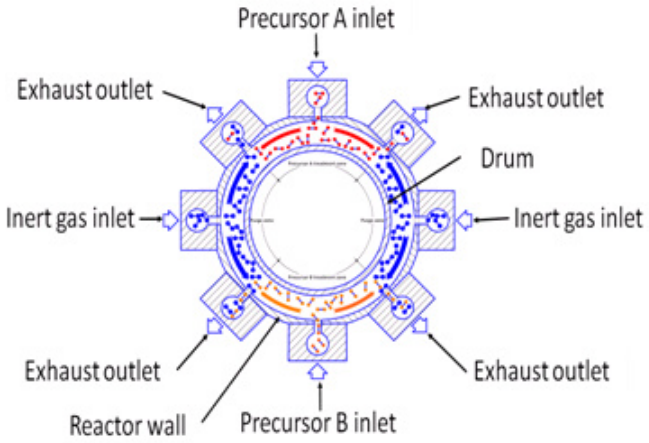

Figure 15. Reactor cross-section of SALD reactor (revision 1).

Promising results with the SALD reactor allowed further development. A new reactor was constructed such that it accommodated more inlet/exhaust slits with a new design that makes reagent separation more efficient. The arrangement of nozzles is depicted in figure 16. Constant precursor gas flow rate takes place between the central nozzle and the exhaust nozzles surrounding it. Additional separation between precursors is provided by inert gas counter flows from the sides of the nozzle arrangement. As can be seen from the picture one rotation of the drum provides sequential exposure of the substrate equivalent to 4 ALD cycles. The drum rotation speed dictates such important parameters as precursor dose and substrate residence time, which is defined here as the length of time that a point on the substrate remains within a particular precursor zone as it rotates. Table 1 shows the drum rotation speed values used in present studies and their relation to residence time and substrate linear speed. The gap between the drum and reactor wall was decreased to 0.5 mm.

Table 1 Drum rotation speed and related parameters used for film deposition

Drum rotation speed, min^{-1}	2	5	8	15	20	25	45	100
Substrate residence time, s	1.146	0.459	0.287	0.153	0.115	0.092	0.051	0.023
Linear speed, m/min	0.628	1.57	2.512	4.71	6.28	7.85	14.13	31.4

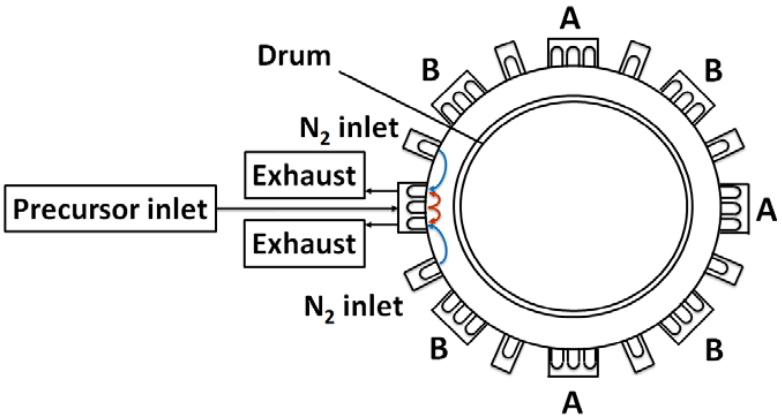

Figure 16. Cross-section view of SALD reactor (revision 2).

B. Roll-to-roll ALD system

This section describes the general layout and vacuum chamber design of the Beneq WCS500 coating system. The coating system is a result of a development work that was carried out on the smaller SALD system. The WCS500 was manufactured by Beneq Oy (Finland).

The system comprises a main vacuum chamber, where the actual coating process takes place, and auxiliary units such as chilling/heating unit, web handling control, precursor storage and delivery system, precursor neutralizing and filter system, and pumping unit. The main chamber accommodates web unwinding and rewinding reels, the main processing drum and coating head which are designed to handle a 500 mm wide web. The

vacuum chamber layout is schematically shown in figure 17. The main drum is 600 mm in diameter, made of stainless steel. The drum is temperature controlled by oil that circulates between the chamber and heating/chilling unit. The reactor features a pendulum-type coating head which is mounted beneath the drum and consists of 29 sections. Each section has a nozzle for reactive gas release and a surrounding exhaust slit.

These nozzles are additionally separated by inert gas curtains to prevent the unwanted spreading and intermixing of reagents. The gap between the coating head and the drum is set to 0.5 mm. The coating head arrangement is schematically shown in figure 18. Additional heating is provided by resistive heaters mounted beneath the coating head. The purpose of the pendulum motion is to increase the relative speed between the moving drum and the coating head allowing multiple passes of the coating head over the web. This enables film thicknesses in the tens of nm to be deposited in a single pass of the web through the coating system.

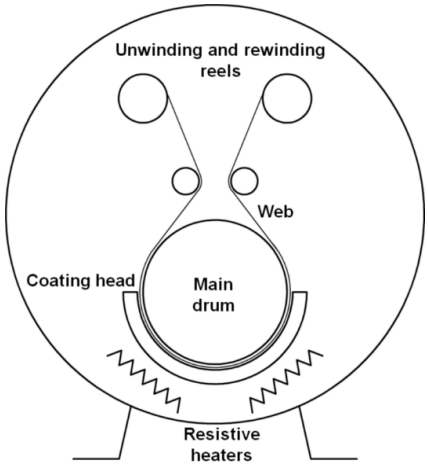

Figure 17. WCS 500 chamber layout.

The coating process is organized as follows: the web leaves the winding reel and moves towards the main drum. While the web is being guided over the drum, it is sequentially exposed to the precursor gas sections of the head. Each pair of sections provides one ALD cycle. As mentioned above, the pendulum motion of the head allows additional deposition cycles to be provided. The coating head is designed to travel 82mm in each direction providing 2 ALD cycles per one full swing. The system can also be operated

without using the intermediate guiding rollers between the winding and unwinding reels and the coating drum.

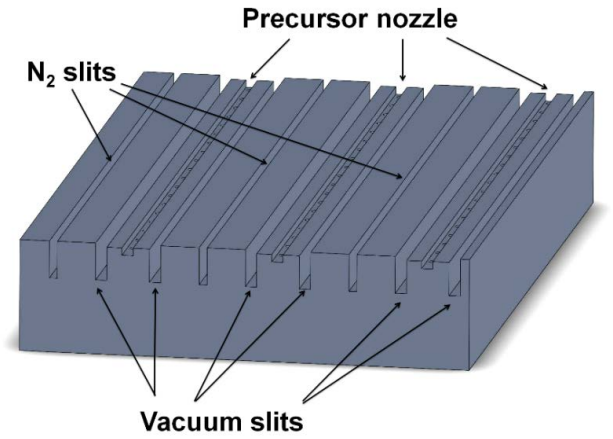

Figure 18. Fragment of coating head showing precursor inlets, exhaust and inert gas slits.

Substrate residence time is an important parameter that affects the process and growth rate to a great extent. It is defined as a time for which the substrate is exposed to one precursor vapour and during which actual gas-surface interaction occurs, that is, the time a point on the substrate surface spends within an individual precursor zone. In the present system it is determined by the web transport speed, the coating head oscillation speed and acceleration/deceleration of the coating head as it changes direction. This means that there will be a difference in the relative speed between the web and the coating head depending on the direction of the pendulum's swing. In the studies reported here, variations in the residence time due to this effect were neglected as the coating head speed is much greater than the web transport speed. Acceleration/deceleration times start to become significant at short residence times. This effect was taken into account and average residence time was used in the present studies. The number of cycles applied to the web is determined by the number of oscillations made by the head while the web is passing through the coating zone.

C. Materials and methods

The current section describes the materials that were used for deposition and process studies. Any variations are noted in the respective part of the Results section.

All depositions were carried out using 98% purity (TMA) delivered by Volatec (Finland). Deionised water with a conductivity of 0.056 uScm^{-1}was used as an oxidising precursor. Ozone was produced from 99.999% purity O_2 (Aga, Finland) by BMT 803N (BMT Messtechnik GmbH, Germany) ozone generator. Ozone concentration was measured by BMT 964 ozone analyzer (BMT Messtechnik GmbH, Germany). Nitrogen for the process was sourced either from bottles (99.999%, Aga, Finland) or from a liquid N_2 evaporation vessel (Aga, Finland). Helium (99.996%, Aga, Finland) was used for gas entrainment tests. Depositions for process studies were made on PET metallized with titanium and on ultrathin 50 um thick crystalline silicon. The purpose of metallization is to create a reflective layer that facilitates optical measurements. Barrier coatings were deposited straight on PEN polymer from Dupont Teijin Films. The particular polymer grade as well process conditions are noted in the respective chapter of the Results section.

A J.A. Woollam M2000FI spectroscopic ellipsometer was used to determine thickness and refractive index of the films. Measurements were carried out at 65, 70 and 75° of incident and reflected beam. A Cauchy model was used for fitting and extracting the thickness and refractive index data.

The WVTR of the Al_2O_3 coated films was measured by using the Aquatran Model 1G (Paper IV) and Aquatran Model 2G (Paper III) test module by MOCON (Minneapolis, MN, USA). In this method, the ALD coated side of a sample is sealed against a test cell by using high vacuum grease. The measurements were carried on at 38 °C/ 90% RH and the active test area of the sample was 50 cm^2.

An optical calcium test was used for evaluation of ultra-barrier levels of the WVTR. In this method, the evaluation of the WVTR is based on the change in transmission of white light through a semi-transparent metallic Ca film with transmission (T) around 10% [87]. It is

known that at low temperature, oxidation of Ca proceeds by reaction with H_2O according the complete reaction

$$Ca + 2H_2O \rightarrow Ca(OH)_2 + H_2 .$$

Ca-films about 60-80 nm thick were deposited on 6" round glass wafers used as substrates in a high vacuum system equipped with a cryo-pump. The Ca-film was deposited in 6 distinct and isolated areas covering about 40% of the total wafer area. Each individual area is between 7 and 20 cm^2 in size. Their distance from the edge ranges from 10 to 15 mm. The Ca film was then encapsulated in situ with a thin oxide film to avoid any initial deterioration by the following handling in atmosphere with residual moisture content. Previous experiments had shown that the oxide film was not a good barrier in accelerated testing at 85ºC/85% RH. Complete oxidation of Ca films protected with this oxide would occur in a few hours of exposure. The ALD barrier to be measured was then glued in a face-sealing configuration on top of the glass plate described above by using a proprietary epoxy adhesive with low WVTR. This configuration shown in figure 19 represents the best simulation for using the ALD barrier in a lamination approach.

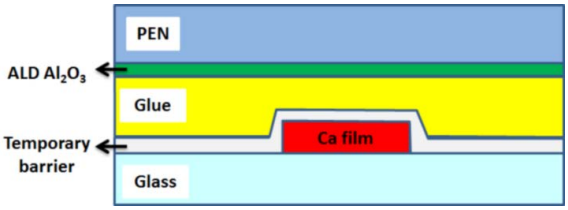

Figure 19. Calcium test setup.

The samples were subjected to accelerated testing at 40 °C/90% RH and 85 °C/85% RH. The change in transmission of the Ca film was monitored at the beginning of the lifetime test, and periodically, with a spectrometer, and the WVTR was calculated. Multiple points were acquired for each area with a spot size of 2-3 mm. In addition, optical observations in transmitted light were carried out to detect the early appearance of transparent pinholes that would indicate a localized failure that may have been below the lateral resolution by the spectrometer.

Optical transmission measurements were carried out using a Thermo Nicolet 500 UV-Vis spectrophotometer.

III. Results and discussion

A. Initial results on deposition behaviour with first revision of SALD reactor.

The current section describes the first results of the deposition behaviour and makes some comments on the approach that was implemented in the studies. It was very important to show that the process possesses ALD's distinctive hallmarks – self-limiting, linear and uniform growth rate.

1. Linearity and uniformity

Linear film growth is a feature of an ALD process when film thickness is strictly proportional to the number of deposition cycles. The film thickness was plotted against the number of cycles at rotational speeds of 20 and 50 rpm as shown in Figure 20. Regardless the rotation speed used for the experiments, the film thickness dependence exhibits straight lines with zero intercept.

In order to assess the uniformity of the ALD growth, film thickness was measured across the substrate in the direction perpendicular to substrate movement. Figure 21 shows the resulting profiles. The process provides uniform film growth at rotation speed up to 40 rpm (375 ms of residence time). However, at higher rotation speeds there is a clear deviation at the edge of the substrate. The reason for that could be the design of the reactor which has the same width of inlet and outlet slits leading to inefficient gas separation at the edges.

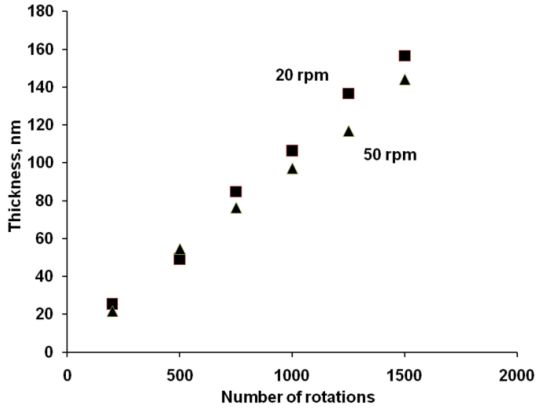

Figure 20. Film thickness as a function of the number of substrate rotations.

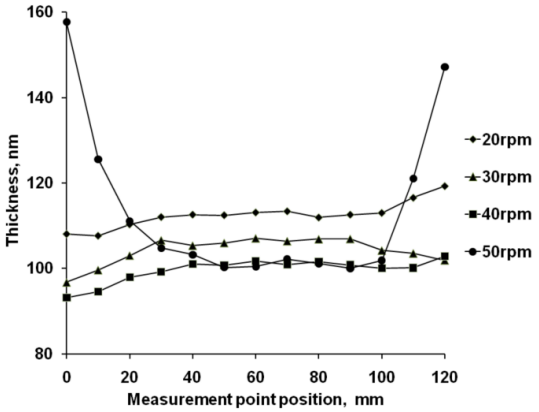

Figure 21. Film thickness as a function of position across the polymer sheet.

2. *Saturation behavior*

For conventional flow-through type ALD system self-limiting behavior can be shown by altering the amount of reagent delivered to the reactor and measuring the growth rate. In the SALD system, the ALD mechanism can be demonstrated by changing the time that the substrate is exposed to the precursor gas zone which has the effect of altering the precursor dose. In the first design of SALD reactor, the substrate residence time is estimated as the time it takes to travel one quarter sector of the reactor.

A series of runs was carried out to demonstrate saturation of the ALD growth rate. 1000 ALD cycles were applied to the substrate in the speed range of 10 to 250 rpm. The resulting saturation curve is shown in figure 22. It can be seen that the curve does not look like a typical ALD saturation curve that can be found in conventional studies. However, a saturation region that occurs at over 300 ms of residence time can be clearly distinguished. The growth rate exhibits a very gradual increase with the residence time that may indicate the presence of CVD growth. The gradual increase of deposition rate that is observed here is typical of the behaviour reported for the Al_2O_3 process in conventional ALD [97]. An abrupt drop of growth rate at residence times below 120 ms due to precursor starvation can be easily recognized as well. In between these regions (1 and 2), there remains a narrow region (3) with abnormally high growth rate values that has to be explained.

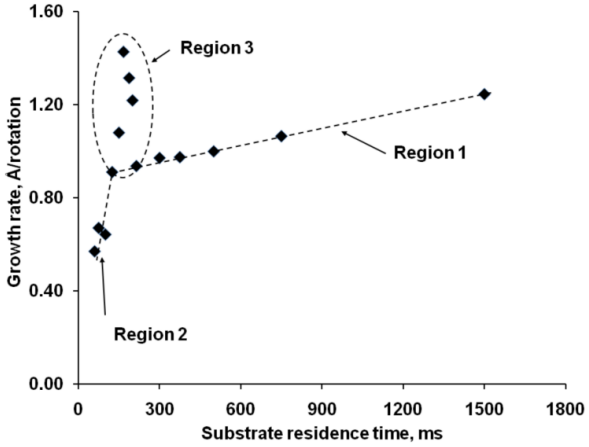

Figure 22. Growth rate per cycle as a function of substrate residence time for 1000 cycles deposition.

It was suggested that anomalous growth is an artifact attributed to gas entrainment effect. Gas entrainment occurs due to viscous friction caused by relative movement between the substrate and gas. This leads to formation of a near-surface boundary layer which in turn may serve as a means of precursor transfer between the zones. The width of the boundary layer and hence the amount of the gaseous reagent that is being dragged is inversely proportional to the square root of relative velocity. Once it arrives to the purging zone it is being disrupted by means of reagent diffusion out of the boundary layer into the N_2 flow. The amount of precursor removed from the boundary layer is proportional to residence

time and thus inversely proportional to substrate velocity. Therefore, we can speculate that there is a certain speed range where the boundary layer is too thick while the corresponding residence time is too short to remove the entire precursor. This situation is illustrated in figure 23. Overall, it will lead to precursor transfer and subsequent reaction with CVD type of growth.

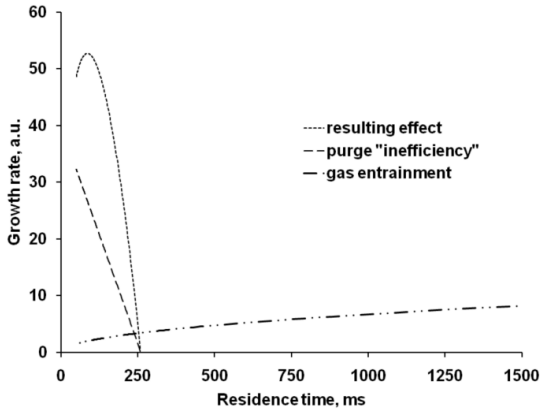

Figure 23. Illustration of factors contributing to anomalous deposition as a function of residence time. Note: purge inefficiency and gas entrainment effects are on arbitrary scales.

Therefore, if we sum all the factors contributing to film growth, specifically growth due to ALD, minor CVD factor and gas entrainment, it is possible that the resulting curve would look like experimental (figure 24). A detailed discussion on the phenomena can be found in the Results section of Paper I.

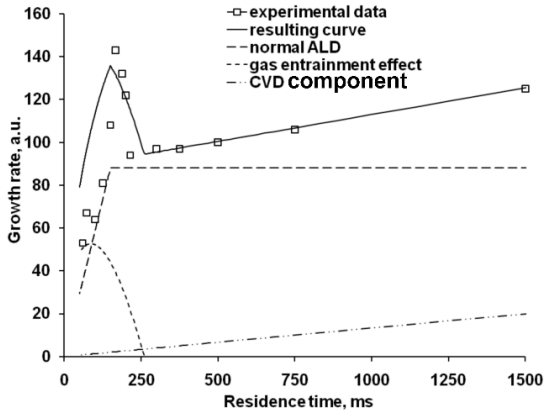

Figure 24. Contributing factors to the growth rate behaviour as a function of residence time: model results compared with measured results.

3. *He leak test*

To either prove or disprove the explanation of the growth anomaly, additional tests were carried out. Helium was employed as a tracing gas to gain a better understanding of the flow distribution and mass transfer in the gas boundary layer. A schematic view of the radial cross-section of the cylindrical reaction chamber indicating the helium injection and measurement ports is shown in figure 25. Helium, without any carrier gas mixture, was injected into the reactor via one precursor inlet with the same partial feeding pressure that was used for the ALD precursor (0.1 mbar). A helium leak detector Smart Test HTL 560 (Pfeiffer Vacuum) was connected via a needle valve to an exhaust port. The helium leak rate was measured at each exhaust port as a function of substrate rotation speed and purging flow. The signal was recorded as an average during a 5 minutes rotation session. The background signal was recorded between each session to avoid any mistake due to background concentration change. Tests were carried at a chamber temperature of 100 °C to reproduce the typical situation during deposition. Measurements were made with rotation speed up to 900 rpm.

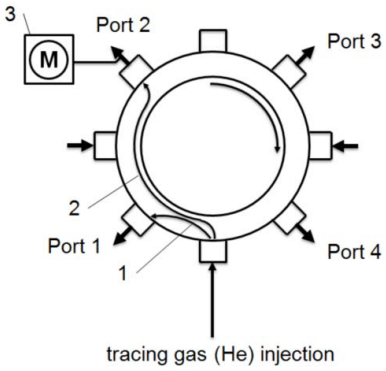

Figure 25. He injection scheme. 1 - main gas flow; 2 - additional gas flow provided by gas entrainment; 3 - leak detector.

The rate of helium flow into the detector mounted on port 1 (immediately adjacent to the He inlet port in the direction of substrate movement – see figure 25) as a function of rotation speed for three different purge gas flow rates is shown in figure 26. As rotation speed increases, the He signal increases in a sub-linear manner.

This dependence can be explained by considering the following factors: (i) constant leak due to He diffusion into the reactor volume; (ii) He leak due to boundary layer effects. While the contribution of first factor is clear, the second factor needs further clarification. As has been mentioned in the previous section, the amount of reagent trapped in the boundary layer depends on its thickness and this is inversely proportional to the square root of the relative velocity. At the same time, the amount of helium that reaches port 1 per unit of time is proportional to the substrate velocity. Thus, the final dependence should follow

$$Q_1 = A + B\sqrt{v} \tag{3}$$

where Q_1 – He signal at port 1, mbar.l/s; v – substrate velocity; A and B are constants for a given speed. A refers to the constant leakage.

As can be seen from figure 26, the model shows a fairly good fit with the experimental data. A detailed discussion and fitting parameters can be found in Paper II.

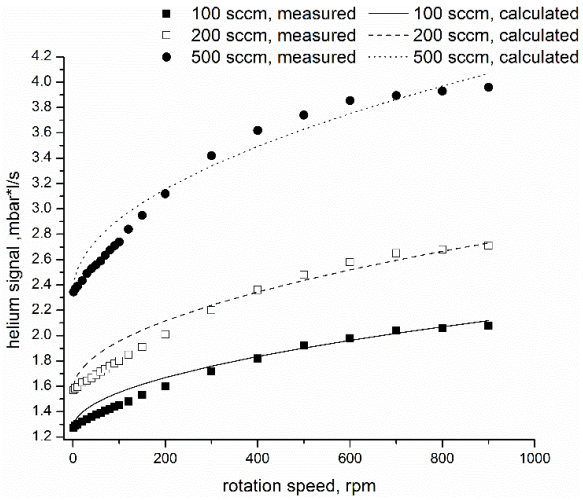

Figure 26. Helium leak rate at port 1 as a function of rotation speed and purge flow.

The helium signal measured at port 2 is depicted in figure 27. This dependence can be understood by considering the following processes. As has been just discussed, the amount of helium that reaches the purging zone per unit of time is proportional to the square root of the substrate velocity. In the purging zone He is being removed from the boundary layer by means of diffusion described by Fick's law. Based on the additional assumption that He has a linear distribution in a boundary layer with zero on its edge and a maximum near the substrate surface, the overall signal at port 2 should be described by following equation:

$$Q_2 = \left[A + B\sqrt{v}\right] \times \left[G_o \exp(-Evt) + K\right] \tag{4}$$

where E and K are the constants.

The model exhibits fairly good fitting with experimental results (figure 27).

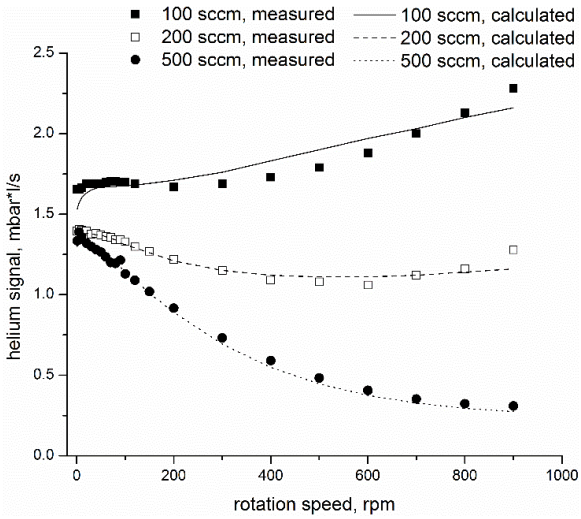

Figure 27. Helium leak rate at port 2 as a function of rotation speed and purge flow.

From the deposition rate date of figure 22, the growth rate anomaly occurs in the rotation speed range of 70-120 rpm. As can be seen from the simulations in figure 27, there is no behaviour at these rotation speeds which could give rise to the anomaly. Therefore, we conclude that gas entrainment is not likely to be the reason for it.

Another hypothesis that explains the abnormal process behaviour is excess of water adsorption on the surface that cannot be eliminated during the purge step. Thus, it is possible that the adsorbed water may be transferred into the TMA zone if the purge time is too short for the complete removal of any excess adsorbed water. When the surface with active reaction sites is exposed to water vapour, the bonding between the surface and the water takes place in two stages: (i) H_2O molecules react with the surface and terminate the reactive sites forming a monolayer of chemically bonded hydroxyl groups. This is the desired effect. (ii) Once the surface is saturated with hydroxyl groups additional water molecules can physisorb to the surface forming a multilayer of adsorbed water. This is the undesired effect. In the former case, the sticking coefficient of water is ~1 and it can be assumed that any water molecule arriving at the surface will undergo a

reaction. In the latter case, the sticking coefficient will be <1. If this adsorbed water is not removed in the purge zone, it will cause extra growth when the substrate arrives in the TMA zone.

This phenomenon was modelled with derivation that can be found in the Results section of Paper II. The excess growth rate was modeled by estimating the adsorption and desorption rates. Assuming that both processes are thermally activated, the overall anomalous growth effect is given by

$$\begin{aligned} \Delta G &= 0 \ \text{ for } \ t < t_m \\ &= bIS\tau\left(1-\exp\left(-\frac{t}{\tau}\right)\right)\exp\left(-\frac{t}{\tau}\right) \text{for } \ t > t_m \end{aligned} \tag{5}$$

where I is the impingement rate of water molecules; S is the sticking coefficient; τ, b are constants; t – residence time; t_m – the time taken to create an OH monolayer.

$IS\tau\left(1-\exp\left(-\frac{t}{\tau}\right)\right)$ describes the water accumulation on the surface while the substrate is passing the precursor zone.

$b\exp\left(-\frac{t}{\tau}\right)$ describes the desorption process that takes place in the purging zone.

It is clear that if the abovementioned hypothesis is right, a varying deposition temperature should have an effect on the presence of growth artifacts. Thus, in order to verify this, an additional series of depositions was performed at 110 and 150 °C reactor temperature. The results are shown in figure 28. Noticeably, increasing the temperature by only 10 °C removes the excessive growth rate. Figure 28 also shows modeled curves calculated by using Eq. 5 assuming an activation energy of 0.69 eV [98]. While the model exhibits a good fit, it is not intended to be an accurate simulation of the deposition rate but it is intended to show that a simple physical model of the processes going on in the continuous ALD system can reproduce the anomalies which are observed in the growth rate during deposition.

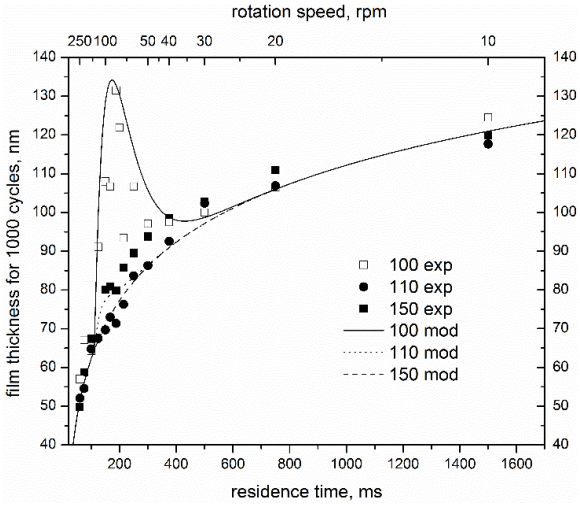

Figure 28. Growth rate as a function of residence time at 100 – 150 °C temperature range (experimental and modeled data).

B. Comparison of ozone and water based processes

There are several ways to solve the problem mentioned in the last section. One would be to extend the purging zone that would allow more time for water molecules to desorb. But as the reactor geometry is usually fixed it is not practically possible to independently change the purge times without changing precursor dose. To do so would require physically changing the purging zone width which is constrained by the reactor size. The substrate speed can be decreased to give more time for water molecules to desorb but that would seriously impact on the process throughput.

Another way to eliminate the water adsorption problem is to use a different oxidizing agent such as ozone or the excited atoms and radicals produced by oxygen plasma. Ozone has been widely used for aluminum oxide ALD processes and has been found to be beneficial for some applications. For example, substitution of water with ozone results in better performance of Al_2O_3 used as a dielectric [99] and in lower impurity levels [100].

Another interesting and important question, especially considering future industrial use of the technology is the ability of oxidizers to produce superior films at the highest possible production rates. The current section is dedicated to a direct comparison between the characteristics of water and ozone as oxygen sources for the Al_2O_3 ALD process using a Spatial ALD reactor. The results described in current section were obtained using the second revision of the SALD reactor. Details on deposition conditions can be found in the Experimental part of Paper III.

1. *Reagent Concentration dependence*

Before comparing the two processes it is essential to study their behaviour as a function of reagent dosage. To do that, a series of runs was performed. Growth rate behaviour was studied as a function of residence time (0.023 – 0.469 s) and precursor mass flows (18.8 - 353 mg/min of TMA; 21.6 -248 mg/min of H_2O).

The resulting saturation curves are shown in figure 29. As expected, the curves are displaced upwards with increasing flow rate until it reaches 160 mg/min of TMA and 176 mg/min for H_2O (series D to B). Doubling the flow rates results in negligible further increase of growth rate (series A).

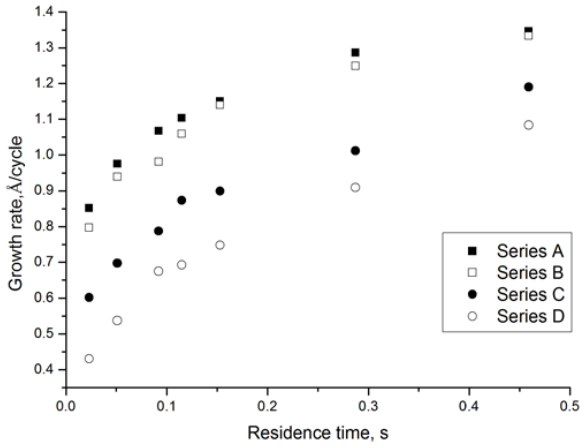

Figure 29. Variation of growth rate as a function of substrate residence time for Al_2O_3 films grown at 120°C of reactor temperature and precursor mass flows: A - 350 mg/min of TMA, 250 mg/min of H_2O; B - 160 mg/min of TMA, 175 mg/min of H_2O; C - 40 mg/min of TMA, 40 mg/min of H_2O; D - 20 mg/min of TMA, 20 mg/min of H_2O.

Analysing the saturation curve the following conclusion can be drawn: there is negligible variation of the growth rate at long residence times and high precursor dosages, which confirms the ALD nature of the process. The growth rate value of 0.13 nm/cycle is within the values obtained for Al_2O_3 ALD process at this temperature; from a practical point of view, the part of the curve at lower residence times is the region of interest as for high production yields it is important obtain highest possible growth rates at possibly shortest residence time. A fairly short residence time of 150 ms provides 0.11 nm/cycle for the growth rate while an extremely short residence time of 23 ms results in a growth rate of 0.085 nm/cycle.

The variation of the refractive index shown in figure 30 suggests that the film density reaches stable values at 150 ms of residence time. The lower refractive index values at shorter residence times indicate a poorer film quality.

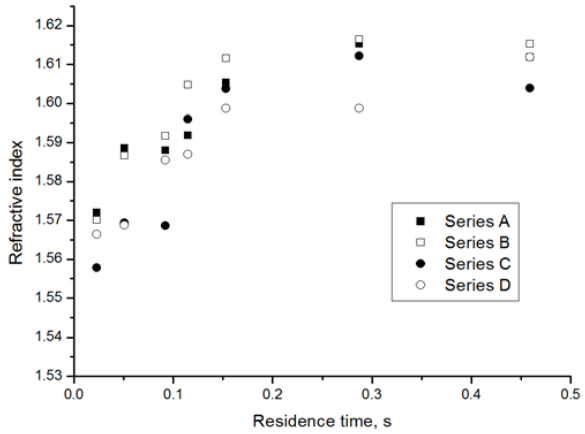

Figure 30. Variation of the refractive index as a function of substrate residence time for Al_2O_3 films grown at 120 °C reactor temperature and precursor mass flows: A - 350 mg/min of TMA, 250 mg/min of H_2O; B - 160 mg/min of TMA, 175 mg/min of H_2O; C - 40 mg/min of TMA, 40 mg/min of H_2O; D - 20 mg/min of TMA, 20 mg/min of H_2O.

The same approach was applied to study the TMA+ O_3 process. Ozone mass flows of 40 and 60 mg/min of O_3 were applied while the TMA flow was fixed at 160 mg/min. Residence time ranged between 0.023 – 1.146 s. Figure 31 shows the resulting saturation curves.

Both ozone mass flow rates provide almost identical growth rate behaviour except for the long residence time region where the growth rate is slightly higher if 60 mg/min of O_3 is used. Generally, it can be concluded that these dosages are sufficient for the process since any further increase of the O_3 flow rate will not benefit the process performance.

The refractive index exhibits an essentially similar behaviour to that observed for growth rate. In the saturated region it exhibits values in the range from 1.575 to 1.590 and drops down to 1.545 for residence times lower than 200 ms.

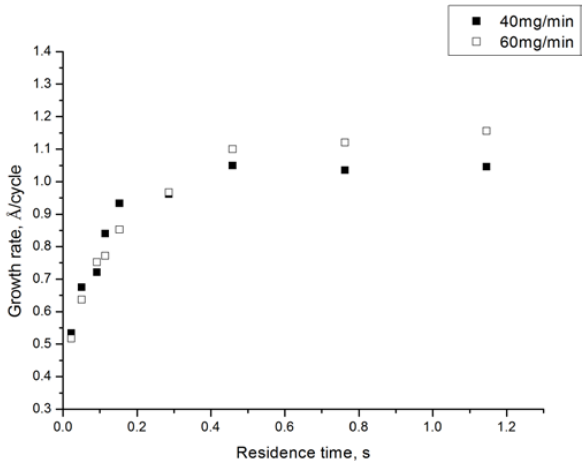

Figure 31. Variation of growth rate as a function of substrate residence time for Al_2O_3 films grown using TMA and O_3 at 120°C of reactor temperature.

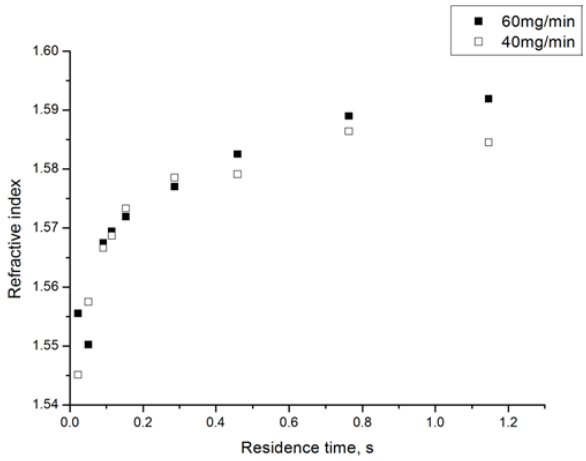

Figure 32. Variation of refractive index as a function of substrate residence time for Al_2O_3 films grown using TMA and O_3 at 120°C of reactor temperature.

The film density was estimated using Lorentz-Lorenz equation:

$$\frac{n^2-1}{n^2+2}=\frac{N_A\rho\alpha}{3M\varepsilon_o} \tag{6}$$

where n is the refractive index, N_A is Avogadro's number, M is the molar mass, ρ is the density and α is the mean molecular polarizability [101]. This gives 2.85 and 2.77 g/cm^3

for the density of films grown using water and ozone, respectively, assuming an electronic polarizability of 4.922×10^{-24} cm^3 [102].

The Specific Precursor Dosage (SPD, mmol/m^2cycle) was introduced as an additional parameter that facilitates process understanding and process transfer between different systems with similar working principles and geometry. The parameter was calculated using the following formula:

$$SPD = \frac{F}{4MSR^2} \quad (7)$$

where F is precursor mass flow, g/min; M is respective molar mass, g/mole; S is substrate area (0.031 m^2); R is the drum rotation speed, min^{-1}.

Figure 33, 34, and 35 show the growth rate per cycle (GPC) and refractive index (RI) for TMA, H_2O and O_3 respectively. Saturation behavior is observed for all three precursors. An SPD of 0.042 mmol/m^2cycle is found to be critical for TMA with a respective growth rate of 1.1 Å/cycle. An abrupt drop of GPC and RI is observed if SPD is applied below the critical value. TMA+H_2O requires 0.2 mmol/m^2cycle of water to be applied to the surface while, for the O_3 process, critical SPD is half this value (0.1 mmol/m^2cycle).

The equation for the Redlich-Peterson Isotherm (RPI) was used to fit the results [103].

$$Q_e = \frac{Q_{max} K_{RP} C_e}{1 + K_{RP} C_e^{n_{RP}}} \quad (8)$$

where Q_e is amount of chemisorbed material mole/m^2, Q_{max} is maximum surface capacity, mole/m^2; K_{RP} and n_{RP} are the RPI constants; C_e –is the equilibrium concentration (in the present case equal to SPD), in mole/m^2.

The experimental amount of adsorbed material Q_e was calculated on the assumption that growth rate is proportional to the surface coverage.

$$Q_e = \frac{Q_{max} GPC}{GPC_{max}} \quad (9)$$

where GPC and GPC_{max} are the equilibrium and maximum growth rates, respectively.

The solid line curves in figure 33a, 34a and 35a show modelled data that were calculated using the RPI equation. The model exhibits a good fit with a correlation coefficient of 0.98 for TMA and 0.96 for water and ozone. All three curves were fitted with a power

exponent n_{RP} of 0.9 which suggest strong saturation behaviour and the absence of uncontrolled condensation. The n_{RP} value of one means that process follows ideal case described by Langmuir equation while a zero n_{RP} value turns the RPI equation into a linear dependence which means condensation of the precursor on the substrate surface.

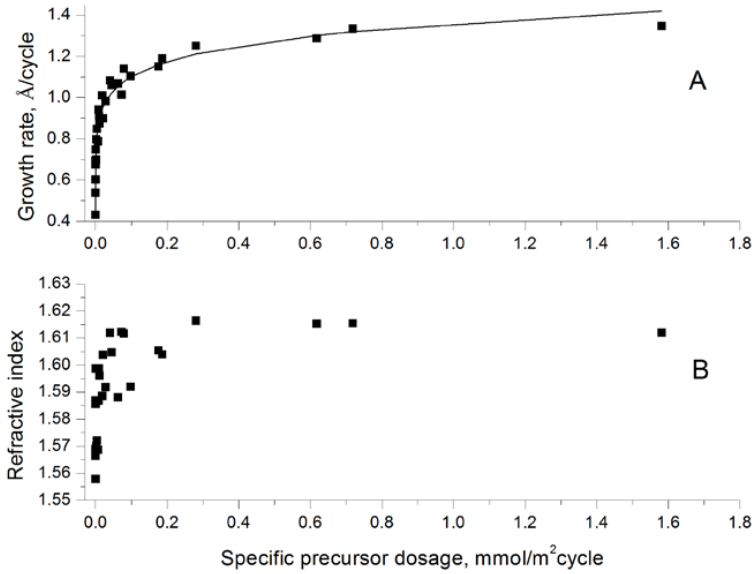

Figure 33. Variation of growth rate (A) and refractive index (B) as a function of applied TMA dosage for Al_2O_3 films grown at 120 °C of reactor temperature, and model fitting using RPI constant n_{RP}=0.90, correlation coefficient R=0.98. Squared marks – experimental data; solid line – model fitting.

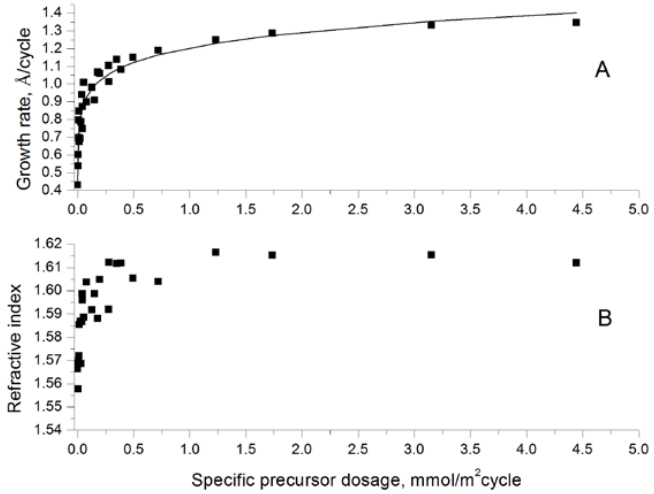

Figure 34. Variation of growth rate (A) and refractive index (B) as a function of the applied H_2O dosage for Al_2O_3 films grown at 120 °C of reactor temperature, and model fitting using RPI constant n_{RP}=0.90, correlation coefficient R=0.96. Squared marks – experimental data; solid line – model fitting.

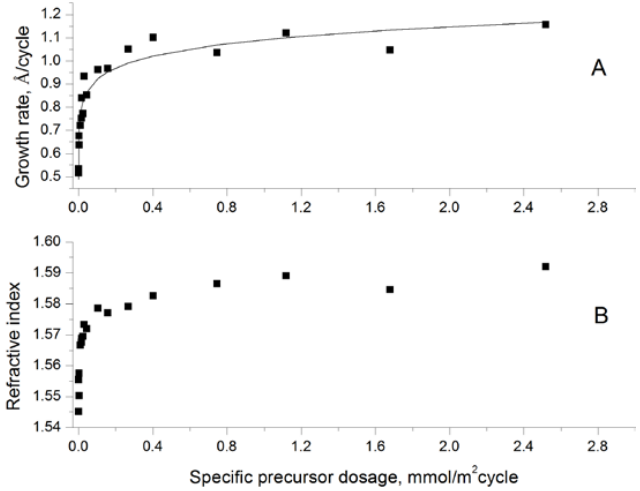

Figure 35. Variation of growth rate (A) and refractive index (B) as a function of applied O_3 dosage for Al_2O_3 films grown at 120 °C of reactor temperature, and model fitting using: RPI constant n_{RP}=0.93, correlation coefficient R=0.96. Squared marks – experimental data; solid line – model fitting.

2. *Temperature dependence*

Changing the process temperature may affect the process and film quality in multiple ways including: (i) growth rate change; (ii) film properties; (iii) process kinetics; (iv) undesirable artefacts which may appear such as excessive growth rates at low temperatures.

Figure 36 shows saturation curves that were built in the 100 – 140 °C temperature range. A noticeable change of growth rate was observed at 100 °C deposition temperature. Lower reactor temperatures result in lower growth rates at short residence time while depositions at substrate speeds faster than 15 rpm (150 ms of residence time) gives sharp increase of growth rate and non-uniform growth rate. This effect was discussed in previous sections. In turn, replacement of water with ozone completely changes the process behaviour at temperatures lower than 100 °C. Figure 37 shows the results of

TMA+O_3 deposition runs made in the 60 – 120 °C temperature range. Generally, ozone as an oxidant provides a much more robust process and more repeatable results. It is notable that the O_3 process at 60 °C exhibits slightly higher growth rate values than higher temperatures. This may happen because of water formation as a by-product in the oxidation step and its subsequent adsorption on the substrate surface [100].

The temperature dependence of the refractive index for H_2O and O_3 oxidation chemistry are shown in figure 38 and 39, respectively. The refractive index of the films decreases with short residence times and low temperatures indicating a lower density and possibly poorer moisture barrier properties.

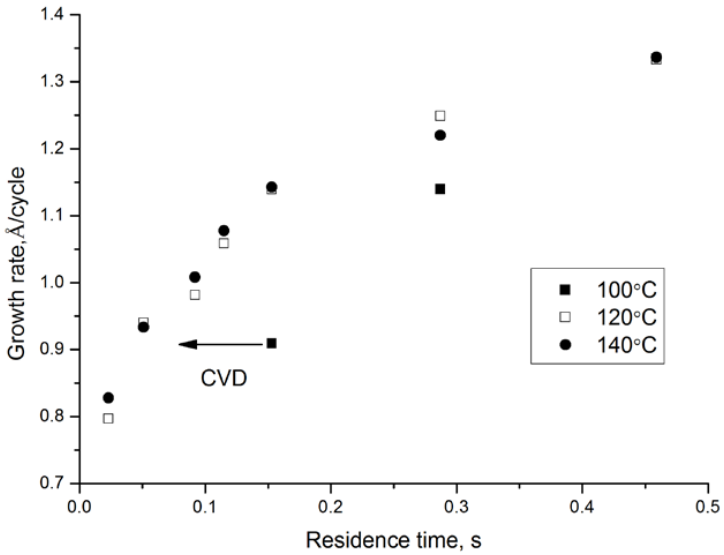

Figure 36. Growth rate as a function of residence for Al_2O_3 (TMA+H_2O) films grown at a temperature range of 100 °C – 140 °C. Data points of 100 °C series at shorter residence are not shown due to a harsh CVD effect and uneven film deposition.

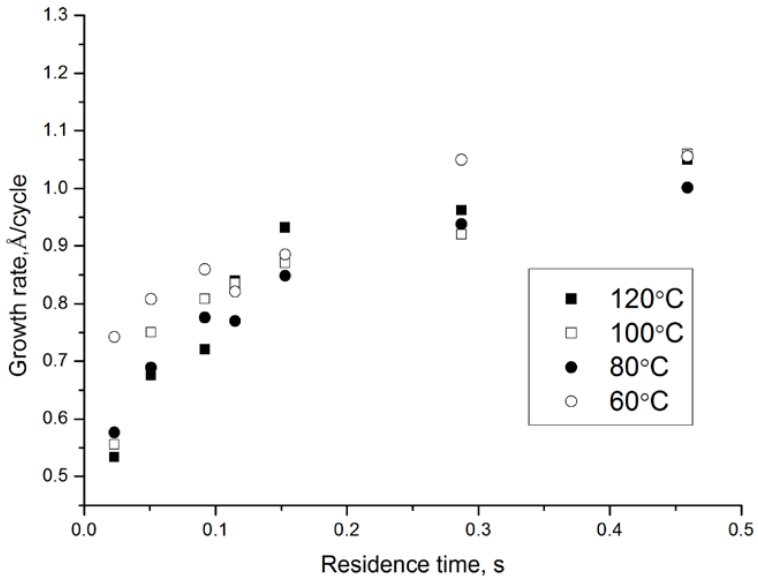

Figure 37. Growth rate as a function of residence for Al_2O_3 (TMA+O_3) films grown at a temperature range of 60 °C – 120 °C.

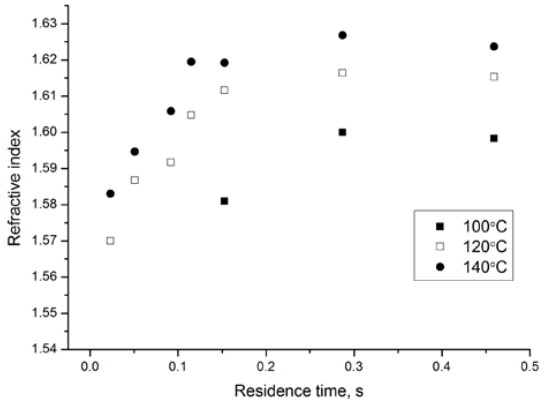

Figure 38. Refractive index as a function of residence for Al_2O_3 (TMA+ H_2O) films grown at a temperature range of 100 °C – 140 °C.

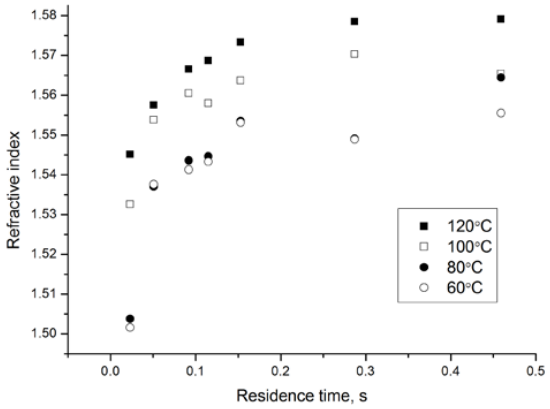

Figure 39. Refractive index as a function of residence for Al_2O_3 (TMA+O_3) films grown at a temperature range of 60 °C – 120 °C.

3. *Water vapour transmission measurements*

To test the moisture barrier performance of the coatings, 20 nm thick Al_2O_3 films were grown on PEN Teonex Q65FA polymer foils. Specific substrate rotation speeds and deposition temperatures were chosen to test favourable, moderate and non-favourable conditions. Table 2 and 3 summarize the experimental parameters and results of water vapour transmission rate measurements for the water and O_3 based processes, respectively.

Table 2 Water vapour transmission rate of 20 nm of Al_2O_3 deposited on PEN Teonex using TMA and H_2O as precursors, in mg/m^{2}day.

T, °C	100 rpm	20rpm	5rpm
120	3.76	0.41	0.64
100	NA	0.70	<0.05*

*Sensitivity level of MOCON Aquatran model 2

Table 3 Water vapour transmission rate of 20nm of Al_2O_3 deposited on PEN Teonex using TMA and O_3 as precursors, in mg/m^{2}day.

T, °C	100 rpm	20rpm	5rpm
120	0.68	0.33	0.40
100	2.39	0.56	0.64
80	64.38	0.7	0.65
60	1177	2.53	0.38

As expected, favourable coating conditions yield better results and lower WVTR values. The high temperature run at substrate rotation speeds up to 20 rpm provides good quality coatings with WVTR level of 10^{-4} g/m^{2}day. Films with lowest WVTR of $5x10^{-5}$ g/m^{2}day were obtained at 100 rpm and 100 °C using water as an oxidant. In turn, the ozone based process gave good results at temperatures ≤100 °C where the water based process fails completely. The use of ozone helps to achieve excellent barrier properties for films coated at 5 and 20 rpm through the entire temperature range. Very low WVTR values of $0.68x10^{-3}$ g/m^{2}day were obtained even at 100 rpm substrate speed. However, the film quality deteriorated at lower temperatures for high speed runs – 100 rpm and 60 °C does not result in any improvement of the WVTR compared with the bare polymer.

C. Roll-to-roll ALD

As has been mentioned in the Introduction section, the final aim of the research project was scaling up the SALD process in order to increase its through-put compared to conventional ALD. Therefore, the implementation of SALD into the roll-to-roll coating mode is a logical and obvious continuation of technology development. A roll-to-roll web coating system was developed and manufactured in conjunction with Beneq Oy (Finland). All tests and process development were carried out in ASTRaL, Lappeenranta University of Technology, Mikkeli, Finland.

1. Basic process studies

The current section describes initial test results that were acquired with a roll-to-roll ALD system. Process conditions are outlined in the Materials and Process section of Paper IV.

In the first place, it is essential to check the growth mechanism when establishing a new process. A series of depositions was carried out using residence times in the range of 49 – 609 ms, corresponding to 0.4–0.02 m/s of coating head speed. The parameters used for the tests are shown in Table 4.

Table 4 Deposition parameters for building saturation curves.

Coating head speed, m/s	Residence time, ms	Web handling speed, m/min	ALD cycles	Growth rate, Å/cycle
0.02	609	0.05	580[a]	1.10
0.03	410	0.044	500	1.06
0.06	211	0.059	700	0.81
0.1	132	0.083	800	0.75
0.2	75	0.117	1000	0.59
0.4	49	0.119	1500	0.494

[a] Web sample was guided 2 times through the coating zone to achieve a large enough number of cycles for easy film thickness measurement.

The resulting saturation curve is shown in figure 40. The curve shows the dependence of the growth rate on residence time.

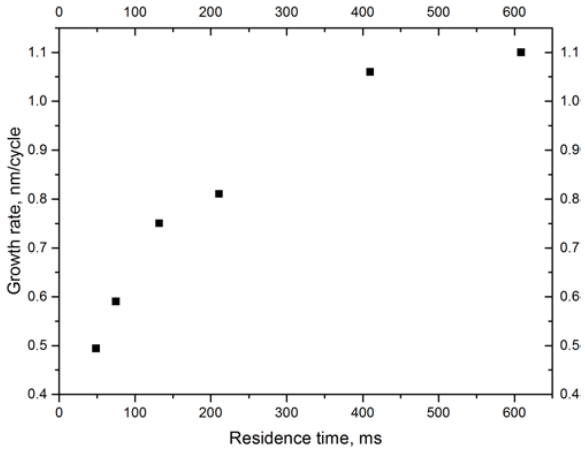

Figure 40. Al_2O_3 growth rate as a function of residence time. Films were grown at 105°C process temperature and 5 l/min of N_2 carrier for each precursor containing 0.6% of TMA and 11% water (volume fraction).

From the graph it can be seen that growth rate stabilizes at 410 ms of residence time or 0.03 m/s of coating head speed. The respective growth rate is 1.1 Å/cycle which is in agreement with previous results [Paper I, III] and conventional ALD studies [21].
It is important to verify the growth rate uniformity, especially when using wide substrates. Deviation of the thickness profile could mean flow distribution imperfections. Extra growth rate would mean a local CVD effect and lower growth rate could mean insufficient precursor flow. 70 nm of Al_2O_3 was deposited on Ti coated web and the thickness profile was measured by spectroscopic ellipsometry. An image of the sample is shown in figure 41. Spectroscopic ellipsometry confirmed uniform coverage with ±5% thickness deviation across the substrate width.

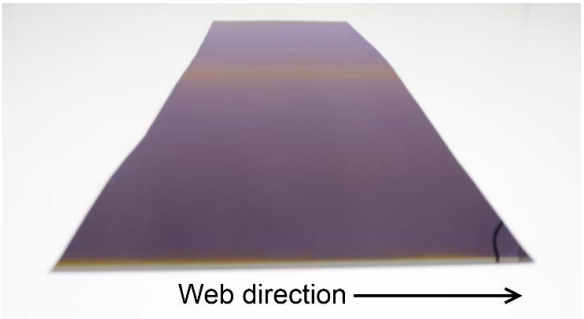

Figure 41. Image of a section of Ti metalized PET substrate coated with 70 nm of Al_2O_3.

2. *Barrier properties*

Finally, the barrier performance of the coating was assessed in order to verify its quality. 20 nm of Al_2O_3 were deposited on PEN OPTFINE® (125 µm thickness) using range of coating head speeds specified in Table 5. It is important to note that the sample for WVTR measurements was cut off before it reached the rewinding reel to avoid possible mechanical damage to the film during rewinding.

Table 5 Deposition parameters for 20 nm Al_2O_3 coatings on PEN.

Coating head speed, m/s	Residence time, ms	Growth rate, Å/cycle	AALD cycles	Web speed, m/min	WVTR, g/m^2 day	SPD TMA dosage mg/m^2 cycle
0.4	49	0.494	405	0.44	0.01043	1.12
0.2	75	0.59	339	0.35	0.00188	1.70
0.1	132	0.75	267	0.25	<0.0005	3.01
0.06	211	0.81	247	0.17	<0.0005	4.80
0.03	410	1.06	189	0.11	<0.0005	9.33

Figure 42 shows the WVTR data plotted against residence time. Excellent barrier properties were obtained for samples deposited using long and moderately short residence times (400 – 132 ms). The measured WVTR values were below the sensitivity level of the MOCON Aquatran Model 1 system. Shortening the residence time leads to a gradual increase in moisture transmission rate up to 10^{-2} g/m^{2}day. A residence time of 132 ms corresponds to an SPD of ~3 mg/m^2 or 0.042 mmol/m^{2}cycle which was found to be critical for the SALD process [Paper III].

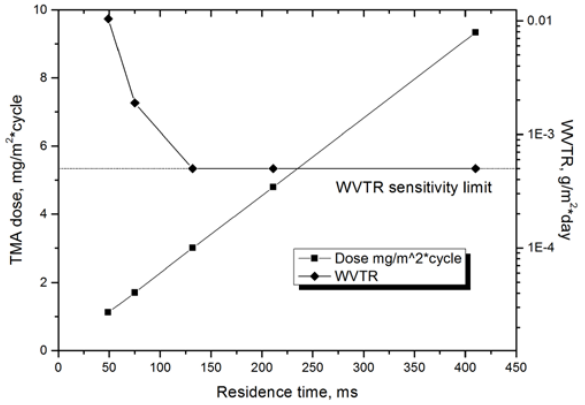

Figure 42. WVTR data and respective specific precursor dosage as a function of residence time.

To overcome the sensitivity limitation of the Aquatran system, a Ca test was employed to measure WVTR values of the samples. For that purpose, Ca/Al_2O_3/PEN structures were produced as described in the Experimental section. 20 nm of Al_2O_3 were deposited at a coating head speed of 0.1 m/s and 0.25 m/min of web speed.

Figure 43 shows an image of the Ca test setup. The encapsulated area is marked with a blue square and therefore only parts of the sample marked with “A” and “B” were considered for the trials. The samples were placed into a climate chamber at 40 °C/90% RH initially for 185 hours. The absence of pinholes and lack of change in the optical transmission of the samples allowed the use of harsher conditions and continuation of the test for another 800 hours at 85 °C/85% RH.

Figure 44 shows images of the sample over time: (a) after 185 hours at 40 °C/90% RH; (b) after 470 hours at 85 °C/85% RH; (c) after 800 hours at 85 °C/85% RH. No change in optical density was observed for the sample throughout the test. At the same time, oxidation can be clearly seen on non-encapsulated areas. However, some oxidation occurs at the edge areas of the sample “A” and “B” (figure 43) due to lateral penetration of moisture through the sealant.

Additionally, the absence of degradation due to local defects in the barrier film was confirmed by optical microscopy. The estimated WVTR is ~3 x 10^{-5} g/m^2day at 38 °C/90%

RH and ~5 x 10^{-6} g/m^2day at 20 °C/50% RH. These figures confirm the superior barrier properties of the coatings.

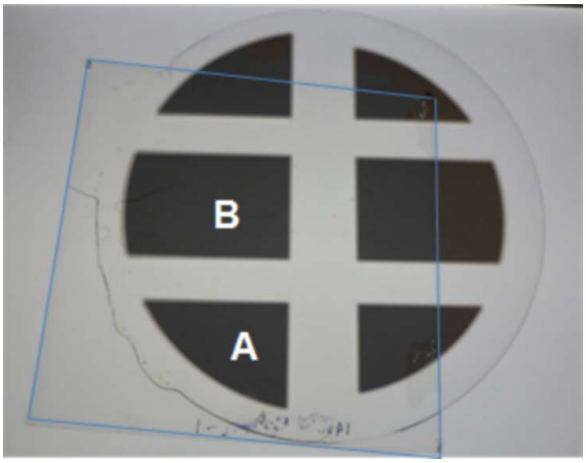

Figure 43. Partially laminated Ca-test wafer. The size of the barrier foil is shown by the overlapped blue contour. Only areas A and B were considered in the WVTR evaluation because they were completely covered with the ALD barrier.

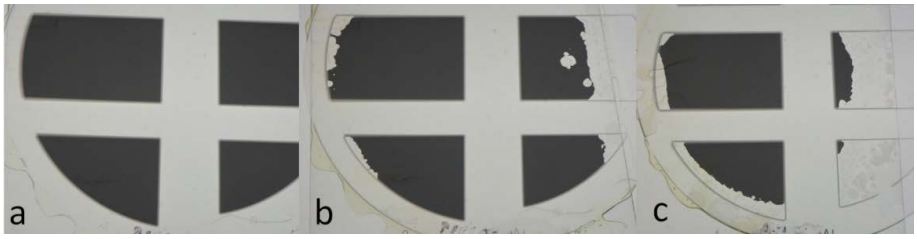

Figure 44. Samples subjected to accelerated Ca test: a) after 185 hours at 40 °C/90% RH; b) 468 hours at 85 °C/85% RH; c) 800 hours at 85 °C/85% RH.

IV. Conclusions

The aim of the present studies was to increase the production rate of the ALD process by implementing the SALD concept. For this purpose a prototype system was built in order to test the feasibility of the SALD approach and to study the basic properties of the process. The development work was done using TMA+H_2O chemistry. It was demonstrated that thin film deposition based on the SALD approach is possible and inherits all the basic properties of the ALD process. The growth rate per cycle of 0.1 nm is similar to batch ALD for Al_2O_3 process. ALD's hallmarks such as self-limiting and linear growth rate were demonstrated as well.

Nevertheless, the process possesses some artefact such as an extra growth rate at certain rotation speeds of the substrate. In relation to this question, such effects as gas entrainment and excessive water physisorption were studied. Flow distribution in the reaction chamber was studied by employing He as a tracing gas. Studies revealed that there is formation of a near-surface boundary layer which is a means of transport of gaseous precursors between the zones that can lead to CVD extra growth. Nevertheless, this occurs at rotation speeds much greater than were used for actual deposition. The effect of excessive water adsorption on the substrate was modelled. It was shown that due to low deposition temperature and slow desorption rate, the presence of extra water on the surface leads to anomalous growth rate values and non-uniform deposition. Both model and experiments confirm that deposition temperatures above 100 °C should be used in order to avoid this effect.

Additionally to water, ozone was evaluated as an alternative oxidizer. The kinetics of both chemistries were directly compared and evaluated. The influence of reactor temperature, residence time and precursor flows on the deposition process were investigated. Using water as an oxidizer helps to achieve higher growth rates and refractive index values. At the same time the production of good films at temperatures below 100 °C fails. In contrast to water, ozone based chemistry performed very well at

temperatures as low as 60 °C. Generally, both oxidation chemistries provide high quality barrier films with WVTR values of 10^{-4} g/m^{2}day.

Based on the acquired experimental data and practical knowledge, a pilot roll-to-roll SALD coating system was built. Self-limiting behaviour of the process was demonstrated indicating the ALD nature of the process. Uniform coatings were obtained on the 500 mm width substrate with a thickness deviation of ±5%.

In order to evaluate the barrier performance of the films 20 nm of Al_2O_3 were deposited on PEN substrate at web speeds up to 0.44 m/min. The barrier performance of Al_2O_3/PEN structures was evaluated using WVTR coulometric and calcium tests. The lowest transmission rate of $5x10^{-6}$ g/m^{2}day was obtained for films coated at 0.25 m/min of web speed. This is equivalent to 180 m^2 of coated web per day.

Generally, SALD coating systems provide a very robust process and repeatable results. It was shown that the SALD concept allows a dramatic increase in production yield compared to conventional ALD without affecting the quality of the films. Barrier films synthesized with SALD technology satisfy the stringent requirements for encapsulation of flexible electronic devices.

References

1 Marketing report IDTechEx, Printed, Organic & Flexible Electronics Forecasts, Players & Opportunities 2014-2024

2 T.W. Kim, M. Yan, A.G. Erlat, P.A. McConnelee, M. Pellow, J. Deluca, T.P. Feist, A.R. Duggal and M. Schaepkens, J. Vac. Sci. Technol. A 23 (2005) 971

3 P.F. Carcia, R.S. McLean, M.H. Reilly, M.D. Groner, S.M. George, Appl. Phys. Lett. 89 (2006) 031915

4 A.P. Ghosh, L. J. Gerenser, C.M. Jarman and J.E. Fornalik, Appl. Phys. Lett. 86 (2005) 223503

5 R.L. Puurunen et al., On the Early History of ALD: Molecular Layering, 14th International Conference on Atomic Layer Deposition, 2014, Kyoto, Japan

6 V.B. Aleskovskii and S. I. Kol'tsov, Some characteristics of molecular layering reactions. Abstract of Scientific and Technical Conference, Goskhimizdat, Leningrad (1965) 67

7 A.M. Shevjakov, G.N. Kuznetsova, V.B. Aleskovskii, Interaction of titanium and germanium tetrachlorides with hydrated silica. Chemistry of high temperature materials. Proceedings of 2nd USSR conference on high temperature chemistry of oxides, November 26-29, 1965, USSR Nauka, Leningrad, USSR, p. 162-168

8 G.S. Sveshnikova, S. I. Kol'tsov, V. B. Aleskovskii, Interaction of titanium tetrachloride with hydroxylated silicon surfaces J. Appl. Chem. USSR., 43 (1970) 432

9 G.V. Sveshnikova, S. I. Kol'tsov, V. B. Aleskovskii, Formation of a silica layer of predetermined thickness on silicon by the molecular-layering method. J. Appl. Chem. USSR, 43 (1970) 1155-1157 in English

10 T. Suntola and J. Antson, U.S. Patent No. 4,058,430 15 November 1977

11 T. Suntola, Mater. Sci. Rep. 4 (1989) 261

12 T. Suntola, Acta Polytech. Scand., Electr. Eng. Ser. 64 (1989) 242

13 T. Suntola, Thin Solid Films 216 (1992) 84

14 T. Suntola, Thin Solid Films 225 (1993) 96

15 T. Suntola, *Handbook of Thin Film Process Technology*, edited by D.A. Glocker and S. I. Shah, IOP, Bristol, United Kingdom, 1995

16 T. Suntola, Appl. Surf. Sci. 100/101 (1996) 391

17 T. Suntola and J.Antson, Finland Patent No. 52,359 10 September 1977

18 T. S. Suntola, A. J. Pakkala, and S. G. Lindfors, U.S. Patent No. 4,389,973 28 June 1983

19 T. S. Suntola, A. J. Pakkala, and S. G. Lindfors, U.S. Patent No.4,413,022 1 November 1983

20 M.D. Groner, Chem. Mater. 15 (2004) 639

21 A.W. Ott, J.W. Klaus, J.M. Johnson, S.M. George, Thin Solid Films, 292 (1997) 135

22 A.C. Dillon, A.W. Ott, J.D. Way, S.M. George, Surf. Sci. 322 (1995) 230

23 J. D. Ferguson, A.W. Weimer, S.M. George, Thin Solid Films 371 (2000) 95

24 J. D. Ferguson, A.W. Weimer, S.M. George, Chem. Mater. 16 (2004) 5602

25 A.W. Ott, J.W. Klaus, J.M. Johnson, S.M. George, Thin Solid Films, 292 (1997) 135

26 M. Juppo, A. Rahtu, M. Ritala and M. Leskelä, Langmuir 16 (2000) 4034

27 A. Rahtu, M. Ritala and T. Alaranta, Langmuir 17 (2001) 6506

28 J. W. Elam, M.D. Groner, S.M. George, Rev. Sci. Instrum. 73 (2002) 2981

29 Y. Widjaja, C. B. Musgrave, Appl. Phys. Lett. 80 (2002) 3304

30 C.A. Wilson, R.K. Grubbs, S.M. George, Chem. Mater. 17 (2005) 5625

31 S.M. George, Chemical Reviews, 110 (2010) 111

32 S.M. George, A.W. Ott, J.W. Klaus, J.M. Johnson, J. Phys. Chem. 100 (1996) 13121

33 M. Ritala, M. Leskelä, Thin Solid Films 409 (2002) 138

34 R. L. Puurunen, J. Appl. Phys. 97 (2005) 121301

35 M. Ritala, M. Leskelä, *Atomic Layer Deposition. Handbook of Thin Film Materials*, San Diego, CA, 2001

36 M. Ritala, M. Leskelä, Nanotechnology 10 (1999) 19

37 L. Niinisto, J. Paivasaari, J. Niinisto, M. Putkonen and M. Nieminen, Phys. Status Solidi A 201 (2004) 1443

38 M. Ritala, M. Leskelä, Angew. Chem., Int. Ed. 42 (2003) 5548

39 M.Knez, K. Niesch and L. Niinisto, Adv. Mater. 19 (2007) 3425

40 T. Suntola and J. Antson, U.S. Patent No. 4,058,430 15 November 1977

41 D.H. Levy, D. Freeman, S.F. Nelson, P.J. Cowdery-Corvan and L.M. Irving, Appl. Phys. Lett. 92 (2008) 192101

42 D.H. Levy , S.F. Nelson and D. Freeman, J. Display. Tech. 5 (2009) 484

43 D. H. Levy, R. S. Jerr and J. T. Carey, U.S. Patent No. 2009/0217878 3 September 2009

44 D.H. Levy, C.R. Ellinger and S.F. Nelson, Appl. Phys. Lett. 103 (2013) 043505

45 P. Poodt, A. Lankhorst, F. Roozeboom, K. Spee, D. Maas, A.Vermeer, Adv. Mater, 22 (2010) 3564

46 P. Poodt, R. Knaapen, A. Illiberi, F. Roozeboom, A. van Asten, J. Vac. Sci. Technol. A, 30 (2012) 01A142

47 P. Poodt, J. van Lieshout, A. Illiberi, R. Knaapen, F. Roozeboom, A. van Asten, J. Vac. Sci. Technol. A, 31 (2013) 01A108

48 P. Poodt, A. Illiberi, F. Roozeboom, Thin Solid Films, 532 (2013) 22

49 P. Poodt, A. Lankhorst, F. Roozeboom, V. Tiba, K. Spee, D. Maas, and A. Vermeer, 10th International Conference on Atomic Layer Deposition, Seoul, R. South Korea, 2010

50 http://www.solaytec.com/technology/spatial-ald Accessed on 12.01.2015

51 F. Werner, B. Veith, V. Tiba, P. Poodt, F. Roozeboom, R. Brendel, J. Schmidt, Appl. Phys. Lett. 97 (2010) 162103

52 http://www.levitech.nl/technology/atomic-layer-deposition/ Accessed on 12.01.2015

53 V.I. Kuznetsov, E.H.A. Granneman, P. Vermont, K. Vanormelingen, ECS Trans. 33 (2010) 441

54 F. Werner, W. Stals, R. Gértzen, B. Veith, R. Brendel and J. Schmidt, Energy Procedia 8 (2011) 301

55 http://lotusat.com/roll-to-roll-ald/ Accessed on 12.01.2015

56 E. R. Dickey and W. A. Barrow, 52nd Annual Technical Conference Proceedings of the Society of Vacuum Coaters, 2009 (unpublished) 720–726

57 E.R. Dickey, US 20130177760, 11 July 2013

58 E.R. Dickey, W.A. Barrow, US 20120219708, 30 August 2012

59 E.R. Dickey, US 20120021128, 26 January 2012

60 E.R. Dickey, W.A. Barrow, US 20100189900, 29 July 2010

61 E.R. Dickey, W.A. Barrow, US 20100143710, 10 June 2010

62 E.R. Dickey, W.A. Barrow, US8187679 B2, 29 May 2012

63 E.R. Dickey, W.A. Barrow, US 11/829,050, 29 May 2012

64 E.R. Dickey, US 13/888159, 11 June 2014

65 P. Poodt, D.C. Cameron, E. Dickey, S.M. George, V. Kuznetsov, G.N. Parsons, F. Roozeboom, G. Sundaram, and A.Vermeer, J. Vac. Sci. Technol. A 30 (2012) 010802

66 B.L. Danforth, E.R. Dickey, Surf. and Coat. Tech. 241 (2014) 142

67 E. Dickey, W.A. Barrow, J. Vac. Sci. Technol. A, 30 (2012) 021502

68 P. R.Fitzpatrick, Z.M. Gibbs, and S.M. George, J. Vac. Sci. Technol. A, 30 (2012) 01A136

69 A. Kamran, C. Kyung-Hyun, J. Jeongdai, L. Yun Woo, Materials Letters 136 (2014) 90

70 H. Chatham, Surf. and Coat. Tech. 78 (1996) 1

71 M.C. Choi, Y. Kim, C.S. Ha, Prog. Polym. Sci. 33 (2008) 581

72 S. J. Yun, Y. W. Ko and J. W. Lim, Appl. Phys.Lett. 85 (2004) 4896

73 S.H. K. Park, J. Oh, C.S. Hwang, J.I. Lee, Y. S. Yang and H. Y. Chu, Electrochemical and Solid-State Letters 8 (2005) H21

74 E. Langereis, M. Creatore, S.B.S. Heil, M.C.M. van de Sanden and W.M.M. Kessels, Appl. Phys.Lett. 89 (2006) 081915

75 M.D. Groner, S.M. George, R.S. McLean and P. F. Carcia, Appl. Phys.Lett. 88 (2006) 051907

76 W.J. Potscavage, S. Yoo, B. Domercq and B. Kippelen, Appl. Phys. Lett. 90 (2007) 253511

77 A.A. Dameron, S.D. Davidson, B.B. Burton, P.F. Carcia, R.S. McLean and S.M. George, J. Phys. Chem. C, 112 (2008) 4573

78 P.F. Carcia, R.S. McLean, M.D. Groner, A.A. Dameron and S.M. George, J. Appl. Phys., 106 (2009) 023533

79 P.F. Carcia, R.S. McLean and S. Hegedus, Sol. Energ. Mat. Sol. Cells, 94 (2010) 2375

80 E.H.H. Jamieson, A.H. Windle, J. Mater. Sci, 18 (1983) 64

81 S.F. Lim, W. Wang and S.J. Chua, Adv. Funct. Mater. 12 (2002) 513

82 Y.G. Tropsha, N.G. Harvey, J. Phys. Chem. B 101 (1997) 2239

83 A.S. da Silva Sobrinho, G. Czeremuszkin, M. Latreche and M.R. Wertheimer, J. Vac. Sci. Technol. A 18 (2000) 149

84 B.M. Henry, F. Dinelli, K.Y. Zhao, C.R.M. Grovenor, O.V. Kolosov, G.A.D. Briggs, A.P. Roberts, R.S. Kumar and R.P. Howson, Thin Solid Films 355–356 (1999) 500

85 http://www.mocon.com/aquatran2.php Accessed on 12.01.2015

86 S. Swann, A Mass Spectrometry Method for Water Vapour Transmission Rate (WVTR) testing to 10^{-6} g/m^2 /day, utilising Deuterium Oxide, VG Scienta corporate presentation (unpublished)

87 G. Nisato, P. C. P. Bouten, P. J. Slikkerveer, W. D. Bennett, G. L. Graff, N. Rutherford, L. Wiese, International Display Research Conference, Asia Display/IDW '01, 2001, p. 1435

88 G. Nisato, M. Kuilder, P. Bouten, L. Moro, O. Philips, N. Rutherford (2003) Thin-film encapsulation for OLEDs: Evaluation of multilayer barriers using the Ca test. SID 03 Digest XXXIV:550

89 R. Paetzold, A. Winnacker, D. Henseler, V. Cesari and K. Heuser, Rev. Sci. Instrum. 74 (2003) 5147

90 C.M. Hansen, L. Just, Prog. Org. Coat 44 (2002) 259

91 A.R. Coulter, R.A. Deeken and G.M. Zentner, Membr. Sci. 65 (1992) 269

92 H. Welding, S.H. Poulsen and C. Ursin, Proceedings of 11th International Conference on Electricity Distribution, CIRED, Liege, Belgium (1991)

93 R. Dunkel, R. Bujas, A. Klein and V. Horndt (2005) Method of measuring ultralow water vapour permeation for OLED displays. Proc IEEE 93:1478–1482

94 C.Y. Chang, C. T. Choua, Y. J. Lee, M.J. Chen, F.Y. Tsai, Organ. Electron. 10 (2009) 1300

95 C.Y. Chang, F.Y. Tsai, J. Mater. Chem., 21 (2011) 5710

96 G. Nisato et al., Comparing water permeation metrologies, LOPEC 2014, Munich, Germany

97 R. Matero, A. Rahtu, M. Ritala, M. Leskelä and T.Sajavaara, Thin Solid Films 368 (2000) 1

98 A. Hodgson, S. Haq, Surf. Sci. Rep. 64 (2009) 381

99 J.B. Kim, D.R. Kwon, K. Chakrabarti, C. Lee, K.Y. Oh and J.H. Lee, J. Appl. Phys. 92 (2002) 6739

100 S.K. Kim, S.W. Lee, C.S. Hwanga, Y. Min, J.Y. Won and J. Jeong, J. Electrochem. Soc. 153 (2006) F69

101 C. Kittel, *Introduction to Solid State Physics*, Wiley, New York (1996)

102 M.R. Saleem, R. Ali, S. Honkanen and J. Turunen, Thin Solid Films 542 (2013) 257

103 O. Redlich and D. L. Peterson, J. Phys. Chem. 63 (1959) 1024

Publication I

P.S. Maydannik, T.O. Kääriäinen, D.C. Cameron
An atomic layer deposition process for moving flexible substrates

Reprinted with permission from Elsevier
Chemical Engineering Journal
Vol. 171, pp. 345-349, 2011

Chemical Engineering Journal 171 (2011) 345–349

Contents lists available at ScienceDirect

Chemical Engineering Journal

journal homepage: www.elsevier.com/locate/cej

An atomic layer deposition process for moving flexible substrates

P.S. Maydannik*, T.O. Kääriäinen, D.C. Cameron

ASTRaL, Lappeenranta University of Technology, Prikaatinkatu 3E, 50100 Mikkeli, Finland

ARTICLE INFO

Article history:
Received 14 October 2010
Received in revised form 7 March 2011
Accepted 28 March 2011

Keywords:
Atomic layer deposition
Flexible substrate
Aluminium oxide

ABSTRACT

A new design of atomic layer deposition (ALD) system for deposition on to moving flexible substrates has been demonstrated. The basic design is a cylindrical drum to which the substrate is attached which rotates inside a reaction chamber fitted with a number of different precursor and purge zones. It is intended as a vehicle for determining the parameters which are important in the design of a roll-to-roll ALD system. The system shows that deposition takes place according to the typical ALD model where there is dose saturation above a certain dose levels and that the thickness of film deposited is proportional to the number of ALD cycles carried out. The deposition rate for a reaction temperature of 100 °C is ~1 Å/cycle. Good uniformity across the width of a 300 mm × 100 mm flexible substrate is demonstrated. The deposition process shows some deviations from classical ALD behaviour which can be understood taking into account the movement of the substrate.

1. Introduction

Atomic layer deposition (ALD) is a technology which can deposit very high-quality thin films which have extreme uniformity even on three-dimensional structures, high density, low porosity and freedom from defects. ALD is the method of choice in depositing high-k dielectrics in microelectronics [1] and shows very promising results in area such as gas barrier layers for encapsulation [2], sensors [3] and protective coatings [4]. More details of applications and capabilities can be found in various reviews [5–7]. These desirable characteristics are brought about by the nature of the ALD process which is based on sequential surface reactions between active chemical groups bonded to the substrate surface and precursor molecules. The gas flow sequencing ensures that there is an inert gas purge process between the exposure of the substrate to the active precursors, which removes any non-attached species and prevents any gas phase reactions. Detailed explanations of the ALD process can be found elsewhere, for example, in Ref. [8].

The typical ALD process requires filling the reaction chamber with precursor so that the surface reactive sites are saturated, purging away the excess, filling with the second precursor and purging away the by-products. This sequence constitutes one cycle of the process and, in principle, forms a monolayer deposit on the surface. The required film thickness can then be obtained by repeating the process the appropriate number of times. The cycle time is determined by (i) the chemical reaction time at the surface, (ii) the reactor filling time and (iii) the reactor purging time. The limiting factors here are typically the reactor filling and purging times since the chemical reaction time is normally very short. This has limited the possibility of commercialisation, even though ALD has shown promising results in many areas. In particular, where barrier layers are needed for encapsulation and packaging purposes, a continuous roll-to-roll process is necessary in order that the encapsulation can be integrated into the production process in an efficient way.

A continuous process system can be envisaged where, instead of using a stationary substrate and a time sequence of pulses of precursor and purge gases, the gas flows can be separated spatially in different zones and the time sequencing can be achieved by moving the substrate between the zones. Several patents have been granted using this approach [9–12]. There have been some recent developments using this concept which have shown promising results. Levy et al. [13] and Poodt et al. [14] have demonstrated atmospheric pressure systems using rigid substrates and Dickey and Barrow [15] has described a roll-to-roll process based on guiding a 100 mm wide plastic web through different gas zones as many times as is desired to achieve a given number of cycles at speeds of 0.2–10 m s^{-1}.

In this paper, we report the results obtained from a new design of continuous ALD (CALD) system for coating flexible substrates. The tool was designed to evaluate the behaviour and characteristics of a moving flexible substrate system in order to facilitate the development of a true roll-to-roll process.

2. Experimental details

The main feature of the CALD system is a rotating aluminium drum 100 mm diameter and 130 mm height to which a thin flexible substrate of 300 × 120 mm size can be fitted. This drum rotates in a heated cylindrical reaction chamber which is equipped with

* Corresponding author. Tel.: +358 40 836 93 08.
E-mail address: philipp.maydannik@lut.fi (P.S. Maydannik).

1385-8947/$ – see front matter © 2011 Elsevier B.V. All rights reserved.
doi:10.1016/j.cej.2011.03.097

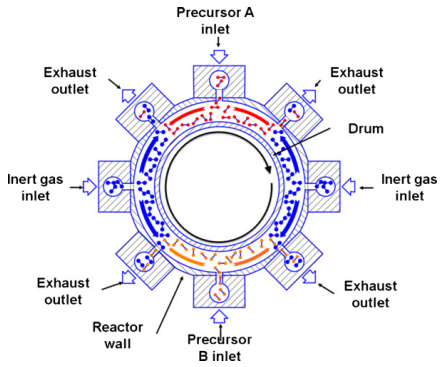

Fig. 1. Schematic radial cross-section of the continuous ALD system.

four vertically aligned slits to allow the inlet of two precursor and two purge gases, with four exhaust slits in the intermediate spaces. The exhaust slits are connected to a rotary vane vacuum pump. A schematic diagram of this layout is shown in Fig. 1. The spacing between the slits and rotating drum is 1 mm and was chosen on the basis that on the one hand, small reactor volume would decrease the precursor consumption and make the gas separation more efficient; while on the other hand large spacing would make mechanical assembly easier because of the need to avoid any drum vibrations affecting the reactor volume and as a result the flow dynamics. Moreover, large spacing gives more freedom in choosing the substrate thickness without affecting the process.

The cylindrical reaction chamber is mounted in a cold wall vacuum vessel. The reaction chamber temperature is varied using radiant heaters. An axial cross section of the reaction chamber is shown in Fig. 2. The principle of operation is as follows: as the drum rotates, the substrate is led through the various gas zones formed by continuous flows between respective precursor and exhaust slits – see Fig. 1. The purge zones and exhaust lines serve to isolate the precursor zones so that no gas phase mixing occurs between the precursors. One rotation of the drum is equivalent to one cycle of the ALD process. Additional gas flows can be set from top and bottom to ensure precursor confinement and stop precursor leakage from the ends of the drum. The drum is rotated by a servo motor and the maximum frequency used was 250 rpm. The CALD system was manufactured by Beneq Oy.

The system was tested using the well studied trimethylaluminium (TMA) and water ALD process for aluminium oxide. This

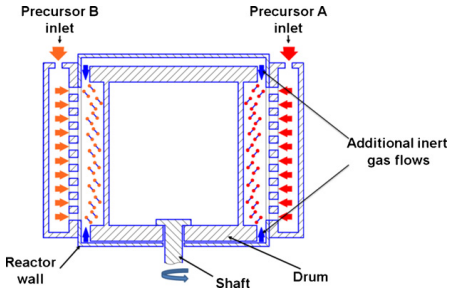

Fig. 2. Schematic axial cross-section of the continuous ALD system.

process was chosen because it is extremely sensitive to unwanted mixing of the precursors and the presence of residual water vapour. It is therefore a good vehicle for showing up imperfections in the process. The process was carried out at a reaction temperature of 100 °C using heated precursors and heated gas lines to avoid any condensation of the precursors. The TMA was 98% purity and deionised water with a conductivity of 0.056 μS cm^{-1} was used. The precursor flows were adjusted with respective needle valves so that there was no noticeable deposition while the substrate was at rest. The flows were estimated by measuring the precursor mass consumption and were approximately 1 and 10 sccm for TMA and water, respectively. Total deposition pressure was ~1 mbar with precursor partial pressure of 0.1 mbar. The purge gas was nitrogen with a purity of 99.999% with total flow of 100 sccm. It should be noted that no additional gas flows from the top and bottom of the drum were used. Films were deposited on flexible silicon pieces and on PET sheets of size 300 × 120 mm. The PET sheets were previously metallised with sputtered titanium, purely as an aid to visibility of the coatings and ease of analysis. Film thickness measurements were carried out by spectroscopic ellipsometry using a J.A. Woollam M2000FI.

3. Results

The main goal of the present studies was to verify that the growth mechanism was indeed ALD and to detect any effects due to the movement of the substrate. In conventional systems, the mechanism is assumed to be ALD if the growth process is shown to be self-limiting, that is the growth rate becomes independent of precursor dose above a certain dose level – so-called saturation behaviour. Film growth rate which is strictly independent of the number of growth cycles (except perhaps for an initial nucleation period) is also necessary. In a batch system, precursor dose can be varied by altering the gas pulse time or by changing the precursor partial pressure. In the CALD system, dose variation can be achieved by changing the time that the substrate is exposed to the precursor gas zones – which we have designated the "residence time". This is achieved by changing the rotation speed. Varying the precursor flow rates can also be used to change dosing but that may have consequent effects on the overall gas flow pattern and cause unreacted precursors to leak out from the reaction zone in the drum. These effects will be explored in future work. It is assumed that the residence time is approximately the time it takes the substrate to travel through a 90° sector of the reaction chamber, that is, between exhaust slits. Thus 60 rpm corresponds to a residence time of 250 ms.

Films were deposited using 1000 rotations at speed range from 10 to 250 rpm corresponding to total process time range of 100–4 min respectively. Fig. 3 shows the growth rate per cycle as a function of the residence time. At first sight, the behaviour looks very complex but it can be understood by considering three regions: region 1 for residence times above 300 ms, region 2 for residence times below 120 ms and region 3 between these values. In region 1, the deposition rate is relatively constant but shows a gradual increase as the residence time increases. The gradual increase may be indicative of a partly CVD-type process taking place. However, even in conventional ALD using TMA and water, the growth rate does not perfectly saturate but continues to increase slowly as the precursor dose is increased, probably due to more complete surface saturation at longer exposure times. The range of the gradual increase of deposition seen here is typical of the behaviour reported [16] for these processes. Taking 300 ms as the point where saturation occurs (as indicated by the start of the curve showing stable or gradually increasing deposition per cycle), this indicates a deposition rate due to ALD of 0.97 Å per cycle. The slope of the growth rate

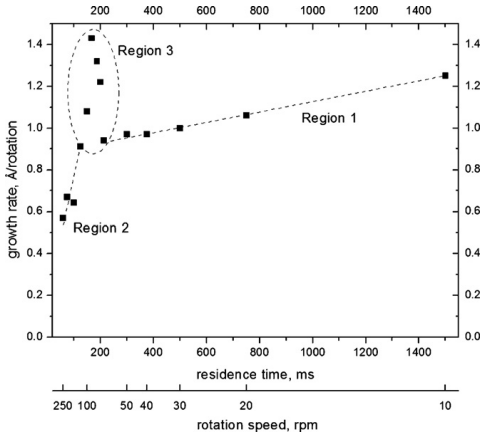

Fig. 3. Growth rate per cycle as a function of substrate residence time for 1000 cycles deposition.

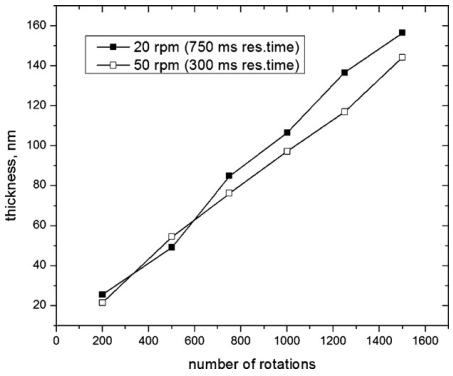

Fig. 4. Film thickness as a function of number of rotations.

curve at longer residence times indicates an additional component, either due to CVD or to the non-ideal behaviour of the TMA – water process, as mentioned above, of ~0.2 nm min^{-1}. For the purposes of this discussion it will be referred to as a CVD component, regardless of its actual cause. The deposition rate due to ALD is comparable to that of a conventional process using the same reaction [17]. Region 2 can be understood if it corresponds to the region where insufficient dose of precursor is applied to the substrate because the residence time is too short. This can lead to incomplete coverage of the substrate surface with precursor. This is also typical of the conventional ALD process. The slope of the curve in this region confirms that the deposition rate is approximately proportional to the residence time, as would be expected from incomplete saturation. Region 3 is somewhat more complicated. As residence time reduces, the deposition rate shows an initial increase followed by a sharp decrease. A possible explanation for this behaviour can be constructed if we consider the different processes which are occurring in the deposition and purge zones. This question is explored further in Section 4 below.

As was mentioned above, a feature of an ALD process is that the film thickness is strictly proportional to the number of deposition cycles. Fig. 4 shows the film thickness as a function of the number of cycles for two rotational speeds, 20 and 50 rpm. It can be seen that both processes are linear with a zero intercept. An important feature of conventional ALD is the uniformity of film thickness across the substrate. Fig. 5 shows the film thickness across the width of the substrate for films obtained from 20 to 50 rpm for 1000 cycles. From 20 to 40 rpm (750–375 ms of residence time) the films show good uniformity across the substrate. At 50 rpm (300 ms of residence time), however, it can be seen that there are deviations towards each edge of the substrate. Part of the reason for this is due to the design of the reaction chamber. In the current design, the inlet and outlet slits are 10 mm narrower than the width of the substrate so there will be an edge zone where the gas flows are different. A detailed explanation is given in Section 4.

4. Discussion

An "ideal" ALD process should have a deposition rate independent of residence time, above the saturation dose, and a deposition rate which decreases approximately linearly to zero as the dose reduces below this saturation level. At high and low residence times the growth behaviour has been observed corresponds to this with addition of a CVD-type component discussed in Section 3. However there is anomalous extra growth which must be explained. An important factor could be gas entrainment by the moving substrate. It has been reported that the relative movement between a surface and a gas gives rise to a near-surface boundary layer with thickness inversely proportional to the square root of the relative velocity [18].

Put simply, the contribution of gas entrainment to the process can be explained by the following relations: (i) formation of a boundary layer with thickness reducing as speed is increasing. Thus, the amount of material that is being dragged per one revolution is decreasing at higher speeds; (ii) at the same time, the boundary layer is disrupted while passing the purging zone. The level of disruption is proportional to the time during which the substrate is exposed to the purging zone, that is, inversely proportional to speed. If we assume that, at a certain speed, on the one hand the boundary layer is thick enough to entrain enough precursor to cause extra growth, while on the other hand the purging is already not effective enough to remove it because substrate exposure time is short, than some of the reactant contained in the boundary layer is transferred to the opposite precursor zone. As

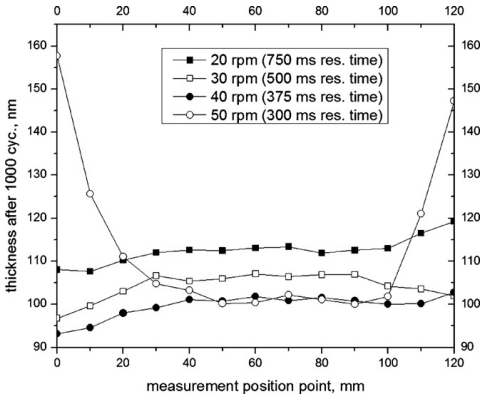

Fig. 5. Film thickness as a function of position across the polymer sheet.

a result we can expect precursor intermixing, a chemical reaction and excess growth. This hypothesis has been illustrated using the relation between substrate speed and boundary layer thickness,δ, [18]

$$\delta \sim \sqrt{\frac{1}{V_s}}$$

Where V_s is the substrate speed. Thus the dependence of concentration of the reactant in the boundary layer is proportional to δ which is then proportional to the square root of the substrate residence time since residence time is inversely proportional to substrate velocity. Based on the assumption that both boundary layer and purging N_2 are flowing in the laminar mode, and the boundary layer removal in the purge zone can be described by Fickian diffusion of reactant from the boundary layer into the pure N_2 of purging flow, an inverse relation between substrate exposure time to the purge gas and reactant residue can be assumed. These tendencies and the resulting curve are depicted in Fig. 6. The curve referred to as "boundary layer thickness" shows the magnitude of the variation in thickness as a function of residence time and rotational speed. The curve referred to as "purge inefficiency" shows the relation between relative residue concentration in the boundary layer after the substrate has passed through the purging zone and the residence time in the zone. If the amount of material being dragged through is multiplied by the fraction that is not purged from the boundary layer, the curve referred as "resulting effect on growth" will show the dependence of the extra growth caused by the gas entrainment effect on residence time or rotational speed. Note that this "resulting effect on growth" is not meant to accurately model the actual behaviour but merely to indicate how the physical processes taking place could feasibly cause the real behaviour which is seen. If we add the ideal ALD process curve where saturation occurs at 300 ms residence time, a component due to CVD or non-ideal behaviour mentioned in Section 3, and an additional component due to gas entrainment as argued above, resulting curve approximately reproduces the shape of the measured data as shown on Fig. 7.

As has been mentioned the inlet and outlet slits are 10 mm narrower than the substrate width at each side. It is obvious that at these edge zones, purging flows are much lower than at the 100 mm central region. This will influence the purging efficiency and it can

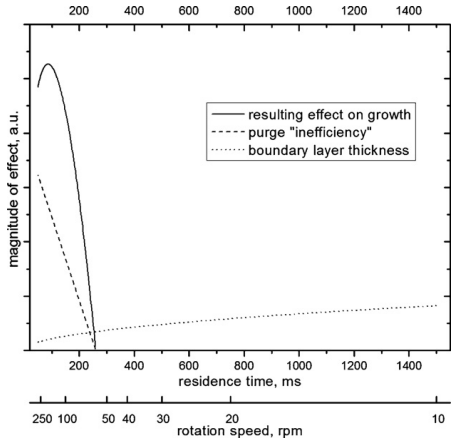

Fig. 6. Factors contributing to gas entrainment effect as a function of residence time.

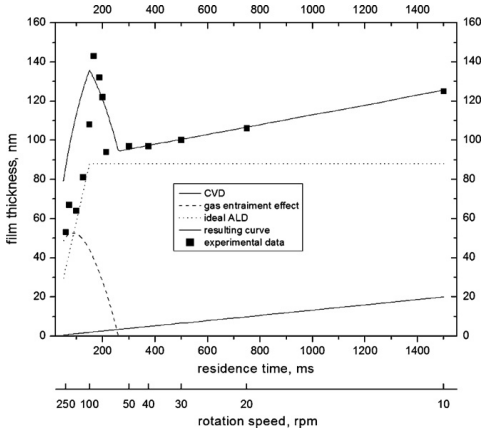

Fig. 7. Contributing factors to growth rate behaviour as a function of residence time.

be expected that excess growth attributed to the gas entrainment effect appears at lower speeds than for the central area. That is what is observed in Fig. 5 at 50 rpm of substrate rotation speed and supports our proposed explanations of anomalous behaviour of growth rate.

5. Conclusion

A novel prototype continuous ALD system has been demonstrated for coating on flexible substrates. The deposition per cycle of ~1 Å is similar to conventional ALD for the TMA + water process at the same deposition temperature. The process has shown typical ALD behaviour, that is, dose saturation (albeit with a small dose dependent component), constancy of deposition rate per cycle and film thickness uniformity over a large area. It has also demonstrated other anomalies under certain process conditions which can be understood by considering gas entrainment and purge inefficiency processes which are dependent on rotational speed. This system has shown itself to be a good test-bed for researching the uniformity and throughput factors which will be important in a roll-to-roll process based on this type of design. It has also demonstrated that additional process factors become significant when a moving substrate system is used.

Acknowledgements

This projected was supported by TEKES under project 70018/08. Thanks also to Beneq Oy for discussions on the deposition mechanisms.

References

[1] M.D. Groner, S.M. George, in: S.P. Murarka, M. Eizenberg, A.K. Sinha (Eds.), Interlayer Dielectrics for Semiconductor Technologies, Academic Press, San Diego, 2003, pp. 327–348.
[2] P.F. Carcia, R.S. McLean, M.D. Groner, A.A. Dameron, S.M. George, J. Appl. Phys. 106 (2009) 023533.
[3] X. Du, S.M. George, Sens. Actuators, B 135 (2008) 152.
[4] N.D. Hoivik, J.W. Elam, R.J. Linderman, V.M. Bright, S.M. George, Y.C. Lee, Sens. Actuators, A 103 (2003) 100.
[5] M. Knez, K. Nielsch, L. Niinistö, Adv. Mater. 19 (2007) 3425.
[6] H. Kim, H.-B.-R. Lee, W.-J. Maeng, Thin Solid Films 517 (2009) 2563.
[7] M. Leskela, M. Ritala, Thin Solid Films 409 (2002) 138.
[8] S.M. George, Chem. Rev. 110 (2010) 111.

[9] D.H. Levy, Patent Application US20070238311 – Process for atomic layer deposition, March 29, 2006.
[10] C.M.A. Heller, A.G. Erlat, E.M. Breitung, Patent WO2008057625 – Systems and methods for roll-to-roll atomic layer deposition on continuously fed objects, June 5, 2006.
[11] J. Yudovsky, Patent Application US20040067641 – Gas distribution system for cyclical layer deposition January 29, 2003.
[12] E.R. Dickey, W.A. Barrow, Patent WO2007112370 Atomic layer deposition system and method for coating flexible substrates, March 26, 2007.
[13] D.H. Levy, D. Freeman, S.F. Nelson, P.J. Cowdery-Corvan, L.M. Irving, Appl. Phys. Lett. 92 (2008) 192101.
[14] P. Poodt, A. Lankhorst, F. Roozeboom, V. Tiba, K. Spee, D. Maas, A. Vermeer, 10th International Conference on ALD, Seoul, Korea, 2010.
[15] E.R. Dickey, W.A. Barrow, 52th Annual Technical Conference Proceedings of the Society of Vacuum Coaters, 2009, pp. 700–726, ISSN 0737-5921.
[16] R. Matero, A. Rahtu, M. Ritala, M. Leskela, T. Sajavaara, Thin Solid Films 368 (2000) 1.
[17] A.W. Ott, J.W. Klaus, J.M. Johnson, S.M. George, Thin Solid Films 292 (1997) 135.
[18] A. Arzate, P.A. Tanguy, Chem. Eng. Sci. 59 (2004) 3527.

Publication II

P.S. Maydannik, T.O. Kääriäinen, D.C. Cameron
Continuous atomic layer deposition: Explanation for anomalous growth rate effects

Reprinted with permission from AIP Publishing
Journal of Vacuum Science & Technology A
Vol. 30, p. 01A122, 2011

Continuous atomic layer deposition: Explanation for anomalous growth rate effects

Philipp S. Maydannik,[a] Tommi O. Kaariainen, and David. C. Cameron
ASTRaL, Lappeenranta University of Technology, Prikaatinkatu 3E, FI-50100, Mikkeli, Finland

(Received 15 August 2011; accepted 13 October 2011; published 29 November 2011)

Spatial atomic layer deposition (ALD) on moving substrates has recently been the subject of increasing interest and development. Recent results of deposition on flexible substrates in a cylindrical rotating continuous ALD system showed that in certain regions of operation, deviations from ideal ALD behavior occurred showing excess deposition during the trimethylaluminium (TMA)/water process for aluminum oxide. It was speculated that this was due to boundary layer gas entrainment at the surface of the moving substrate and consequent drag-through of precursors between the different precursor vapor zones. In this paper a study has been made of these gas entrainment effects by using helium as a tracer gas to determine how the transport between zones takes place. A simple model of the process based on physical principles has been constructed which replicates the observed helium transport behavior in the boundary layer. Based on this, it has been shown that gas entrainment is not the reason for the anomalous excess growth in this system. As an alternative explanation, adsorption of excess water molecules on the substrate surface and their carry over to the TMA zone has been proposed as the cause of the anomalous growth. A physical model for this process has been constructed and it has been shown that simulations based on this model reproduce the observed behavior over a range of substrate temperatures. © *2012 American Vacuum Society*. [DOI: 10.1116/1.3662861]

I. INTRODUCTION

Atomic layer deposition (ALD) has been shown to be a very promising technique for various applications where dense and nonporous thin films with extreme thickness control are needed.[1] These features are brought about by the nature of the ALD process. Film deposition is carried out in a step-by-step manner and growth is limited by process chemistry. At first sight, ALD is very similar to the chemical vapor deposition (CVD) technique. However, in contrast to CVD, deposition occurs not due to reaction between incoming precursors and subsequent condensation of the reaction products on a surface, but via the reaction between the precursors and the surface species of the substrate. This can bring extreme thickness control and perfectly uniform surface coverage over the substrate area. The typical ALD system consists of vacuum chamber where the substrate is at rest. Pulses of precursors and purge gases are controlled by pulsing valves and the excess gases and by-products are removed by a vacuum pump. Precursor pulsing is performed in such a way that only one of them is in the reaction chamber at any time. This avoids any reaction between them which would cause a CVD process. To ensure proper precursor separation either, excess precursors are removed by a pulse of an inert purging gas such as nitrogen or by pumping the chamber down to pressures at which the precursor concentration is negligible.

Unfortunately, the conventional ALD scheme is not able to provide very high deposition rates as it is limited by precursor filing and purging times. High throughput is achievable only by using large batch mode systems which can coat a large number of substrates at the same time. For industrial utilization, particularly with flexible substrates, a continuous roll-to-roll process is necessary. This requires a "spatial ALD" concept in which a mobile substrate travels between each gas zone which is permanently filled with the particular precursor or purge gas. The zones are allocated so that when substrate passes through them in sequence film deposition occurs as in conventional ALD. The important advantage of the concept is that it allows coating of continuous flexible web materials which is not possible when using the conventional process. In the spatial ALD system, the issue of gas separation between the various zones becomes very challenging since precursors are fed to them simultaneously and there can be no impermeable physical barrier between them.

The spatial ALD concept has been successfully implemented by several research groups. Description of those can be found elsewhere.[2–4] Our implementation of this concept is the result of collaboration between the Advanced Surface Technology Research Laboratory (ASTRaL), Lappeenranta University of Technology, Finland, and Beneq Oy, Finland. This system, known as continuous ALD (CALD) was built as a test bed for optimizing the parameters and obtaining process understanding as well as to prove feasibility of technical concept as a precursor to development of a roll-to-roll system.

The CALD system features a cylindrical-shaped aluminum reactor and a 100 mm diameter aluminum rotating drum centered inside. The volume between the reactor and the rotating drum forms the reaction space. The reactor has overall eight slit-shaped gas ports—four inlet and four outlet

[a]Electronic mail: philipp.maydannik@lut.fi

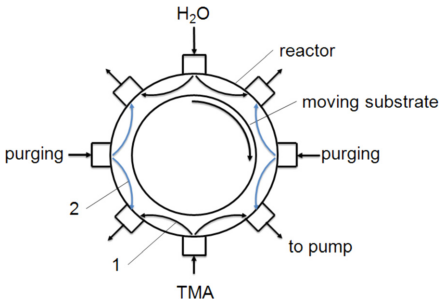

FIG. 1. (Color online) Flow scheme for the CALD reactor of TFS 200 R system: 1—precursor flow; 2—purging flow.

arranged symmetrically around the reaction chamber, as shown in Fig. 1. Precursors and purge gases are injected continuously through their respective ports and extracted from the exhaust ports. The purge zones act as a gas barrier to prevent intermixing of precursors. One ALD cycle is provided by one rotation of the drum with the substrate mounted in it through the gas zones. A detailed description of the system is given in Ref. 5.

The tool provides deposition in true ALD mode and has shown itself to be a good vehicle for studying the continuous process. However, a growth anomaly was observed during the deposition of aluminum oxide using trimetylaluminium (TMA) and water as precursors. The anomaly shows up as excess growth rate within a certain range of substrate rotation speed. This is shown in Fig. 2. The growth rate increases above the normal, expected rate which is indicative of CVD type of growth due to precursor intermixing. In the light of the fact that this excess growth was observed only when substrate was rotating, precursor intermixing was believed to be caused by gas entrainment in which precursors can be transported from one zone to another as a part of a near-surface boundary layer. This procedure was outlined in a previous paper.[5]

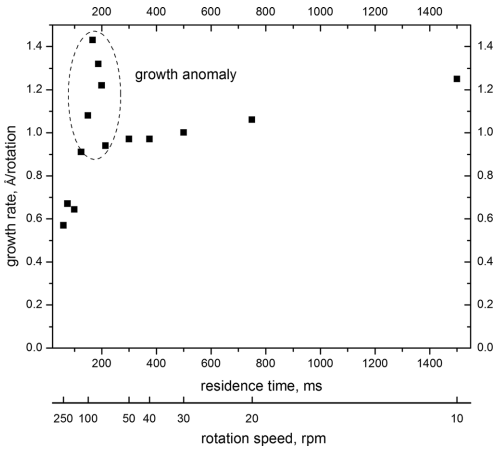

FIG. 2. Growth rate curve of Al_2O_3 films deposited at 100 °C.

The current paper deals with detailed studies of the gas transfer between the reactor ports under conditions which simulate the ALD process and then a comparison between these results and a model of the effect of mass transfer in the gas boundary layer in the CALD reactor. It is shown that the growth anomaly cannot be explained by gas entrainment effects. However, an alternative model based on the desorption rate of excess adsorbed water has been shown to closely reproduce the observed behavior.

II. EXPERIMENT

The measurements were carried out using a Beneq TFS200R ALD reactor. Two types of experiments were done: one series with He as a tracing gas and the other series with actual deposition of Al_2O_3. For the first series, there were no precursors used but the flow of one of the precursors was replaced by helium (99.996%, Aga). A radial cross-section of the cylindrical reaction chamber indicating the helium injection and measurement ports is shown on Fig. 3. Helium, without any carrier gas mixture, was injected into the reactor via one precursor inlet with the same partial feeding pressure that was used for the ALD precursor (0.1 mbar). A helium leak detector Smart Test HTL 560 (Pfeiffer Vacuum) was connected via a needle valve to an exhaust port. The helium leak rate was measured at each exhaust port as function of substrate rotation speed and purging flow. The signal was recorded as an average during 5 min rotation session. The background signal was recorded between each session to avoid any mistake due to background concentration change. Nitrogen (grade 99.999%, Aga) was used as the purging gas. Tests were carried at chamber temperature of 100 °C to reproduce the typical situation during deposition. Measurements were made with rotation speed up to 900 rpm.

The aluminum oxide deposition was carried out using TMA (98%, Volatec Oy, Finland) and deionized water as

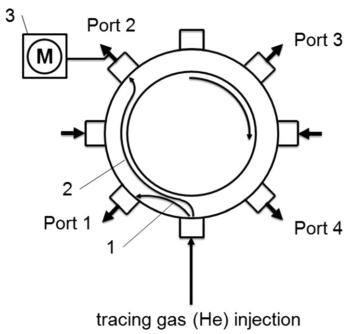

FIG. 3. Scheme of the experimental setup for gas transfer studies. 1—main gas flow; 2—additional gas flow provided by gas entrainment; 3—mass spectrometer.

precursors and the reaction temperature was varied from 100 to 150 °C. Both precursors were delivered to the reactor due to their own vapor pressure without any carrier gas. Accurate measurements of growth rate were made by depositing on flexible silicon pieces and measuring the thickness using a spectroscopic ellipsometer (F2000UI, J W Woollam). Further details of the deposition conditions are given in Maydannik *et al*.[5]

III. RESULTS AND DISCUSSION

The rate of helium flow into the detector mounted on port 1 (immediately adjacent to the He inlet port in the direction of substrate movement—see Fig. 3) as a function of rotation speed for three different purge gas flow rate is shown on Fig. 4. As rotation speed increases, the He signal increases in a sublinear manner. The He signal can be considered to consist of two components. The main component is the result of He leakage from high pressure inlet to low pressure exhaust through the reaction space and across the ends of the rotating drum. This component is assumed to be constant as a function of rotation speed for a given purging flow. An additional component comes about by gas entrainment effects. This component depends on the width of the boundary layer dragged by the substrate and the relative speed between the gas and the moving substrate surface. It is to be expected that as the rotation speed increases, more He will be trapped in the boundary layer and reach port 2 while the rotation will prevent leakage back to port 4. This behavior can be modeled by using the following argument.

The width of the boundary layer is inversely proportional to the square root of relative velocity between the gas and the moving substrate. For simplicity, we have ignored the gas flow velocity in this simulation. This may change the absolute values of the He flow detected but is not likely to

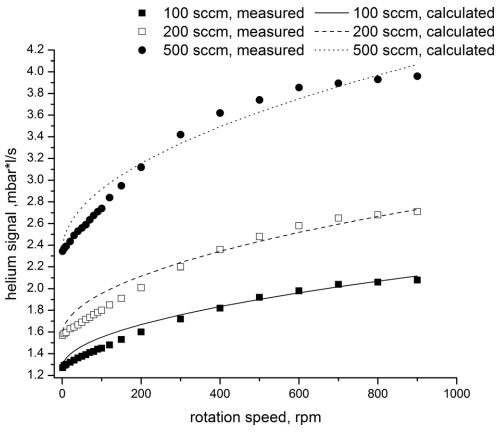

FIG. 4. Measured and calculated data for He signal on port 1 with 100, 200, 500 sccm of N_2 purge flows at 100 °C.

TABLE I. Parameters for model fitting at port 1.

Purge flow rate (sccm)	*B*	*A*
100	0.002044	1.27
200	0.002800	1.57
500	0.004153	2.35

significantly change the general trend in behavior. Moreover, the He flow detected is not an absolute quantity since the detector is only sampling the exhaust gas stream through a leak valve and can therefore not be accurately calibrated. The width of the boundary layer, w, is given by[6]

$$w \propto \frac{1}{\sqrt{v}}, \tag{1}$$

where v is the relative linear velocity of the moving surface and the purge gas. However, the *quantity* of gas arriving at the exhaust port per unit time due to the boundary layer, Q_b, is proportional to the width of the layer multiplied by the substrate velocity, that is,

$$Q_b \propto wv \propto \sqrt{v}. \tag{2}$$

So, the total He signal at port 1 can be modeled as

$$Q_1 = A + B\sqrt{v}, \tag{3}$$

where A and B are constants for a given speed. A refers to the constant leakage

This will also be affected by the purge gas flow rate which will alter the gas flows and change the likelihood that He will pass into the purge zone thus A and B will depend on purge gas flow rate. Figure 4 shows the experimental and calculated data for port 1 at 100, 200, and 500 sccm of purging flow. The modeled curve shows a reasonable fit to the experimental data although with some deviation at lower rotation speeds. The coefficients A and B are displayed in Table I.

The He signal measured at port 2 is shown in Fig. 5. The He entering the purge zone after port 1 will be the amount which is able to resist extraction at the exhaust, does not exit at port 1and is therefore carried into the purge zone. Of the He which enters this purge zone, a fraction of it will be removed as it desorbs and diffuses out of the boundary layer. Thus the signal measured at port 2 will be proportional to the signal at port 1 multiplied by the probability of its removal in the purge zone plus a leakage term independent of rotation speed. The removal of He from the boundary layer in the purge zone is based upon two further assumptions:

(1) As before, boundary layer width $w \propto 1/\sqrt{v}$, where v is the relative linear velocity of the moving substrate surface and the purge gas.
(2) Precursor concentration falls linearly from maximum at the substrate surface to zero at the boundary layer edge. This enables a very simple expression to be obtained for the rate of diffusion out of the boundary layer. In practice, there may not be a linear variation but if, for

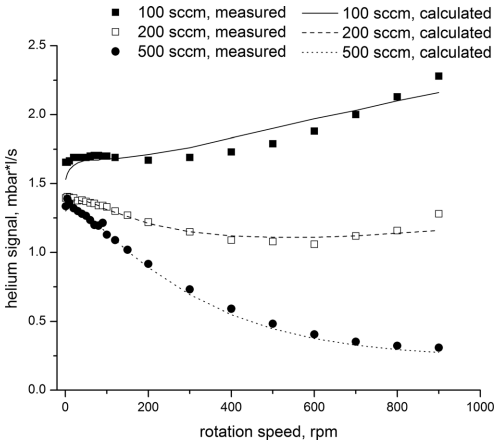

FIG. 5. Measured and calculated data for He signal on port 2 with 100, 200, 500 sccm of N_2 purge flows at 100 °C.

example, there were an exponential variation, this would only give rise to a different constant for the magnitude of the rate without changing its dependency on the speed therefore this simplification is justifiable.

With these assumptions, the total quantity of precursor in the boundary layer $G = [1/2]C_s w$ (per unit area) where C_s is the concentration at the substrate surface which will reduce in time as the substrate progresses through the purge zone.

The flux of precursor out of the boundary layer will depend on the concentration gradient, that is,

$$F(t) = -D\frac{dC}{dx} \approx -D\frac{C_s}{w} = -D\frac{2G}{w^2}, \tag{4}$$

where G is the quantity of He in the boundary layer.

The rate of change of G,

$$\frac{dG}{dt} = F = -D\frac{2G}{w^2} \tag{5}$$

$$\text{thus} \quad G = J\exp\left(-\frac{t}{\tau}\right), \tag{6}$$

where J is a constant and

$$\tau = \frac{w^2}{2D} \tag{7}$$

when $t = 0$, $G = G_o$, therefore $J = G_o$,

$$\text{so} \qquad G = G_o\exp\left(-\frac{2Dt}{w^2}\right) \tag{8}$$

$$\text{but} \qquad w = \frac{\text{const}}{\sqrt{v}}, \tag{9}$$

$$\text{therefore} \quad G = G_o\exp(-Evt) (E \text{ is a constant}). \tag{10}$$

The amount of He signal at port 2 is then given by

$$H = G_o\exp(-Evt) + K, \tag{11}$$

TABLE II. Parameters for model fitting at port 2.

Purge gas flow rate (sccm)	K	G_0	E
100	2.70	1	4.18×10^{-5}
200	1	1	2.61×10^{-5}
500	0.1	1	2.09×10^{-5}

where K allows for direct leakage to port 2 (for example, through the reactor space or across the ends of the reactor). The overall flow at port 2 can then be estimated by multiplying Eqs. (11) and (3), that is,

$$Q_2 = \left[A + B\sqrt{v}\right] \times [G_o\exp(-Evt) + K]. \tag{12}$$

The outcome of these factors gives a good fit to the measured data as shown in Fig. 5. The factors in the equation are shown in Table II.

From the deposition rate date of Fig. 2, the growth rate anomaly occurs in the rotation speed range of 70–120 rpm. As can be seen from the simulations in Fig. 5, there is no behavior at these rotation speeds which could give rise to the anomaly. Therefore, we conclude that gas entrainment is not likely to be the reason for it.

As mentioned in the Introduction, the results shown in Fig. 2 were obtained using the TMA/water precursor system. Water vapor adsorbs on surfaces which are exposed to it. It is possible that the adsorbed water may be transferred into the TMA zone if the purge time is too short for the complete removal of any excess adsorbed water. We will show that this process can be simply modeled to give a good approximation to the observed behavior. When the surface with active reaction sites is exposed to water vapor, the bonding between the surface and the water takes place in two stages: (i) H_2O molecules react with the surface and terminate the reactive sites forming a monolayer of chemically bonded hydroxyl groups. This is the desired effect. (ii) Once the surface is saturated with hydroxyl groups additional water molecules can physisorb to the surface forming a multilayer of adsorbed water. This is the undesired effect. In the former case, the sticking coefficient of water is ~1 and it can be assumed that any water molecule arriving at the surface will undergo a reaction. In the latter case, the sticking coefficient will be < 1.[7] If this adsorbed water is not removed in the purge zone, it will cause extra growth when the substrate arrives in the TMA zone.

The final thickness of the multilayer will depend on two factors: the arrival rate of water molecules and their rate of desorption. The rate of desorption in turn, depends on the surface concentration, Q, and the probability that water molecules will desorb. This probability depends on the binding energy of the adsorbed molecules according to the Boltzmann equation giving a desorption rate per molecule of

$$R_d = L\exp\left(-\frac{qE}{kT}\right), \tag{13}$$

where L is a constant which includes the molecular vibrational frequency, E is the molecule binding energy (eV), q, k, T are the electronic charge (C), Boltzmann's constant ($\mathrm{J\,K^{-1}}$) and temperature (K), respectively.

The rate of water molecules accumulation is

$$\frac{dQ}{dt} = IS - QR_d, \tag{14}$$

where Q is the surface concentration, I is the impingement rate of water molecules, and S is the sticking coefficient. For a surface exposed to vapor with pressure p the number of molecules reaching the surface per unit of time is

$$I = \frac{pN_A}{\sqrt{(2\pi MkT)}}, \tag{15}$$

where N_A is Avogadro's number, M is the molar mass (kg), and p is the partial pressure of the water vapor (Pa). The solution to this equation is

$$Q = IS\tau\left(1 - \exp\left(-\frac{t}{\tau}\right)\right), \tag{16}$$

where the time constant τ is given by

$$\tau = \frac{1}{R_d} = \frac{1}{L}\exp\left(\frac{qE}{kT}\right). \tag{17}$$

The amount of excess water adsorbed as a function of time spent in the precursor zone is approximately given by

$$\begin{aligned} Q_o &= 0 \text{ for } t < t_m \\ &= IS\tau\left(1 - \exp\left(-\frac{t}{\tau}\right)\right) \text{for } t > t_m, \end{aligned} \tag{18}$$

where t_m is the time takes to create an OH monolayer. It is assumed that the initial water exposure will only cause the formation of the chemisorbed OH layer until all the surface sites have been reacted with. The total surface concentration of adsorbed water, $Q_{o,}$ will be limited by t_r, the residence time in the water zone. As the substrate then rotates through the purge zone, it will desorb water in a thermally activated way such that the amount of water remaining on the substrate is given by

$$Q = Q_o \exp\left(-\frac{t}{\tau}\right), \tag{19}$$

where t is the time substrate spend in the purge zone and τ is the same as defined above. The excess growth rate, ΔG, will depend on the amount of water remaining on the surface and will be

$$\Delta G = bQ = bQ_o \exp\left(-\frac{t}{\tau}\right), \tag{20}$$

where b is a constant.

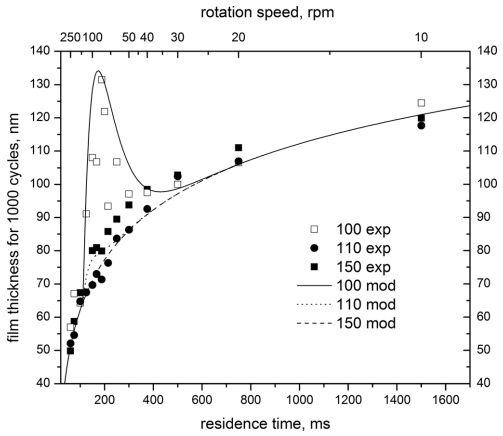

FIG. 6. Growth rate as a function of residence time at 100–150 °C temperature range (measured and modeled data).

The overall anomalous growth effect is given by

$$\begin{aligned} \Delta G &= 0 \text{ for } t < t_m \\ &= bIS\tau\left(1 - \exp\left(-\frac{t}{\tau}\right)\right)\exp\left(-\frac{t}{\tau}\right) \text{for } t > t_m, \end{aligned} \tag{21}$$

where $IS\tau\left(1 - \exp\left(-\frac{t}{\tau}\right)\right)$ describes the water accumulation on the surface while substrate is passing the precursor zone and $b\exp(-t/\tau)$ describes desorption process that takes place in the purging zone.

Since the time constants will depend on the temperature because of the Boltzmann equation, depositions at different temperatures should show marked differences in the amount of this anomalous growth. Depositions were done in the range from 100 to 150 °C using the same conditions as those where the anomaly was observed. The results are shown in Fig. 6. The graph also shows the modeled curves based on the above equation. These curves give a reasonable fit if the activation energy for desorption of water molecules is set to 0.69 eV, within the range of that given by Hodgson.[7] The other parameters are adjusted for the best fit. The modeled results are not intended to be an accurate simulation of the deposition rate but they are intended to show that a simple physical model of the processes going on in the continuous ALD system can reproduce the anomalies which are observed in growth rate during deposition.

IV. CONCLUSION

He tracing gas and mass spectrometry have been used to study gas flow behavior and detect possible gas transfer between zones in the continuous ALD reactor. The method has shown high sensitivity and reproducible results. The test results show that the moving substrate influences the gas flow in a way which can be modeled using gas entrainment in a boundary layer attached to the moving substrate. It is also shown that this does not explain the anomalous behavior of the deposition rate in the rotation speed range of 70–120 rpm.

An alternative reason for the anomalous growth rate has been proposed in which excess water is adsorbed on the substrate. This is then carried through to the TMA zone where it reacts to give extra deposition. This process has also been modeled and it has been shown that the model can reproduce the effects of deposition at different temperatures if a binding energy of the water molecules to the substrate surface of 0.69 eV is assumed. This indicates that to avoid these anomalous effects, temperatures higher than 100 °C must be used to speed up the desorption of excess adsorbed water. However, that poses problems for deposition on flexible polymer substrates because temperatures above the glass transition point cause mechanical stress and make them prone to film cracking. In that situation, an oxidizing precursor other than water must be used, e.g., ozone or a water-free plasma process.

ACKNOWLEDGMENT

Acknowledgment is given to TEKES, the Finnish Agency for Technology and Innovation, for their support for this work.

[1]S. M. George, Chem. Rev. **110**, 111 (2010).
[2]D. H. Levy, D. Freeman, S. F. Nelson, P. J. Cowdery-Corvan, and L. M. Irving, Appl. Phys. Lett. **92**, 192101 (2008).
[3]E. R. Dickey and W. A. Barrow, 52th Annual Technical Conference Proceedings of the Society of Vacuum Coaters, Santa Clara, CA, 2009 (unpublished), pp. 700–726.
[4]P. Poodt, A. Lankhorst, F. Roozeboom, K. Spee, D. Maas, and A. Vermeer, Adv. Mater. **22**, 3564 (2010).
[5]P. S. Maydannik, T. O. Kaariainen, and D. C. Cameron, Chem. Eng. J. **171**, 345 (2011).
[6]A. Arzate and P. A. Tanguy, Chem. Eng. Sci. **59**, 3527 (2004).
[7]A. Hodgson and S. Haq, Surf. Sci. Rep. **64**, 381 (2009).

Publication III

P.S. Maydannik, A. Plyushch, M. Sillanpää and D.C. Cameron
Spatial Atomic Layer Deposition: performance of low temperature H2O and O3 oxidant chemistry for flexible electronics encapsulation

Reprinted with permission from AIP Publishing
Journal of Vacuum Science & Technology A
Vol. 33, p. 031603, 2015

Spatial atomic layer deposition: Performance of low temperature H_2O and O_3 oxidant chemistry for flexible electronics encapsulation

Philipp S. Maydannik,[a] Alexander Plyushch, and Mika Sillanpää
Advanced Surface Technology Research Laboratory Team (ASTRaL), Laboratory of Green Chemistry, Lappeenranta University of Technology, Sammonkatu 12, Mikkeli 50130, Finland

David C. Cameron
R&D Center for Low-Cost Plasma and Nanotechnology Surface Modification, Masaryk University, Kotlářská 2, 611 37 Brno, Czech Republic

(Received 5 December 2014; accepted 17 February 2015; published 6 March 2015)

Water and oxygen were compared as oxidizing agents for the Al_2O_3 atomic layer deposition process using spatial atomic layer deposition reactor. The influence of the precursor dose on the deposition rate and refractive index, which was used as a proxy for film density, was measured as a function of residence time, defined as the time which the moving substrate spent within one precursor gas zone. The effect of temperature on the growth characteristics was also measured. The water-based process gave faster deposition rates and higher refractive indices but the ozone process allowed deposition to take place at lower temperatures while still maintaining good film quality. In general, processes based on both oxidation chemistries were able to produce excellent moisture barrier films with water vapor transmission rate levels of 10^{-4} g/m^2 day measured at 38 °C and 90% of relative humidity on polyethylene naphthalate substrates. However, the best result of $<5 \times 10^{-5}$ was obtained at 100 °C process temperature with water as precursor. © *2015 American Vacuum Society*. [http://dx.doi.org/10.1116/1.4914079]

I. INTRODUCTION

Atomic layer deposition (ALD) is a thin film technology that allows the deposition of various functional materials in an extremely controllable manner on a wide range of substrates including complex shaped and porous materials. These technology features provide outstanding material properties such as uniformity, conformality, and film integrity, which can facilitate development in a range of applications.

ALD materials find their niche in several applications. Nowadays, especially, their use is very pronounced in the flexible electronics field where very thin and high quality films are needed. One of the most demanding applications is device encapsulation for organic light emitting diodes (OLEDs) and solar cells to provide moisture barrier qualities. The requirements for barrier layer coatings are very stringent—the coating must (1) provide a water vapor transmission rate (WVTR) as low as 10^{-6} g/m^2 day; (2) be continuous and conformal; (3) be pinhole-free and at the same time; (4) be flexible; and (5) be transparent in the visible range.[1] A number of studies have shown that ALD technology fulfills these requirements. The excellent performance of Al_2O_3 films has been demonstrated by Carcia *et al.*[2] Accelerated calcium water permeation tests were performed at 60 °C and 85% relative humidity (RH) on 25 nm of Al_2O_3 grown on polyethylene naphthalate (PEN). Tests exhibited a WVTR level of 10^{-5} g/m^2 day corresponding to 6×10^{-6} g/m^2 day at room temperature.[2] In addition, Ghosh *et al.* demonstrated that 180 nm of Al_2O_3 deposited by ALD can protect actual OLED devices for 1000 h during harsh accelerated WVTR testing at 85 °C/85 RH.[3] Similar results have been shown for copper indium gallium selenide solar cells moisture protection.[4]

Nevertheless, despite promising results at the research and development stage, ALD technology possesses some drawbacks that restrain its development in the high volume manufacturing area. Conventional ALD uses a batch coating scheme where the substrate is sequentially exposed to precursor gases, interposed with inert gas purging. This sequence, known as the ALD cycle, needs to be repeated sufficient times to achieve the desired film thickness. The ALD cycle time depends on the gas filling and purging times for the reaction chamber. While the precursor injection pulse can be quite short (tens of milliseconds), purging must be long enough to remove all the unreacted precursor and byproducts. The exact time this takes is very dependent on the reactor volume and its configuration, as well as chemistry of the process, but may be more than several seconds even in case of small R&D reactors. Additionally, the downtime for loading/unloading and heating/cooling must be taken into account for reactors utilizing the batch scheme.

One of the ways to increase the production yields and decrease the manufacturing costs is to implement a roll-to-roll substrate handling scheme into the coating process. The recently developed spatial ALD (SALD) concept allows such a process to be implemented.[5] Spatial ALD utilizes an alternative approach to batch ALD where a moving substrate is alternatively exposed to active and inert gas zones in a way that replicates the exposure sequence of conventional ALD cycle. First of all, it allows continuous substrate coating and thus roll-to-roll handling, and second, it eliminates precursor filling and purging times. Thus, the coating speed depends solely on process chemical kinetics and substrate moving speed.

Currently, the SALD concept is under active development. Both home-made and commercial systems are

[a]Electronic mail: philipp.maydannik@lut.fi

available nowadays. The state-of-the-art of hardware development was recently comprehensively reviewed.[6–8]

Nevertheless, further studies are needed for better process understanding. Most of the research published so far is application driven and dealing with material development rather than process studies. Materials that have been obtained using SALD based ALD systems include: Al_2O_3,[9–12] TiO_2,[11] and ZnO.[13]

George *et al.* studied a "multiple slit gas source head" system at atmospheric pressure.[12] Such a system was tested and described by Levy[13] and is one of the ways in which the SALD concept can be implemented. The effects of gap spacing between the coating head and substrate, and exhaust pumping speed and nitrogen separation flows were investigated. The features of a low pressure Al_2O_3 SALD process were studied using a cylindrical shape type reactor.[9,14] Chemical vapor deposition (CVD) excess growth rate effects due to excess water adsorption and/or gas boundary formation were revealed under certain conditions.

As can be seen from the abovementioned studies, the main difficulty in the process is to keep two reagents separate from each other to avoid gas-phase reactions or multilayer surface deposition. Since both precursors are fed into different segments of one reactor volume it is very important to show that there is no intermixing and that inert gas separation works efficiently. As in conventional ALD studies, this is done by building so-called saturation curves that demonstrate that the precursor dose has no effect on growth rate once a saturation level has been reached.

Recent studies on the SALD process show that process artifacts may occur due to relative movement between substrate and precursor gases. Formation of near surface boundary layer leads to entrainment of gaseous precursors and can result in CVD type of growth.[9] Another type of artifact can be observed at low temperature when water is used as oxidizing agent. At low deposition temperatures water molecules tend to form multilayers instead of monolayer and if the purging is insufficient, it can result in a higher than expected growth rate.[14,15] This effect is well known in conventional ALD studies and usually solved by applying much longer purging pulses compared to high temperature runs. In SALD studies, this effect is more dramatic and not straightforward to solve. As the reactor geometry is usually fixed, then it is not practically possible to independently change the purge times without changing precursor dose. To do so would require physically changing the purging zone width, which is constrained by the reactor size. The substrate speed can be decreased to give more time for water molecules to desorb but that would seriously impact on the process throughput.

One way to eliminate the water adsorption problem is to use a different oxidizing agent such as ozone or the excited atoms and radicals produced by an oxygen plasma. Ozone has been widely used for aluminum oxide ALD processes and has been found to be beneficial for some applications. For example, substitution of water with ozone results in better performance of Al_2O_3 used as a dielectric[16] and in lower impurity levels.[17]

The aim of the present study is a direct comparison between the characteristics of water and ozone as oxygen sources for the Al_2O_3 ALD process using a low pressure spatial ALD reactor. For successful industrialization, a deep understanding of the relationships between parameters such as precursor dosage and concentration, process speed and material properties and quality are essential.

II. EXPERIMENT

Depositions were carried out using modified spatial ALD TFS200R reactor (Beneq Oy, Finland). The general description and layout can be found elsewhere.[9] The reactor features a cylindrical drum that serves as a substrate holder and an annular reaction chamber fitted with nozzles for either gas delivery or exhaust. The arrangement of nozzles is depicted in Fig. 1. Constant rate precursor gas flow takes place between the central nozzle and the exhaust nozzles surrounding it. Additional separation between precursors is provided by inert gas counter flows from the sides of the nozzle arrangement. As can be seen from the picture, one rotation of the drum provides sequential exposure of the substrate equivalent to four ALD cycles. Drum rotation speed dictates important parameters such as precursor dose and substrate residence time, which is defined here as the length of time that a point on the substrate remains within a particular precursor zone as it rotates. Table I shows the drum rotation speed values used in present studies and their relation to residence time and substrate linear speed. The gap between the drum and reactor wall is set to 0.5 mm. Nitrogen for the carrier and curtain process gas was sourced from liquid nitrogen supplied by Aga, Finland. Trimethylaluminum (TMA), 98% (Volatec, Finland), and deionized water precursors were evaporated using heated sources and delivered to the reactor by 100 sccm of carrier gas, respectively. Precursor concentration was adjusted by needle valves, and the respective dosages were determined by measuring reagent weight loss in the precursor container. Four thousand six hundred standard cubic centimeters per minute of N_2 curtain flows were used in order to separate precursor flows and prevent intermixing. Ozone was produced by a BMT 803N (BMT Messtechnik GmbH, Germany) ozone generator from 99.999% purity oxygen (Aga, Finland). O_3 concentration was measured with BMT 964 ozone analyzer (BMT Messtechnik GmbH, Germany). Thin films were deposited

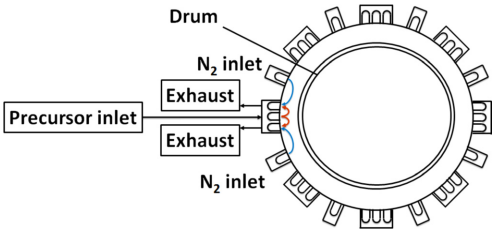

FIG. 1. (Color online) Schematic view of modified SALD TFS200R reactor with drum and N_2 and precursor inlet, and exhaust ports.

TABLE I. Drum rotation speed and related parameters used for film deposition.

Drum rotation speed (min^{-1})	2	5	8	15	20	25	45	100
Substrate residence time (s)	1.146	0.459	0.287	0.153	0.115	0.092	0.051	0.023
Linear speed (m/min)	0.628	1.57	2.512	4.71	6.28	7.85	14.13	31.4

onto 50 μm thick flexible silicon pieces and titanium metalized polymer foils in order to monitor thickness variation across the substrate. Film thickness and refractive index (RI) data were extracted using spectroscopic ellipsometry (J.A. Woollam M2000FI). Al_2O_3 films for the moisture barrier measurements were deposited on 125 μm thick Teonex® Q65FA foils. WVTR measurements were carried out using an Aquatran model 2 (Mocon, USA) at 38 °C and 90% RH.

III. RESULTS AND DISCUSSION

Successful industrialization requires the adaptation of ALD technology into a continuous operating mode (roll-to-roll or sheet-to-sheet) in order to achieve high-production yields. As was mentioned in Sec. I, the SALD concept allows continuous treatment of web substrates. In SALD technology, process conditions must provide simultaneous achievement of high growth rate values and fast substrate moving speed. As far as chemical kinetics are concerned, the rate of a particular chemical reaction depends on the reagent concentration and temperature. The first part of the studies is dedicated to investigation of the effect of reagent concentration on the film growth and properties while the second part focuses on how temperature affects the process behavior.

A. Reagent concentration dependence

Before comparing two processes, it is essential to study their behavior as a function of reagent dosage. It is important to show that the chemical reaction is not limited by reagent supply. In conventional batch flowthrough-type ALD systems dosage can be altered either by changing reagent pulsing time or increasing reagent vapor pressure. In case of SALD, the same task can be fulfilled in two ways: by changing reagent flow rate or by changing time during which substrate is being exposed to the precursor vapors (substrate residence time). In terms of process throughput decreasing substrate residence time is beneficial. Thus, loss of exposure time has to be compensated by applying higher reagent dosages per unit of time. To explore the process limits, a series of depositions was performed using the following precursor dose ranges: 18.8–353 mg/min of TMA, 21.6–248 mg/min of H_2O, and 40–60 mg/min of O_3 mass flow rates. Substrate residence times ranging from 0.023 to 1.146 s were studied. Growth rate curves for the TMA + H_2O process are shown in Fig. 2. It can be seen that with increasing mass flow rates of reagents, the growth rate curves rise (series D to B) until the flow rates reach 160 mg/min of TMA and 176 mg/min for H_2O. Further increase of flow rates by 100% results only

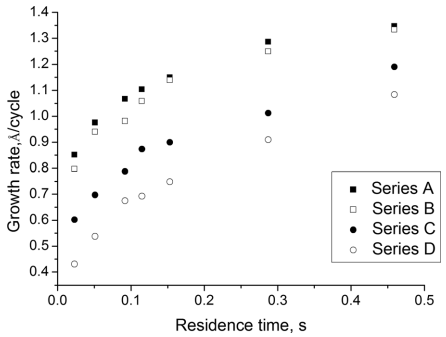

FIG. 2. Variation of growth rate as a function of substrate residence time for Al_2O_3 films grown at 120 °C of reactor temperature and precursor mass flows: A—350 mg/min of TMA, 250 mg/min of H_2O; B—160 mg/min of TMA, 175 mg/min of H_2O; C—40 mg/min of TMA, 40 mg/min of H_2O; and D—20 mg/min of TMA, 20 mg/min of H_2O.

in a slight increase of growth rate by up to 5% at higher speeds (curve A). At 150 ms of residence time, these conditions provide a saturated growth rate value (0.11 nm/cycle) that is normally observed in batch ALD studies. It is known that the TMA + H_2O ALD process does not exhibit true saturation, and in the present studies, 0.13 nm/cycle of growth rate was reached. Already, fairly high growth rate values of 0.085 nm/cycle were observed at the low residence time of only 23 ms. Refractive index data in Fig. 3 suggest that film quality maximizes at $\geq$150 ms of residence time. The refractive index is 1.61 in the saturated region of the curve and exhibits a gradual decrease for lower residence times, indicating a lower density and perhaps lower quality of those films.

To illustrate the effect of ozone, instead of water, as a precursor, Fig. 4 shows the saturation curves for film growth at 40 and 60 mg/min of O_3 and TMA mass flows fixed at 160 mg/min. It can be seen that the growth rate behavior

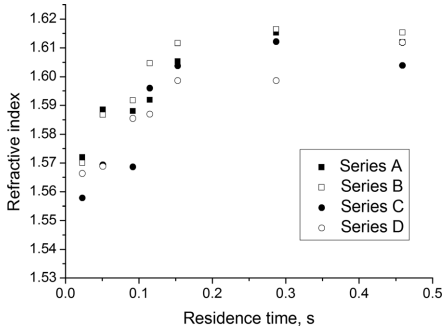

FIG. 3. Variation of refractive index as a function of substrate residence time for Al_2O_3 films grown at 120 °C reactor temperature and precursor mass flows: A—350 mg/min of TMA, 250 mg/min of H_2O; B—160 mg/min of TMA, 175 mg/min of H_2O; C—40 mg/min of TMA, 40 mg/min of H_2O; and D—20 mg/min of TMA, 20 mg/min of H_2O.

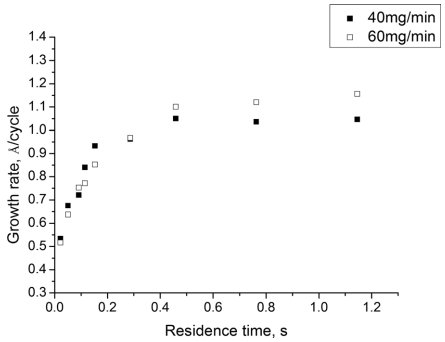

FIG. 4. Variation of growth rate as a function of substrate residence time for Al_2O_3 films grown using TMA and O_3 at 120 °C of reactor temperature.

does not change with O_3 mass flow rate, indicating that a sufficient amount of O_3 is present. In particular, the reduction of growth rate with decreasing residence time is pronounced in the unsaturated part of the curves, which are evidently very sensitive to precursor feed rates. Growth rate stabilizes at 0.11 nm/cycle above 400 ms residence time, which is slightly lower than 0.13 nm/cycle obtained previously using conventional ALD reactors.[18] The refractive index curves shown on Fig. 5 can be divided into two parts. From the figure it can be clearly seen that below 200 ms residence time the index decreases rapidly down to 1.545, while above 200 ms, the index exhibits very gradual increase from 1.575 to 1.590, indicating better film quality.

Generally, refractive index values are in agreement with previous experiments with films being denser if water is used.[15,17] The Lorentz–Lorenz equation relates the refractive index to the molecular density according to

$$\frac{n^2-1}{n^2+2}=\frac{N_A\rho\alpha}{3M\varepsilon_o}, \tag{1}$$

where n is the refractive index, N_A is Avogadro's number, M is the molar mass, ρ is the density, and α is the mean molecular polarizability.[19] This gives 2.85 and 2.77 g/cm^3 for the density of films grown using water and ozone, respectively, assuming an electronic polarizability of 4.922×10^{-24} cm^3.[20] It has been shown that the Lorentz–Lorenz equation may not predict the exact value of the film's density but it gives fairly good agreement with other analytical methods.[15] Hence, it can be used to study the change of density as a function of process parameters.

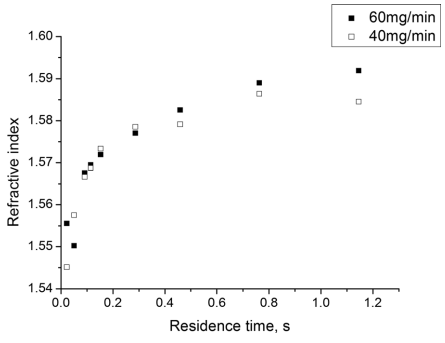

FIG. 5. Variation of growth rate as a function of substrate residence time for Al_2O_3 films grown using TMA and O_3 at 120 °C of reactor temperature.

Previous studies using batch ALD reactors do not provide any experimental data on quantitative chemical kinetics. Some information can be extracted from time resolved quartz crystal microbalance (QCM) studies.[21–23] Nevertheless, growth rate is usually plotted against valve pulsing time, which also includes time required to deliver chemical reagent into the reactor. Poodt *et al*. carried out studies on Al_2O_3 ALD process kinetics using a rotary spatial ALD reactor.[24] In this study, almost full surface saturation was already reached at ~15 ms of residence time at 150 °C reactor temperature. Notably, much higher dosages of water were used than in this work. The water sticking coefficient increases at lower temperature and this leads to formation of water multilayers on the surface and sequentially to CVD type of growth. Thus, there is always a tradeoff between process temperature and water dosage that will affect the maximum achievable speed.

To develop a better understanding of process behavior and its limitations, growth per cycle (GPC) and RI were plotted against the amount of reagent applied per one ALD cycle and square meter of substrate for each precursor. Hereinafter referred as specific precursor dosage (SPD, mmol/m^{2}cycle). Applied dosage was calculated for each run using the following formula:

$$\mathrm{SPD}=\frac{F}{4MSR^2}, \tag{2}$$

where F is precursor mass flow (g/min); M is respective molar mass, (g/mole); S is substrate area (0.031 m^2); and R is the drum rotation speed (min^{-1}).

In conventional ALD studies, the saturation point is reached once growth rate per cycle become independent of the reagent amount that the substrate is exposed to per half cycle. In practical application, full saturation is not essential if two conditions are fulfilled: (1) the requirements for film quality are met and (2) the film grows uniformly over the substrate area. In these cases, running the process at higher substrate speeds is much more beneficial in a production situation rather than achieving complete saturation.

Figure 6 shows growth rate and refractive index as a function of SPD of TMA. It can be seen that both parameters exhibit clear saturation as a function of applied dosage. 0.042 mmol/m^2 cycle of TMA is required for process to reach growth rate value of 1.1 Å/cycle and refractive index of 1.61 that are commonly reported in batch ALD studies. However, full saturation of 1.3 Å/cycle is reached once 0.6 mmol/m^2 cycle of reagent is applied. An SPD of 0.042 mmol/m^2 cycle is equivalent to 3 mg/m^2 cycle. Below that level, an abrupt drop of growth rate and RI is observed. This is in good agreement with the result obtained previously

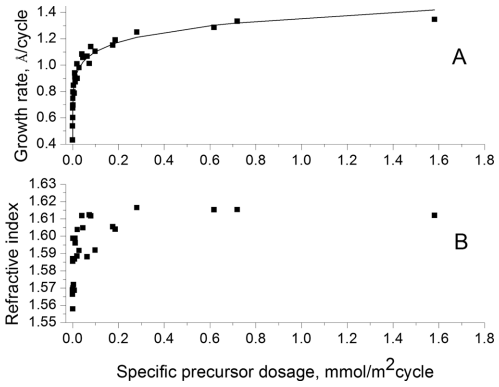

FIG. 6. Variation of growth rate (a) and refractive index (b) as a function of applied TMA dosage for Al_2O_3 films grown at 120 °C of reactor temperature. And model fitting using Redlich–Peterson isotherm: RPI constant $n_{RP} = 0.90$, correlation coefficient $R = 0.98$. Squared marks—experimental data and solid line—model fitting.

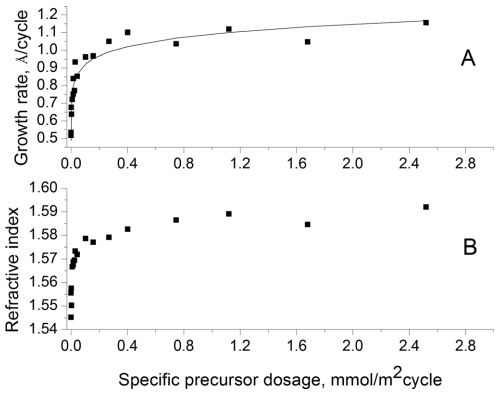

FIG. 8. Variation of growth rate (a) and refractive index (b) as a function of applied O_3 dosage for Al_2O_3 films grown at 120 °C of reactor temperature. And model fitting using Redlich–Peterson isotherm: RPI constant $n_{RP} = 0.93$, correlation coefficient $R = 0.96$. Squared marks—experimental data and solid line—model fitting.

using a scaled up SALD reactor where 3 mg/m^2 cycle was found to be critical dosage for WVTR properties of the films.[5] Growth rate and refractive index curves for water and ozone are shown in Figs. 7 and 8. Similar to TMA, both oxidizing agents exhibit saturation behavior with abrupt drop if dosage goes below certain level. The critical reagent dose for water is 0.2 mmol/m^2 cycle, which is twice larger than that for ozone (0.1 mmol/m^2 cycle).

It is interesting to compare these quantities with actual surface uptake measured by QCM. There is some inconsistency between QCM measurements of TMA uptake −34 ng/cm^2 (Ref. 23) and 39 ng/cm^2.[15] To calculate the number of molecules attached per unit of area we assume that TMA undergoes ligand exchange reaction on the surface and half of the TMA

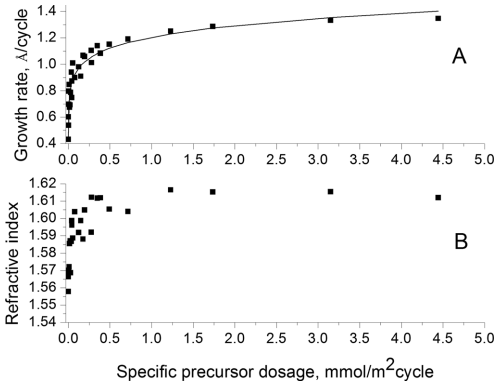

FIG. 7. Variation of growth rate (a) and refractive index (b) as a function of applied H_2O dosage for Al_2O_3 films grown at 120 °C of reactor temperature. And model fitting using Redlich–Peterson isotherm: RPI constant $n_{RP} = 0.90$, correlation coefficient $R = 0.96$. Squared marks—experimental data and solid line—model fitting.

molecules are attached through exchange of one methyl group and half lose two methyl groups. Based on the aforementioned assumptions and TMA uptake of 39 ng/cm^2, the resulting amount of TMA chemisorbed on the surface is 0.788×10^{-2} mmol/m^2 according to QCM data. Thus, if we compare it with present studies, it can be concluded that the process requires up to 100 times as much supply of reagent excess to reach saturation under given conditions. At the same time, chemisorption is shown to be very efficient. If we assume a value of 0.788×10^{-2} mmol/m^2 cycle as an applied dosage, then it results in 0.51×10^{-2} mmol/m^2 of adsorbed TMA with reagent utilization of 65%. Water mass gain behaves in a somewhat different fashion. Mass gain exhibits values of 10 ng/cm^2 immediately after exposure and then decreases to 5 nm/cm^2 probably due to desorption of byproducts.[15] Based on 10 ng/cm^2 figure, the number of reacted water molecules is 0.555×10^{-2} mmol/m^2. Thus, reagent excess of 500 is required for complete saturation. These figures highlight the importance of water reagent supply during the process.

The equation for the Redlich–Peterson isotherm (RPI) was used to fit the results[25]

$$Q_e = \frac{Q_{\max} K_{RP} C_e}{1 + K_{RP} C_e^{n_{RP}}}, \tag{3}$$

where Q_e is amount of chemisorbed material (mol/m^2); $Q_{\max}$ is maximum surface capacity (mol/m^2); K_{RP} and n_{RP} are the RPI constants; and C_e is the equilibrium concentration (in the present case equal to SPD) (mol/m^2).

The experimental amount of adsorbed material Q_e was calculated on the assumption that growth rate is proportional to the surface coverage

$$Q_e = \frac{Q_{\max} \mathrm{GPC}}{\mathrm{GPC}_{\max}}, \tag{4}$$

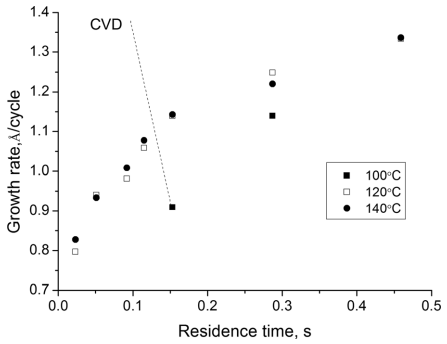

FIG. 9. Growth rate as a function of residence for Al_2O_3 (TMA + H_2O) films grown at temperature range of 100–140 °C. Data points of 100 °C series at shorter residence are not shown due to harsh CVD effect and uneven film deposition. Dashed line does not represent actual behavior but only indicates presence of CVD growth.

where GPC and GPC_{max} are equilibrium and maximum growth rates, respectively.

As can be seen from Figs. 6(a), 7(a), and 8(a), the model exhibits excellent fit for TMA and both oxidizing agent with correlation coefficient R of 0.98 and 0.96, respectively. The Redlich–Peterson equation combines features of Langmuir and Freundlich isotherms. An important parameter here is the power exponent n_{RP}, which indicates saturation behavior of the process. Values of n_{RP} constant lie between 1 and 0. In the first case, the RPI equation turns to Langmuir equation isotherm and in the second case into a linear law. Derivation of Langmuir equation assumes ideal case of adsorption with homogeneous energy site distribution and what is important in our case formation of only one monolayer of adsorbate. A linear law clearly means condensation of material onto the substrate (CVD type of growth). All the curves were fitted with n_{RP} of more than 0.9 that suggest strong saturation behavior and absence of condensation.

It should be noted that SPD is a characteristic of particular reactor arrangement and likely to vary with reactor

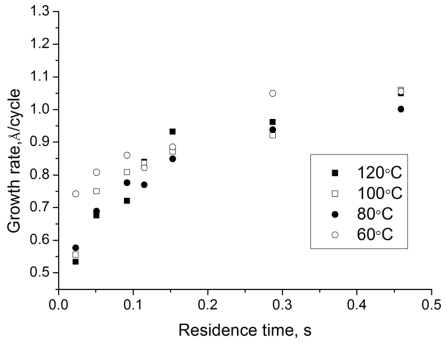

FIG. 10. Growth rate as a function of residence for Al_2O_3 (TMA + O_3) films grown at temperature range of 60–120 °C.

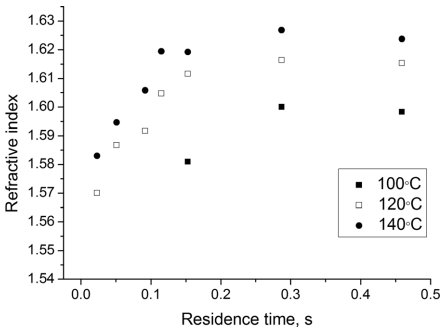

FIG. 11. Refractive index as a function of residence for Al_2O_3 (TMA + H_2O) films grown at temperature range of 100–140 °C.

volume and process parameters. On the other hand, it is a good approach to evaluating the efficiency of the process and comparing it between different reactor setups. Despite the fact that SPD is an integrated unit that takes into account both residence time and mass flow, it is clear that in the case of the particular ALD reaction studied here, process speed is limited solely by precursor supply rather than time of chemical reaction. If substrate rotation speed were not enough to provide necessary reaction time then GPC curve would show a gradual decrease with speed regardless of high SPD values being applied.

B. Temperature dependence

Changing the process temperature affects the process and film quality in a several ways. First, growth rate change usually occurs. Nevertheless, process throughput is mainly affected by substrate moving speed rather than growth rate value. Temperature is one of the parameters that has a significant effect on the refractive index, hence the density of the films. As a rule, a decrease of the temperature results in lower refractive index and can be considered as undesirable. The sticking coefficient of water increases at lower temperatures, which makes it difficult to remove excess water

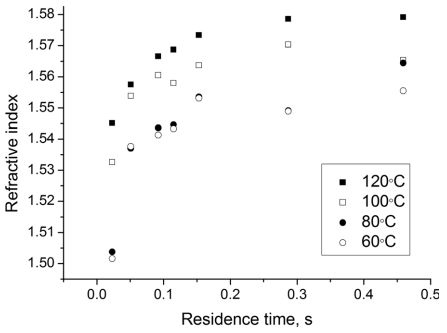

FIG. 12. Refractive index as a function of residence for Al_2O_3 (TMA + O_3) films grown at temperature range of 60–120 °C.

TABLE II. Water vapor transmission rate of 20 nm of Al_2O_3 deposited on PEN Teonex using TMA and H_2O as precursors.

T (°C)	100 rpm	20 rpm	5 rpm
120	3.76	0.41	0.64
100	NA	0.70	<0.05[a]

[a]Sensitivity level of MOCON Aquatran model 2.

molecules from the surface. Tens of seconds may be required for complete purging of a conventional ALD reactor at temperatures less than 120 °C.[23] This issue is especially pronounced with SALD reactors with fixed geometry that does not allow the purging and exposure time to be changed independently.[14,24] Differences in thermal expansion coefficients between substrate and the film may cause mechanical stress and cracking; thus, lower process temperatures should be used if possible. And finally, the rate of chemical reaction is highly determined by temperature.

Figure 9 shows how process temperature affects saturation behavior of TMA + water process. Decrease of reactor temperature from 120 to 100 °C leads to slower reaction that appears as lower growth rate values at short residence time values. Another observation is that temperatures of 100 °C and residence time shorter than 150 ms result in an abrupt increase of growth rate and nonuniform growth due to CVD effects. This has been observed previously and has been a motivation for the current studies. The process based on O_3 oxidation chemistry behaves much more robustly at lower temperatures, exhibiting relatively low variation of growth rate compared to the water-based process (Fig. 10). It is notable that the O_3 process at 60 °C exhibits slightly higher growth rate values than higher temperatures. This may happen because of water formation as a byproduct of the oxidation step and its subsequent adsorption on the substrate surface.[17]

Refractive index decreases with the temperature both for water and ozone based processes (Figs. 11 and 12). Generally, the water-based process is able to produce films with higher refractive index values. The overall trend and values are in agreement with previous studies.[17] Lowest RI values are observed for low temperature samples obtained at high substrate speeds predicting low density and poor moisture barrier performance.

C. Water vapor transmission measurements

Samples for WVTR measurement were prepared using parameters that represent favorable, moderate, and unfavorable conditions for ALD growth based on the data presented above. Twenty nanometer thick Al_2O_3 films were grown on PEN Teonex Q65FA foils at 5, 20, and 100 rpm. Tables II and III summarize the experimental parameters and results of water vapor transmission rate measurements for water and O_3 based processes, respectively.

TABLE III. Water vapor transmission rate of 20 nm of Al_2O_3 deposited on PEN Teonex using TMA and O_3 as precursors.

T (°C)	100 rpm	20 rpm	5 rpm
120	0.68	0.33	0.40
100	2.39	0.56	0.64
80	64.38	0.7	0.65
60	1177	2.53	0.38

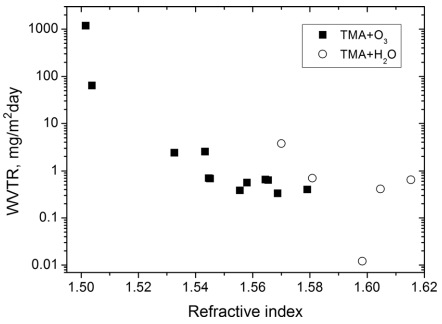

FIG. 13. WVTR as a function of refractive index of films deposited using TMA + H_2O and TMA + O_3 processes.

First, it can be seen that there is a fairly good correlation between WVTR and refractive index of the samples (Fig. 13). Shortening of residence time results in worse barrier properties, and this effect is even more pronounced at lower temperatures. Best barrier performance of less than 5×10^{-5} g/m^2 day was achieved at 5 rpm and 100 °C of process temperature using water as an oxidant. Apparently, this provides the most favorable conditions that allow proper surface saturation and produce less stress between coating and substrate during cooling. At the same time, the ozone based process produces better barrier film at conditions where water process fails. For example, high speed runs at 100 rpm and 120 °C results in relatively low WVTR of 0.68×10^{-3} g/m^2 day. As expected, runs performed at high speed and low temperatures were not able to produce high quality films. The corresponding refractive values were also very low confirming poor film density, which explains the WVTR results.

IV. CONCLUSION

A SALD reactor was employed to study the behavior of Al_2O_3 ALD process based on H_2O and O_3 oxidation chemistry. It showed itself as an excellent vehicle for studying process kinetics as it allows precise alternation of exposure time. The performance of both processes was evaluated as a function of key parameters (precursor flow, exposure time, and reactor temperature). WVTR measurements were carried out to assess film quality and suitability for flexible electronics encapsulation application. The usage of H_2O chemistry resulted in higher growth rate and refractive index values. However, adequate ALD coatings at temperatures below 100 °C cannot be produced. Coatings with a moisture permeation rate of $<5 \times 10^{-5}$ g/m^2 day were obtained using 100 °C and 0.459 s of exposure time. Employing O_3 allows decreasing process temperature down to 60 °C. It has been

found that the WVTR results correlate with refractive index of the coatings. In the light of that fact can be concluded that there is a relation between film density and barrier performance.

The Redlich–Peterson isotherm was used to model growth rate as a function of applied precursor dosage. The isotherm shows a very good fit with experimental data, showing that film growth is based on gas–solid interaction.

Current studies show that successful ALD intensification requires consideration of many factors. Precursor flows should provide sufficient reagent for saturation at low exposure time while purge time should be kept long enough to allow water excess removal. Temperature should be chosen in the way that it favors shorter chemical reaction time from one hand and does not produce mechanical stress between coating and the substrate from the other hand. Specific precursor dosage is a useful parameter that enables process efficiency assessment as well as making easier process transfer between different systems, which facilitated process up scaling.

ACKNOWLEDGMENTS

This research was funded by the Finnish Funding Agency for Technology and Innovation (TEKES). Support of Beneq Oy on hardware development is gratefully acknowledged. The authors would like to thank Chaker Necibi and Eveliina Repo for useful discussions on adsorption isotherms.

[1]W. S. Wong and A. Salleo, *Flexible Electronics: Materials and Application* (Springer, New York, 2009).
[2]P. F. Carcia, R. S. McLean, M. H. Reilly, M. D. Groner, and S. M. George, Appl. Phys. Lett. **89**, 031915 (2006).
[3]A. P. Ghosh, L. J. Gerenser, C. M. Jarman, and J. E. Fornalik, Appl. Phys. Lett. **86**, 223503 (2005).
[4]P. F. Carcia, R. S. McLean, and S. Hegedus, Sol. Energy Mater. Sol. Cells **94**, 2375 (2010).
[5]P. S. Maydannik *et al.*, J. Vac. Sci. Technol. A **32**, 051603 (2014).
[6]J. A. van Delft, D. Garcia-Alonso, and W. M. M. Kessels, Semicond. Sci. Technol. **27**, 074002 (2012).
[7]P. Poodt, D. C. Cameron, E. Dickey, S. M. George, V. Kuznetsov, G. N. Parsons, F. Roozeboom, G. Sundaram, and A. Vermeer, J. Vac. Sci. Technol. A **30**, 010802 (2012).
[8]D. Muñoz-Rojas and J. MacManus-Driscoll, Mater. Horiz. **1**, 314 (2014).
[9]P. S. Maydannik, T. O. Kääriäinen, and D. C. Cameron, Chem. Eng. J. **171**, 345 (2011).
[10]P. Poodt, A. Lankhorst, F. Roozeboom, K. Spee, D. Maas, and A. Vermeer, Adv. Mater. **22**, 3564 (2010).
[11]E. Dickey and W. A. Barrow, J. Vac. Sci. Technol. A **30**, 021502 (2012).
[12]P. R. Fitzpatrick, Z. M. Gibbs, and S. M. George, J. Vac. Sci. Technol. A **30**, 01A136 (2012).
[13]D. H. Levy, D. Freeman, S. F. Nelson, P. J. Cowdery-Corvan, and L. M. Irving, Appl. Phys. Lett. **92**, 192101 (2008).
[14]P. S. Maydannik, T. O. Kääriäinen, and D. C. Cameron, J. Vac. Sci. Technol. A **30**, 01A122 (2012).
[15]M. D. Groner, F. H. Fabreguette, J. W. Elam, and S. M. George, Chem. Mater. **16**, 639 (2004).
[16]J. B. Kim, D. R. Kwon, K. Chakrabarti, C. Lee, K. Y. Oh, and J. H. Lee, J. Appl. Phys. **92**, 6739 (2002).
[17]S. K. Kim, S. W. Lee, C. S. Hwanga, Y. Min, J. Y. Won, and J. Jeong, J. Electrochem. Soc. **153**, F69 (2006).
[18]S. D. Elliott, G. Scarel, C. Wiemer, and M. Fanciulli, Chem. Mater. **18**, 3764 (2006).
[19]C. Kittel, *Introduction to Solid State Physics* (Wiley, New York, 1996).
[20]M. R. Saleem, R. Ali, S. Honkanen, and J. Turunen, Thin Solid Films **542**, 257 (2013).
[21]J. W. Elam, M. D. Groner, and S. M. George, Rev. Sci. Instrum. **73**, 2981 (2002).
[22]C. A. Wilson, R. K. Grubbs, and S. M. George, Chem. Mater. **17**, 5625 (2005).
[23]R. A. Wind and S. M. George, J. Phys. Chem. A **114**, 1281 (2010).
[24]P. Poodt, J. van Lieshout, A. Illiberi, R. Knaapen, F. Roozeboom, and A. van Asten, J. Vac. Sci. Technol. A **31**, 01A108 (2013).
[25]O. Redlich and D. L. Peterson, J. Phys Chem. **63**, 1024 (1959).

Publication IV

P.S. Maydannik, T.O. Kääriäinen, K. Lahtinen, D.C. Cameron, M. Söderlund, P. Soininen, P. Johansson, J. Kuusipalo, L. Moro, X. Zeng

Roll-to-roll atomic layer deposition process for flexible electronics encapsulation applications

Reprinted with permission from AIP Publishing
Journal of Vacuum Science & Technology A
Vol. 32, p. 051603, 2014

Roll-to-roll atomic layer deposition process for flexible electronics encapsulation applications

Philipp S. Maydannik,[a] Tommi O. Kääriäinen,[b] Kimmo Lahtinen, and David C. Cameron[c]
Advanced Surface Technology Research Laboratory, Lappeenranta University of Technology, Sammonkatu 12, 50130 Mikkeli, Finland

Mikko Söderlund and Pekka Soininen
Beneq Oy, P.O. Box 262, 01511 Vantaa, Finland

Petri Johansson and Jurkka Kuusipalo
Tampere University of Technology, Paper Converting and Packaging Technology, P.O. Box 589, 33101 Tampere, Finland

Lorenza Moro and Xianghui Zeng
Samsung Cheil Industries, San Jose R&D Center, 2186 Bering Drive, San Jose, California 95131

(Received 20 June 2014; accepted 7 August 2014; published 19 August 2014)

At present flexible electronic devices are under extensive development and, among them, flexible organic light-emitting diode displays are the closest to a large market deployment. One of the remaining unsolved challenges is high throughput production of impermeable flexible transparent barrier layers that protect sensitive light-emitting materials against ambient moisture. The present studies deal with the adaptation of the atomic layer deposition (ALD) process to high-throughput roll-to-roll production using the spatial ALD concept. We report the development of such a process for the deposition of 20 nm thickness Al_2O_3 diffusion barrier layers on 500 mm wide polymer webs. The process uses trimethylaluminum and water as precursors at a substrate temperature of 105 °C. The observation of self-limiting film growth behavior and uniformity of thickness confirms the ALD growth mechanism. Water vapor transmission rates for 20 nm Al_2O_3 films deposited on polyethylene naphthalate (PEN) substrates were measured as a function of substrate residence time, that is, time of exposure of the substrate to one precursor zone. Moisture permeation levels measured at 38 °C/90% relative humidity by coulometric isostatic–isobaric method were below the detection limit of the instrument ($<5 \times 10^{-4}$ g/m^2 day) for films coated at web moving speed of 0.25 m/min. Measurements using the Ca test indicated water vapor transmission rates $\sim 5 \times 10^{-6}$ g/m^2 day. Optical measurements on the coated web showed minimum transmission of 80% in the visible range that is the same as the original PEN substrate. © *2014 American Vacuum Society*.
[http://dx.doi.org/10.1116/1.4893428]

I. INTRODUCTION

Flexible organic light-emitting diode (OLED) displays are among the fastest emerging applications in the market areas of electronic devices. OLED technology provides flexibility together with lightness, improved brightness, wider viewing angle, power efficiency, and extremely low response time. Another advantage of OLED displays is their potential low cost if high-throughput production processes such as roll-to-roll methods are used. It has been shown that flexible OLEDs can be produced on polymeric substrates such as polyethylene terephthalate (PET).[1] The possibility of implementing ink-jet printing technologies in the manufacture of flexible OLED panels would provide very cost efficient production.[2]

One of the major challenges in producing reliable flexible OLEDs is the necessity for proper encapsulation of the device, as the polymer films used as substrate material are not able to provide the required barrier properties. The components of the OLED, particularly the organic light-emitting materials and the electron injection layer at the cathode interface, are very sensitive to moisture and oxygen and require a very high level of protection. Commonly stated requirements for the gas barrier performance that can be found in the literature are on order of 10^{-6} g/m^2 day of water vapor transmission rate (WVTR). Additionally, requirements such as high optical transparency and flexibility must be fulfilled.[3]

Inorganic coatings are used for this purpose. $SiON_x$,[4] Al_2O_3,[5] TiO_2,[6] ZnO,[7] and SiO_2[8] are among the materials that have been tested. Atomic layer deposition (ALD) is a thin film deposition technique that has shown promising results and is being considered as a potential technology for OLED encapsulation. The ALD process is based on the chemical interaction between chemisorbed surface species on the substrate and gaseous reagents. The nature of the process provides a number of advantages, such as strong adhesion, excellent uniformity, and precise thickness control, which cannot be fulfilled by any other deposition technique. Twenty five nanometer Al_2O_3 layers deposited by ALD have shown WVTR values of 10^{-6} g/m^2 day; this complies with abovementioned requirements.[5]

At the same time, the chemical nature of the process brings some drawbacks. The main disadvantage of the

[a]Electronic mail: philipp.maydannik@lut.fi
[b]Present address: University of Colorado Boulder, Chemistry & Biochemistry, 215 Cristol Chemistry, Boulder, CO 80309.
[c]Present address: Miktech Oy, Sammonkatu 12, 50130 Mikkeli, Finland.

method in its traditional implementation is that it is slow due to intrinsic process features. In the standard batch process, the substrate is sequentially exposed to the active precursors one at a time. The reagent chemically binds to surface sites forming a monolayer of material. A following inert gas purge stage is required to remove leftover reagents and byproducts. While the precursor feeding time is quite short—of the order of tens or hundreds of milliseconds, the purging time at low process temperatures can be significantly longer—of the order of seconds—in order to ensure that all active materials are removed from the reaction chamber. The actual time sequence also depends on the reactor shape and volume. Thus, taking into account the low growth rate per cycle and also unavoidable downtime for loading/unloading and heating/cooling, this makes the process unsuitable for low cost, large area production.

To overcome the drawbacks mentioned above and enable large-scale continuous production in a roll-to-roll configuration, the ALD process must be reconfigured to handle a moving continuous web substrate. The spatial atomic layer deposition (SALD) concept allows this. During the SALD process, the substrate moves between spatially separated zones filled with the respective precursor gases and reagents in such a manner that the exposure sequence replicates the conventional ALD cycle. The working principle of the SALD concept is illustrated in Fig. 1. SALD processes have been described by a number of authors,[9–12] and concepts for developing these into a roll-to-roll process have been proposed.[13–15] Previously, only one implementation has been constructed, which enables narrow webs to be coated in a roll-to-roll basis with a very restricted number of deposition cycles in one pass.[13,14]

Up until now, there has been no roll-to-roll SALD system reported, which can deposit barrier layer coatings on a scale suitable for industrial production. In this paper, we report the results of a true roll-to-roll SALD process, which enables the deposition of 20 nm aluminum oxide moisture barrier layers with $<5 \times 10^{-4}$ g/m^2/day on polymer web substrates of 500 mm width with a web speed of 0.25 m/min.

II. EXPERIMENT

A. ALD roll-to-roll web coating system

The roll-to-roll ALD was carried out in a Beneq WCS500 coating system. The system comprises a main vacuum chamber, where the actual coating process takes place, and auxiliary units such as chilling/heating unit, web handling control, precursor storage and delivery system, precursor

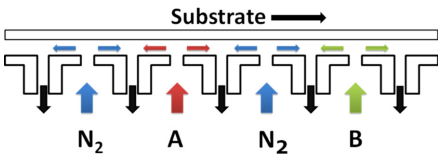

FIG. 1. (Color online) Schematic diagram of spatial atomic layer deposition coating head.

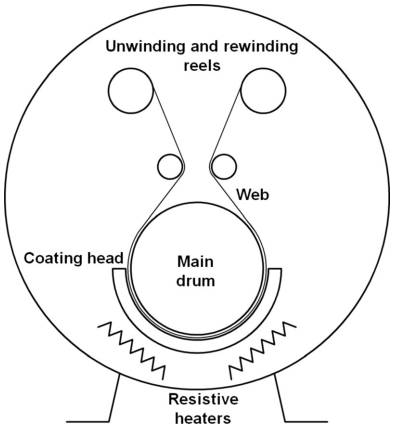

FIG. 2. WCS 500 vacuum chamber layout showing configuration of main components.

neutralizing and filter system, and pumping unit. The main chamber accommodates web winding and rewinding reels, the main processing drum and coating head, which are designed to handle a 500 mm wide web. The vacuum chamber layout is schematically shown in Fig. 2. The main drum is 600 mm in diameter made of stainless steel. The drum is temperature controlled by oil that circulates between the chamber and heating/chilling unit. The reactor features a pendulum-type coating head which is mounted beneath the drum and consists of 29 sections. Each section has a nozzle for reactive gas release and a surrounding exhaust slit. These nozzles are additionally separated by inert gas curtains to prevent the unwanted spreading and intermixing of reagents. The gap between the coating head and the drum is set to 0.5 mm. The coating head arrangement is schematically shown in Fig. 3. Additional heating is provided by resistive heaters mounted beneath the coating head. The purpose of the pendulum motion is to increase the relative speed between the moving drum and the coating head, allowing multiple passes of the coating head over the web. This

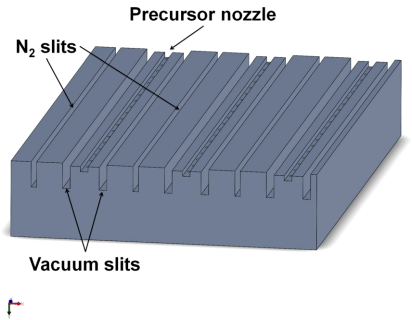

FIG. 3. (Color online) Schematic diagram of part of coating head showing configuration of precursor and purge gas nozzles and vacuum exhaust slits.

enables film thicknesses in the tens of nanometer to be deposited in a single pass of the web through the coating system.

The coating process is organized as follows: the web leaves the winding reel and moves toward the main drum. While the web is being guided over the drum, it is sequentially exposed to the precursor gas sections of the head. Each pair of sections provides one ALD cycle. As mentioned above, the pendulum motion of the head allows additional deposition cycles to be provided. The coating head is designed to travel 82 mm in each direction providing two ALD cycles per one full swing. The system can also be operated without using the intermediate guiding rollers between the winding and unwinding reels and the coating drum.

Substrate residence time is an important parameter that affects the process and growth rate to a great extent. It is defined as a time for which the substrate is exposed to one precursor vapor and during which actual gas–surface interaction occurs, that is, the time a point on the substrate surface spends within an individual precursor zone. In the present system, it is determined by the web transport speed, the coating head oscillation speed and acceleration/deceleration of the coating head as it changes direction. This means that there will be a difference in the relative speed between the web and the coating head depending on the direction of the pendulum's swing. In the studies reported here, variations in the residence time due to this effect were neglected as the coating head speed is much greater than the web transport speed. Acceleration/deceleration times start to become significant at short residence times. This effect was taken into account and average residence time was used in the present studies. The number of cycles applied to the web is determined by the number of oscillations made by the head while the web is passing through the coating zone.

B. Materials and process

The ALD web coating system was tested using the trimethylaluminum (TMA) + water process for Al_2O_3 deposition. This process was chosen because it is very sensitive to the presence of moisture and to reagent intermixing and thus can easily highlight possible imperfections. TMA (98%) (Volatec, Finland) and deionized water were evaporated at 35 °C and 45 °C, respectively, and delivered to the coating head using 5 l/min of N_2 as a carrier gas. Precursor dosage was adjusted by needle valves to 0.6% and 11% of the volume fraction, for TMA and water, respectively. Carrier gas flows were controlled via mass flow controllers. The process temperature was kept at 105 °C. Previously, it was found that for the spatial ALD process the temperature should be above 100 °C to allow excess water molecules to desorb from the surface during the purging stage.[16] On the other hand, the temperature should be low enough so that the polymer web is not affected. An overall flow rate of 60 l/min was used for the inert curtain gas. Nitrogen for the carrier and curtain process gas was sourced from liquid nitrogen supplied by Aga, Finland.

Additional experiments were carried out using a TFS200R (Beneq Oy, Vantaa, FI) continuous ALD system (Beneq, Finland). A detailed description of the system can be found elsewhere.[12,16] The reactor in this system features similar space geometry, size of the inlet and exhaust nozzles and substrate to nozzle gap to that of the large scale WCS 500 ALD system. Comparisons of performance between the systems have shown that they both behave in a similar manner. Therefore, use of the TFS200R allows process development at a smaller scale and direct transfer of the parameters to the larger system. Precursors were delivered to the reactor using 200 sccm of N_2 flow and 4600 sccm of N_2 were used as an inert gas curtain flow in order to separate two precursors within the reactor. Precursor concentrations were adjusted by needle valves.

For process tests, PET web metalized with Ti was used as a substrate. The purpose of Ti metallization was to provide a reflective surface for accurate thickness measurements using spectroscopic ellipsometry (J.A. Woollam M2000FI). Al_2O_3 films for diffusion barrier coating application were deposited on polyethylene naphthalate (PEN) OPTFINE® (125 μm) supplied by Dupont Teijin Films.

Optical transmission measurements were performed using a Thermo Nicolet Evolution 500 UV-Vis spectrophotometer.

C. Moisture barrier tests

WVTR of the Al_2O_3 coated films was measured by using Aquatran Model 1G by MOCON (Minneapolis, MN, USA). In this method, the ALD coated side of a sample is sealed against a test cell by using high vacuum grease. The measurements were carried on at 38 °C/90% relative humidity (RH) and the active test area of the sample was 50 cm^2.

An optical calcium test was used for evaluation of ultrabarrier levels of WVTR. In this method, the evaluation of WVTR is based on the change in transmission of white light through a semitransparent metallic Ca film[17] with transmission (T) around 10%. It is known that at low temperature, oxidation of Ca proceeds by reaction with H_2O according the complete reaction

$$Ca + 2H_2O \rightarrow Ca(OH)_2 + H_2.$$

Following this reaction, the originally metallic Ca becomes transparent Ca hydroxide. Therefore, the light transmitted through the film increases. By calibrating the transmission of the Ca film versus Ca thickness and measuring the transmittance change of the film, it is possible to evaluate the amount of water reacting with the metallic Ca and from it calculate the WVTR of the barrier. Ca-films about 60–80 nm thick were deposited on 6 in. round glass wafers used as substrates in a high vacuum system equipped with a cryopump. The Ca-film was deposited in 6 distinct and isolated areas covering about 40% of the total wafer area. Each individual area is between 7 and 20 cm^2 in size. Their distance from the edge ranges between 10 and 15 mm. The Ca film was then encapsulated *in situ* with a thin oxide film to avoid any initial deterioration by the following handling in atmosphere with residual moisture content. Previous experiments had shown that the oxide film was not a good barrier in accelerated testing at 85 °C/85% RH. Complete

oxidation of Ca films protected with this oxide would occur in a few hours of exposure. The ALD barrier to be measured was then glued in a face-sealing configuration on top of the glass plate described above by using a proprietary epoxy adhesive with low WVTR. This configuration shown in Fig. 4 represents the best simulation for using the ALD barrier in a lamination approach.

The samples were subjected to accelerated testing at 40 °C/90% RH and 85 °C/85% RH. The change in transmission of the Ca film was monitored at the beginning of the lifetime test, and periodically, with a spectrometer, and the WVTR was calculated. Multiple points were acquired for each area with a spot size of 2–3 mm. In addition, optical observations in transmitted light were carried out to detect the early appearance of transparent pinholes that would indicate a localized failure that may have been below the lateral resolution by the spectrometer.

III. RESULTS AND DISCUSSION

A. ALD behavior

ALD technology is valuable because it is able to produce conformal pinhole-free films on complex shape surfaces or even porous structures. Quality films are produced only if the process follows the unique self-limiting mechanism that signifies ALD film growth. Particle and void formation and nonuniform growth occur when precursor separation is not efficient and reagent mixing takes place in the gas phase. Thus, it is essential to check the growth mechanism when establishing a new process. The issue is especially critical in spatially separated atomic layer deposition where precursors are simultaneously introduced in one reaction chamber volume and confined within their zones by means of inert gas. One way of proving the ALD process mechanism is by showing self-limiting growth behavior. This is done by building so-called saturation curves, which show the dependence of growth rate on the precursor dose, which in the case of SALD is defined by the precursor residence time, if the precursor flow rate is fixed. To verify this, a series of depositions was carried out using residence times in the range of 49–609 ms, corresponding to 0.4–0.02 m/s of coating head speed. The parameters used for the tests are shown in Table I.

The resulting saturation curve is shown in Fig. 5. The curve shows dependence of growth rate on residence time. It should be noted that in contrast to the conventional ALD process, altering the residence time affects the applied dosage of both precursors simultaneously. Nevertheless, in the present case, the conditions were chosen in such a way that water is largely in excess. It was shown in previous studies that water flow rate greatly affects the resulting growth rate.[18]

TABLE I. Deposition parameters for building saturation curve.

Coating head speed (m/s)	Residence time (ms)	Web handling speed (m/min)	ALD cycles	Growth rate (Å/cycle)
0.02	609	0.05	580[a]	1.10
0.03	410	0.044	500	1.06
0.06	211	0.059	700	0.81
0.1	132	0.083	800	0.75
0.2	75	0.117	1000	0.59
0.4	49	0.119	1500	0.494

[a]Web sample was guided two times through the coating zone to achieve a large enough number of cycles for easy film thickness measurement.

From the curve, it can be seen that process reaches saturation approximately at 410 ms residence time and additional time does not increase the growth rate. It confirms that no precursor is being deposited on the surface once all reactive sites on the surface have been occupied. Saturation growth rate of 1 Å/cycle and residence time value is consistent with the results obtained from a similar SALD system[16] and, indeed, from conventional TMA + water ALD processes.[19]

Another important feature is growth rate uniformity over the substrate area. In case of spatially separated ALD, this test can show how uniform gas flows are and help to detect possible process imperfections. Increased thickness is usually attributed to CVD growth and reduced thickness to low precursor concentration. Figure 6 shows an image of the Ti metalized substrate web sample coated with 70 nm of Al_2O_3using roll-to-roll mode. Spectroscopic ellipsometry reveals ±5% deviation thickness deviation across the substrate width. The thickness variation value agrees with earlier studies.[16]

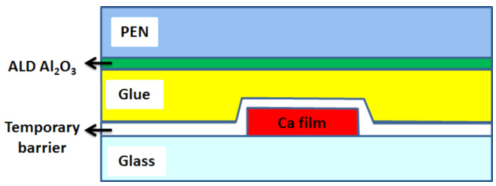

FIG. 4. (Color online) Setup structure for accelerated Ca test.

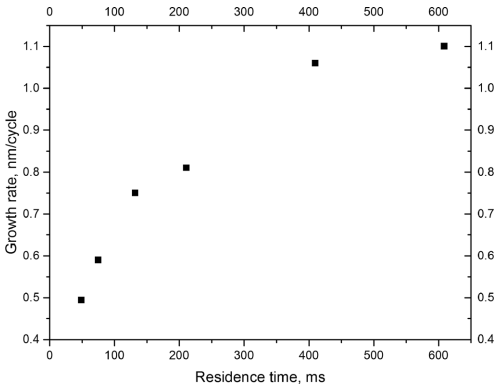

FIG. 5. Al_2O_3 growth rate as a function of residence time at 0.6% and 11% of the volume fraction of TMA and water respectfully.

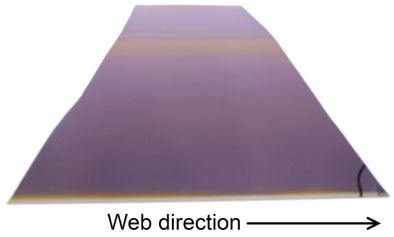

FIG. 6. (Color online) Image of a section of Ti metalized PET substrate coated with 75 nm of Al_2O_3.

B. Barrier properties

One of the potential applications mentioned in Sec. I is a gas diffusion barrier for flexible electronics. To evaluate the barrier properties of the film, PEN OPTFINE (125 μm) polymer web was coated with 20 nm of Al_2O_3 at a range of parameters depicted in Table II. The last column in the table shows the respective TMA dosage for each run. Noncoated PEN OPTFINE exhibits WVTR of 1.3 g/m^2 day. Samples for the WVTR measurements were cut off the web before it reached the idle roller. Thus, the surface was kept intact to prevent possible mechanical damage from the rewinding. Certainly, this is one of the issues to be addressed in the future. One of the possible solutions could be usage of lamination techniques to protect sensitive coatings (e.g., pressure sensitive adhesives, UV curable coatings). However, the aim of this work is to determine the basic properties and capabilities of a roll-to-roll process. It is important to note that the actual thickness of the Al_2O_3 film on the PEN substrate is likely to be less than the 20 nm, which was measured on a metalized foil. It is known that during ALD on polymers there is some penetration of the precursor into the polymer resulting in a lower thickness than expected.[20] It is difficult on a routine basis, however, to measure the thickness of a nm scale transparent film on a transparent substrate.

WVTR data and TMA precursor dosage as a function of residence time are shown in Fig. 7. From the WVTR curve, it can be seen that barrier films perform well in the range of 132–400 ms giving values below the Aquatran detection limit ($\sim 5 \times 10^{-4}$ g/m^2 day). Further decrease of the residence time causes critical worsening of barrier performance. This behavior is predictable as the minimal dosage of TMA required for complete surface saturation derived from conventional ALD experiments is $\sim$3 mg/m^2, thus lower doses will give incomplete surface coverage per individual cycle.

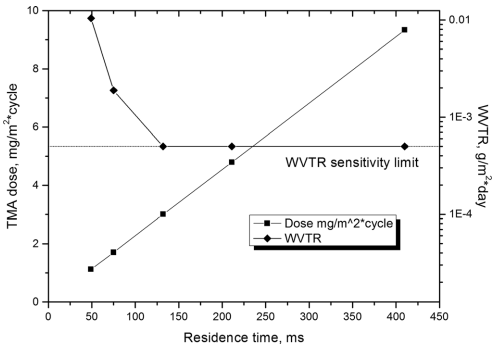

FIG. 7. WVTR data and respective specific precursor dosage as a function of residence time.

Ca tests were carried out to measure extremely low permeation rates down to the 10^{-6} g/m^2 day range because commercially available WVTR measurement equipment do not possess the required sensitivity for measuring ultrahigh barrier films. Barriers of 20 nm of Al_2O_3 on PEN obtained using 0.1 m/s of coating head speed were assembled for Ca-tests as described in Sec. II.

Accelerated lifetime testing was carried on by aging the samples at 40 °C/90% RH initially for 185 h, then at 85 °C/85% RH. Because of the limited size of the PEN foil with ALD barrier, only a part of the Ca test vehicle was covered with barrier foil. With reference to Fig. 8, only the Ca areas labeled "A" and "B" were considered in the evaluation of the WVTR of the barrier. The samples were first aged at 40 °C/90% RH for 185 h. Because no transmission change was measured and no pinhole had appeared in areas A and B, the samples were moved to an aging chamber set for more aggressive accelerated test conditions at 85 °C/85% RH.

Figure 9 shows the image of the sample prior to the test, after 470, and 800 h at 85 °C/85%RH. It can be seen that the optical density of the central part of areas A and B does not change with time in accelerated testing at high temperature and humidity. The transmission versus aging time curves were also flat. This confirms the superior barrier quality of the films. In contrast, Ca oxidation occurred rapidly in the areas not covered by the film confirming the negligible contribution of the protective oxide to the overall barrier performance evaluation. At longer aging time, further oxidation

TABLE II. Deposition parameters for 20 nm Al_2O_3 coatings on PEN.

Coating head speed (m/s)	Residence time (ms)	Growth rate (Å/cycle)	AALD cycles	Web speed (m/min)	WVTR (g/m^2 day)	TMA dosage (mg/m^2 cycle)
0.4	49	0.494	405	0.44	0.01043	1.12
0.2	75	0.59	339	0.35	0.00188	1.70
0.1	132	0.75	267	0.25	<0.0005	3.01
0.06	211	0.81	247	0.17	<0.0005	4.80
0.03	410	1.06	189	0.11	<0.0005	9.33

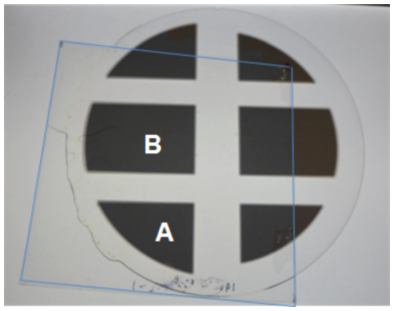

FIG. 8. (Color online) Partially laminated Ca-test wafer. The size of the barrier foil is shown by the overlapped blue contour. Only areas A and B were considered in WVTR evaluation because they were completely covered with the ALD barrier.

occurs at the periphery of the encapsulated Ca-area by water due to penetration through edge of the sealant.

Absence of local degradation in the central areas of zone A and B was confirmed by the absence of any pinhole upon observation by optical microscopy. Estimated WVTR of the samples according to Ca test is $\sim 5 \times 10^{-6}$ g/m^2 day at 20 °C/50% RH. This value is equivalent to $\sim 3 \times 10^{-5}$ g/m^2 day at 38 °C/90% RH, about one order of magnitude lower than the detection limit of the MOCON Aquatran Model G1.

To explore the effect of the specific precursor dose on the WVTR performance, as mentioned earlier, additional experiments were performed using the small scale TFS200R Spatial ALD reactor. The system features a reactor with identical design to the large scale system with respect to nozzle arrangement and geometrical dimensions except nozzles length reduced to 100 mm (compare to 500 mm of WCS500). A series of depositions was carried out in order to study the effect of TMA precursor dosage on the film properties. Applied precursor dosage was adjusted in two ways: (a) changing the speed of the substrate and hence the residence time and (b) adjusting the precursor concentration using the respective needle valve. In order to take into account the influence of both factors, the amount of precursor applied per unit of area and per one ALD cycle was calculated, and hereinafter, this is referred to as the specific precursor dosage (mg/m^2 cycle). Ranges of 23–459 ms for residence time and 20–350 mg/min for precursor flow were used, which results in a wide range of specific precursor dosage of 0.37–51.8 mg/m^2 cycle.

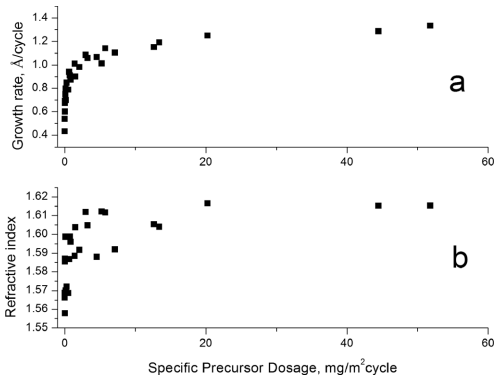

FIG. 10. Growth rate and refractive index of the ALD films as a function of specific precursor dosage.

Respective growth rate and refractive index values were measured and plotted against the specific precursor dosage calculated for each deposition run. Growth rate and refractive index curves are shown in Fig. 10. From Fig. 10(a), it can be seen that film growth rate exhibits typical saturation behavior for the TMA + H_2O process once the specific precursor dosage exceeds 14 mg/m^2 cycle and a dramatic drop from 1 to 0.43 Å/cycle if dosage less than 3 mg/m^2 cycle is applied.

Refractive index data in Fig. 10(b) also shows great dependence on the applied dosage in a range below 3 mg/m^2 cycle. If refractive values of 1.610–1.615 are consistently achieved within the saturated region, the values for the non-saturated range (below 3 mg/m^2 cycle) exhibit an abrupt drop from 1.600 to 1.566. Mass density calculation using the Lorentz–Lorenz equation[21] reveals density values of 3.33–3.35 g/cm^3 for films synthesized at high dosages and 3.28–3.13 g/cm^3 for low dosage films. It can be concluded that poorer barrier properties of the films are caused by lower film density as a result of incomplete surface saturation.

Obviously, the critical dosage of 3 mg/m^2 cycle characterizes a particular type of reactor assembly rather than chemistry of the process itself. Previous studies of the Al_2O_3 ALD process using a quartz crystal microbalance show that actual precursor uptake by the substrate surface is 10 times less −0.35 mg/m^2 cycle.[22] It is worth mentioning that precursor uptake depends on the substrate type, e.g., some polymer materials require much more reagent quantity during the

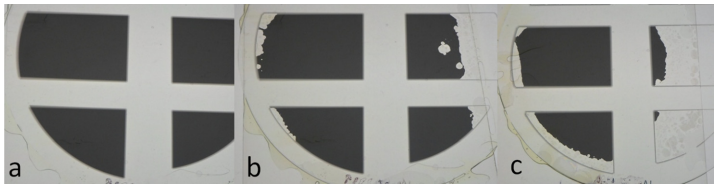

FIG. 9. (Color online) Samples subjected to accelerated Ca test: (a) after 185 h at 40 °C/90% RH; (b) 468 h at 85 °C/85% RH; (c) 800 h at 85 °C/85% RH.

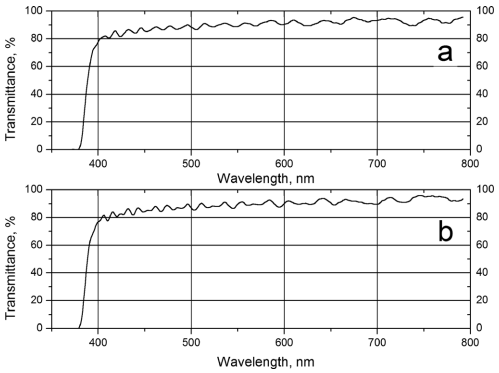

FIG. 11. Optical transmittance of (a) noncoated PEN; (b) 20 nm Al_2O_3/PEN.

nucleation period—up to 10 times more compared to a quartz surface.[20]

C. Optical transmission

Optical clarity is one of the essential requirements for flexible photovoltaics and display applications. Transmission measurements of Al_2O_3/PEN were taken at 350–800 nm wavelength range. As an example, spectrum of 410 ms sample was compared with noncoated polymer (Fig. 11). It can be seen that 20 nm Al_2O_3 coating does not affect the optical clarity in the visible range with minimum transmission of approximately 80%.

IV. SUMMARY AND CONCLUSIONS

A true ALD roll-to-roll process for thin Al_2O_3 coatings has been developed and investigated. The ALD nature of the process has been proven by demonstrating self-limiting behavior. Other ALD thin films features such as growth uniformity and high moisture barrier performance have also been shown in the present study. Effect of precursor dosage on the film properties were studied as well. It has been shown that 3 mg/m^2 cycle is the critical value for applied specific precursor dosage below which surface saturation is incomplete and leads to poorer moisture barrier performance. WVTR measurements by the coulometric method at tropical conditions (MOCON Aquatran Model 1) have shown values of $\leq 5 \times 10^{-4}$ g/m^2 day for 20 nm Al_2O_3 films, obtained at 0.1 m/s of coating head speed and 0.25 m/min web speed which equal to 180 m^2 of coated web per day. Additional accelerated Ca test at 85 °C/85% RH during 800 h has confirmed the superior quality of the films with the final WVTR figure equal to $\sim 5 \times 10^{-6}$ g/m^2/day at 20 °C/50%RH. Production yields can be potentially increased in a similar machine design by using wider webs and/or a larger coating head and drum as the system exhibits a very stable and robust process.

ACKNOWLEDGMENT

This research was supported by Finnish Funding Agency for Technology and Innovation (TEKES) under Project 70033/10.

[1]G. Gustafsson, Y. Cao, G. M. Treacy, F. Klavetter, N. Colaneri, and A. J. Heeger, Nature **357**, 477 (1992).
[2]D. A. Pardo, G. E. Jabbour, and N. Peyghambarian, Adv. Mater. **12**, 1249 (2000).
[3]W. S. Wong and A. Salleo, *Flexible Electronics: Materials and Application* (Springer, New York, 2009).
[4]S. Iwamori, Y. Gotoh, and K. Moorthi, Vacuum **68**, 113 (2002).
[5]P. F. Carcia, R. S. McLean, M. H. Reilly, M. D. Groner, and S. M. George, Appl. Phys. Lett. **89**, 031915 (2006).
[6]S. Cho, K. Lee, and A. J. Heeger, Adv. Mater. **21**, 1941 (2009).
[7]D. Choi, S.-J. Kim, J. H. Lee, K.-B. Chung, and J.-S. Park, Curr. Appl. Phys. **12**, S19 (2012).
[8]A. G. Erlat, R. J. Spontak, R. P. Clarke, T. C. Robinson, P. D. Haaland, Y. Tropsha, N. G. Harvey, and E. A. Vogler, J. Phys. Chem. B **103**, 6047 (1999).
[9]D. H. Levy, D. Freeman, S. F. Nelson, P. J. Cowdery-Corvan, and L. M. Irving, Appl. Phys. Lett. **92**, 192101 (2008).
[10]P. Poodt, A. Lankhorst, F. Roozeboom, K. Spee, D. Maas, and A. Vermeer, Adv. Mat. **22**, 3564 (2010).
[11]F. P. Ryan, Z. M. Gibbs, and S. M. George, J. Vac. Sci. Technol., A **30**, 01A136 (2012).
[12]P. S. Maydannik, T. O. Kääriäinen, and D. C. Cameron, Chem. Eng. J. **171**, 345 (2011).
[13]E. R. Dickey and W. A. Barrow, J. Vac. Sci. Technol., A **30**, 021502 (2012).
[14]E. R. Dickey and W. A. Barrow, *52th Annual Technical Conference Proceedings of the Society of Vacuum Coaters* (2009), pp. 700–726.
[15]P. Poodt, R. Knaapen, A. Illiberi, F. Roozeboom, and A. van Asten, J. Vac. Sci. Technol., A **30**, 01A142 (2012).
[16]P. S. Maydannik, T. O. Kääriäinen, and D. C. Cameron, J. Vac. Sci. Technol., A **30**, 01A122 (2012).
[17]G. Nisato, P. C. P. Bouten, P. J. Slikkerveer, W. D. Bennett, G. L. Graff, N. Rutherford, and K. Heuser, *International Display Research Conference, Asia Display/IDW '01* (2001), p. 1435.
[18]R. Matero, A. Rahtu, M. Ritala, M. Leskelä, and T. Sajavaara, Thin Solid Films **368**, 1 (2000).
[19]A. W. Ott, J. W. Klaus, J. M. Johnson, and S. M. George, Thin Solid Films **292**, 135 (1997).
[20]C. A. Wilson, R. K. Grubbs, and S. M. George, Chem. Mater. **17**, 5625 (2005).
[21]M. R. Saleem, R. Ali, S. Honkanen, and J. Turunen, Thin Solid Films **542**, 257 (2013).
[22]J. W. Elam, M. D. Groner, and S. M. George, Rev. Sci. Instrum. **73**, 2981 (2002).

ACTA UNIVERSITATIS LAPPEENRANTAENSIS

603. SSEBUGERE, PATRICK. Persistent organic pollutants in sediments and fish from Lake Victoria, East Africa. 2014. Diss.

604. STOKLASA, JAN. Linguistic models for decision support. 2014. Diss.

605. VEPSÄLÄINEN, ARI. Heterogenous mass transfer in fluidized beds by computational fluid dynamics. 2014. Diss.

606. JUVONEN, PASI. Learning information technology business in a changing industry landscape. The case of introducing team entreneurship in renewing bachelor education in information technology in a university of applied sciences. 2014. Diss.

607. MÄKIMATTILA, MARTTI. Organizing for systemic innovations – research on knowledge, interaction and organizational interdependencies. 2014. Diss.

608. HÄMÄLÄINEN, KIMMO. Improving the usability of extruded wood-plastic composites by using modification technology. 2014. Diss.

609. PIRTTILÄ, MIIA. The cycle times of working capital: financial value chain analysis method. 2014. Diss.

610. SUIKKANEN, HEIKKI. Application and development of numerical methods for the modelling of innovative gas cooled fission reactors. 2014. Diss.

611. LI, MING. Stiffness based trajectory planning and feedforward based vibration suppression control of parallel robot machines. 2014. Diss.

612. KOKKONEN, KIRSI. From entrepreneurial opportunities to successful business networks – evidence from bioenergy. 2014. Diss.

613. MAIJANEN-KYLÄHEIKO, PÄIVI. Pursuit of change versus organizational inertia: a study on strategic renewal in the Finnish broadcasting company. 2014. Diss.

614. MBALAWATA, ISAMBI SAILON. Adaptive Markov chain Monte Carlo and Bayesian filtering for state space models. 2014. Diss.

615. UUSITALO, ANTTI. Working fluid selection and design of small-scale waste heat recovery systems based on organic rankine cycles. 2014. Diss.

616. METSO, SARI. A multimethod examination of contributors to successful on-the-job learning of vocational students. 2014. Diss.

617. SIITONEN, JANI. Advanced analysis and design methods for preparative chromatographic separation processes. 2014. Diss.

618. VIHAVAINEN, JUHANI. VVER-440 thermal hydraulics as computer code validation challenge. 2014. Diss.

619. AHONEN, PASI. Between memory and strategy: media discourse analysis of an industrial shutdown. 2014. Diss.

620. MWANGA, GASPER GODSON. Mathematical modeling and optimal control of malaria. 2014. Diss.

621. PELTOLA, PETTERI. Analysis and modelling of chemical looping combustion process with and without oxygen uncoupling. 2014. Diss.

622. NISKANEN, VILLE. Radio-frequency-based measurement methods for bearing current analysis in induction motors. 2014. Diss.

623. HYVÄRINEN, MARKO. Ultraviolet light protection and weathering properties of wood-polypropylene composites. 2014. Diss.

624. RANTANEN, NOORA. The family as a collective owner – identifying performance factors in listed companies. 2014. Diss.

625. VÄNSKÄ, MIKKO. Defining the keyhole modes – the effects on the molten pool behavior and the weld geometry in high power laser welding of stainless steels. 2014. Diss.

626. KORPELA, KARI. Value of information logistics integration in digital business ecosystem. 2014. Diss.

627. GRUDINSCHI, DANIELA. Strategic management of value networks: how to create value in cross-sector collaboration and partnerships. 2014. Diss.

628. SKLYAROVA, ANASTASIA. Hyperfine interactions in the new Fe-based superconducting structures and related magnetic phases. 2015. Diss.

629. SEMKEN, R. SCOTT. Lightweight, liquid-cooled, direct-drive generator for high–power wind turbines: motivation, concept, and performance. 2015. Diss.

630. LUOSTARINEN, LAURI. Novel virtual environment and real-time simulation based methods for improving life-cycle efficiency of non-road mobile machinery. 2015. Diss.

631. ERKKILÄ, ANNA-LEENA. Hygro-elasto-plastic behavior of planar orthotropic material. 2015. Diss.

632. KOLOSENI, DAVID. Differential evolution based classification with pool of distances and aggregation operators. 2015. Diss.

633. KARVONEN, VESA. Identification of characteristics for successful university-company partnership development. 2015. Diss.

634. KIVYIRO, PENDO. Foreign direct investment, clean development mechanism, and environmental management: a case of Sub-Saharan Africa. 2015. Diss.

635. SANKALA, ARTO. Modular double-cascade converter. 2015. Diss.

636. NIKOLAEVA, MARINA. Improving the fire retardancy of extruded/coextruded wood-plastic composites. 2015. Diss.

637. ABDEL WAHED, MAHMOUD. Geochemistry and water quality of Lake Qarun, Egypt. 2015. Diss.

638. PETROV, ILYA. Cost reduction of permanent magnet synchronous machines. 2015. Diss.

639. ZHANG, YUNFAN. Modification of photocatalyst with enhanced photocalytic activity for water treatment. 2015. Diss.

640. RATAVA, JUHO. Modelling cutting states in rough turning of 34CrNiMo6 steel. 2015. Diss.